INSTITUTO SUPERIOR TÉCNICO
Universidade Técnica de Lisboa

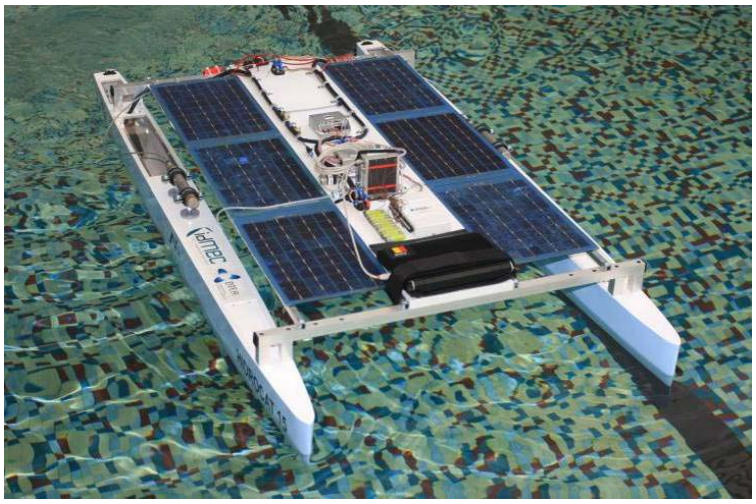

Hydrogen / Solar-based Boat Propulsion System: Design, Modelling and Implementation on a Scale Model

Julien Mélot ing.

M.Sc. thesis for obtaining the degree of Master of Science in

Naval Architecture and Marine Engineering

Jury

President:	Prof. Carlos Antonio Pancada Guedes Soares
Supervisor:	Prof. Nuno Miguel Magalhaes Duque da Fonseca
Co-Supervisor:	Dr. Rui Pedro da Costa Neto
Member:	Prof. Sergey Sutulo

October 2010

Acknowledgements

First and foremost, I am heartily grateful to my Supervisor, Pr. Nuno Fonseca, who invited me at an early stage of my master programme to join the Hidrocat team and offered me the opportunity to carry out my M.Sc. thesis in the scope of this project. His belief that Naval Architects can contribute to a cleaner world through projects such as the Hidrocat has been a constant driver throughout my thesis. Finally, his guidance and expertise have been of tremendous help to achieve the goals of the present M.Sc. thesis.

I would like to express my sincere gratitude to my co-Supervisor, Dr. Rui Neto, who shared his know-how in fuel cell technology, chemical and electrical engineering with infinite generosity. Thanks to Rui's positive attitude, working in the laboratory has been very enjoyable and instructive. I will never forget his day-to-day support and good mood.

I am very thankful to Prof. Falcão de Campos who, despite being always very busy, has always been available and offered his help in the complex field of propulsion whenever I needed it.

Dr. Gonçalo Goncalves has supported me in many ways in the course of this project by facilitating the material purchase, by providing expert advices and by giving a hand any time it was needed. I am very grateful to him.

I would like to thank Prof. Toste de Azevedo for his generosity and aid that greatly contributed to meeting the objectives of this study, Prof. Duarte Fonseca who kindly provided the hydrogen fuel cell used for this project and Ir. Filipe Duarte for the Rhino 3-D models of the Hidrocat.

To all Professors of the CENTEC with whom I had the chance to have classes, I would like to show my gratitude as they all contributed to the quality of the present thesis.

I am indebted to many of my colleagues whose support and help have been crucial throughout the course of this project. Special thanks to Jose Luis, Quian, Pedro, Thomas, Gonçalo, Manases and André.

Many thanks to my flatmates Eduardo and Eduardo for the good times and peaceful atmosphere at home that indirectly contributed to achieving this project.

Finally, I thank my parents who showed continuous trust in a successful ending of my endeavour, for supporting me throughout this master programme in Lisbon. Despite the distance between us, they always have been by my side to help me look at the bright side in hard times and to share happy moments of life.

Abstract

As climate change becomes a more widely recognized global problem, electrical propulsion of vehicles appears to be a promising solution to cut green house gases emissions. While the automotive industry makes rapid strides towards a mature electric car market, very few initiatives have arisen in the maritime sector thus far. Existing recreational electric boats are often powered either by batteries only, photovoltaic panels and batteries, or fuel cell and batteries, with range and performances dependent upon sun radiation and hydrogen storage capacity. This study contemplates an electric propulsion system for a boat, encompassing battery, photovoltaic panels and a hydrogen fuel cell, which provide incomparable range and flexibility of use. This propulsion system has been designed for a 1/8 scale model (2 m long) of the Hidrocat catamaran in order to reach required speed and to offer suitable range. The elements of the propulsion system have been characterized individually in a laboratory and a simulation model has been created based on this testing campaign. It permits simulation of various sailing schemes as well as study and prediction of energy flows and consumptions. Several trials with the catamaran scale model were conducted while monitoring the circuit components. The experimental data acquired during live testing of the scale model were compared to the output of the simulations and both were consistent which confirmed the reliability of the simulator model. The behaviour of the propulsion system encompassing two renewable sources energy was efficient and the technological choices have been validated.

Keywords: Electric boat propulsion; renewable energies; fuel cell; photovoltaic panel; simulator model

Resumo

Enquanto as mudanças climáticas são um problema global cada vez mais reconhecido, os sistemas de propulsão eléctrica de veículos parecem oferecer uma solução adequada para reduzir as emissões de gases com efeito de estufa. Enquanto a indústria automóvel progride rapidamente em direção a uma maturidade do mercado de veículos eléctricos, no sector marítimo as iniciativas que têm surgido até agora foram muito limitadas. As embarcações de recreio existentes com propulsão eléctrica são geralmente alimentadas apenas por baterias ou por painéis fotovoltaicos ou célula de combustível e baterias, cuja autonomia e desempenho são dependentes da radiação solar e volume de armazenamento de hidrogénio. Este estudo incide sobre um sistema de propulsão elétrica para uma embarcação, que engloba uma bateria, painéis fotovoltaicos e pilha de combustível de hidrogénio que permitem uma incomparável autonomia e flexibilidade de uso. Este sistema propulsor foi concebido para um modelo à escala 1/8 (2 m de comprimento) do catamarã Hidrocat, a fim de atingir requisitos de velocidade e autonomia. Os elementos do sistema de propulsão foram caracterizados individualmente em laboratório e um modelo de simulação foi criado, baseado nos testes em laboratório. Este permite a simulação de vários esquemas de navegação, bem como o estudo e previsão dos fluxos de energia e consumo. Foram realizados vários testes com o catamarã à escala, monitorizando os componentes do circuito. Os dados experimentais adquiridos durante os testes do modelo à escala foram confrontados com o resultado das simulações e ambos foram consistentes, o que confirmara a fiabilidade do simulador. O comportamento do sistema de propulsão, englobando duas fontes de energia renováveis foi eficiente e as opções tecnológicas foram validadas.

Palavras-chave: propulsão elétrica de barco; energias renováveis; pilha de combustível; painel fotovoltaico; modelo de simulação

Contents

List of tables

List of figures

Acronyms

AP	Aft Peak
B	Breadth (moulded)
BLDC	Motor - Brushless Direct Current Motor
CPP	Controllable Pitch Propeller
DAR	Developed Area Ratio
DC	Direct Current
EAR	Expanded Area Ratio
EHP	Effective Horse Power
FP	Fore Peak
FPP	Fixed Pitch Propeller
H_2	Hydrogen
I	Current
LBP	Length Between Perpendiculars
LCB	Longitudinal Centre of Buoyancy
LCG	Longitudinal Centre of Gravity
LHV	Lower Heating Value
LOA	Length Over All
LWL	Length at Waterline
NA	Not Available
OC	Open Circuit
OPC	Overall Propulsive Coefficient
PAR	Projected Area Ratio
PEM	Proton Exchange Membrane
PV	Photovoltaic
R/C	Radio Control
RH	Relative Humidity
RPM	Revolutions Per Minute
SC	Short Circuit
SHP	Shaft Horse Power
SOC	State Of Charge
T	Draft
TCG	Transversal Centre of Gravity
V	Voltage
VCB	Vertical Centre of Buoyancy
WL	Waterline

Nomenclature

Symbol	***Unit***	***Description***
A_w	m^2	Wetted area
α	-	Scale Factor
c	-	Blade Area Ratio
c_a	-	Correlation Margin
C_D	-	Drag Coefficient
C_F	-	Frictional Coefficient
D	m	Propeller Diameter
F	$C.mol^{-1}$	Faraday Constant
J	-	Advance Coefficient
Kq	-	Torque Coefficient
Kt	-	Thrust Coefficient
n	s^{-1}	Rotation Speed
n	$mole.l^{1}$	Number of moles per litre
ν	$m^2.s^{-1}$	Kinematic Velocity
p	Pa	Pressure
R	$J.K^{-}1.mol^{-1}$	Ideal Gas Constant
Re	-	Reynolds Number
t	-	Thrust Deduction Factor
$\overline{u}_m$	$m.s^{-1}$	Average Speed in Model Wake
V	m^3	Volume
V_a	$m.s^{-1}$	Advance Speed
V_m	$m.s^{-1}$	Model Speed
V_s	$m.s^{-1}$	Ship Speed
w_m	-	Wake Fraction of the Model
w_s	-	Wake Fraction of the Ship
Z	-	Number of Blades

Units

A	Ampere
C	Coulomb
g	gram
GHz	Gigahertz
K	Kelvin
kts	knots
μm	micron
l	litre
m	metre
m^2	square metre
mAh	milliampere hour
min	minute
MJ	Megajoules
mV	millivolt
Pa	Pascal
s	second
t	metric tonne
V	Volt
W	Watt
Wh	Watt hour

Chapter I - Introduction

1.1. Global Context

The “Hidrocat” project aims at building a 15 metre tourist catamaran propelled solely by electricity.

The relevance of projects of this nature is obvious in today’s global context when people are coming to realize that oil dependency is a threat at multiple levels, the first one being environmental. As this thesis was being carried out, no less than two major oil spills broke out, both destroying hundreds of kilometres of protected coastal area and natural habitat.

The awareness of this issue has already arisen widely among the automotive industry as well as in the power production sector. However, the maritime area has seen only very nominal small scale projects aiming at implementing green energy power sources on boats or merchant vessels.

In this sense, the Hidrocat project is truly unique since it benefits from a strong university based research and development and aims at encompassing multiple renewable energy sources in order to offer operation performances as high as those of a traditional combustion engine while making optimized use of electrical sources.

We, Actors of this project, treasure the hope that the Hidrocat - and other similar projects - will open a new way to clean and safe operation of boats and ships. Therefore, all our efforts are directed to carrying out this project in the most rational, meticulous and efficient way.

The major difference between electric vehicles and conventional internal combustion vehicles is the energy storage mechanism (i.e. battery instead of a liquid fuel such as gasoline) and the engine (i.e. an electric motor instead of an internal combustion engine). From an environmental standpoint the use of batteries, which provide “zero emissions” is preferred over liquid fuels, which typically generates hydrocarbon and other pollutants. Nevertheless, batteries merely move the source of the pollution from the vehicle to an electric utility which produces power to recharge the batteries - unless the energy comes from green energy sources [40].

Although internal engines generate pollutants and are inefficient, energy can be conveniently stored in reasonable quantities in the vehicle and is readily available on demand. Furthermore, this kind of vehicle can be conveniently and quickly refuelled. On the other hand, batteries are currently inherently limited in terms of both operating range and recharge rate.

In order to circumvent the two above mentioned drawbacks of traditional electric vehicles (indirect pollution and restricted range due to battery capacity limitation) other technologies have been incorporated into this propulsion system.

Photovoltaic (PV) panels supply emission free and directly available electricity to an extent related to the solar radiation. A hydrogen fuel cell (FC) produces electricity from hydrogen through an electro-chemical reaction (that is further described in *Chapter VI - Component Testing in Laboratory*). The main advantage versus batteries is that the energy concentration per weight unit is much higher with hydrogen when the latter is stored under certain conditions [13].

Combining those two electric sources enables the boat to make very limited use of pre-charged batteries and even of hydrogen when the sun intensity is sufficient. An optimized energy management hence will allow the boat to sail with a very low or no carbon footprint. It is important to note that if renewable energy sources - such as wind, solar or hydro - are used to produce the hydrogen and to recharge the batteries, the propulsion system of the Hidrocat becomes 100% emission free.

1.2. Scope

This M.Sc. thesis consists of the design, modelling, implementation and monitoring of a solar / hydrogen based electric propulsion system on a 1/8 scale catamaran (approx. 2 metres long).
Its scope is to design a suitable electric propulsion system enabling to reach required speeds and offering suitable range while consuming as little hydrogen and energy from the pre-charged batteries as possible. The propulsion system components have consequently been selected with this objective in mind together with weight constraints. The entire propulsion system will be monitored and the data stored for subsequent analysis. A computer-based model of the system will be built in order to simulate various sailing schemes, study and predict energy flows and consumptions. The output of the simulations will be confronted to experimental data acquired during live testing of the scale model. All work carried out in the scope of the present thesis will serve as a knowledge foundation for the choice of technology and design of the propulsion system of the real scale Hidrocat.

1.3. Objectives

The overall objective of this M.Sc. thesis is to develop and implement a new procedure to support the design and assessment of the electric propulsion system of ships based on photovoltaic panels and hydrogen fuel cells. This new procedure is based on the development of a comprehensive propulsion system simulator, together with the characterization of the propulsion system components in laboratory. The simulation tool is realistic since it simulates

the energy fluxes and electric characteristics of all the propulsion system components under operational conditions. This procedure can be used to design the propulsion system components and to assess the efficiency of the electric propulsion system. To achieve the overall objective, a work program was developed which is reflected in the structure of this thesis.

Following this introduction, this Dissertation is organized in 8 more chapters. The second chapter presents a wide electric propulsion boat market study aiming at defining the state-of-the-art, the technical solutions applied in function of the type of boat and the extent of the supply on this market. This introductory phase included a literature revision of the scientific papers on electric propulsion in nautical applications, manufacturer websites and catalogues and association consultation. Following this theoretical stage, the 1/8 Hidrocat scale model was prepared for hosting propulsion and steering equipment. This includes the design and installation of a platform to link the two hulls and host photovoltaic panels, a part of the energy production equipment and data acquisition material. A description and the characteristics of the scale model are found in Chapter 3. Chapter 4 describes the propeller design project which was undertaken in order to design the optimal propeller for the real scale Hidrocat and use its adimensional characteristic curves for the computer-based simulator of the scale model.
Subsequently, the hull hydrodynamic resistance of the Hidrocat scale model was calculated based on the real scale data. From these results and including the motor, transmission and propeller efficiency, the minimum propulsive power was determined. In conjunction with a sailing scheme and a minimal autonomy requirement, the capacity of the battery, power of the fuel cell and photovoltaic panels were defined. Components matching best the requirements have been selected as can be seen in Chapter 5. These components underwent testing in laboratory involving real time data acquisition techniques in order to obtain there characteristic curves. Experiment descriptions and results are related in the sixth chapter. After individual testing, the elements composing the propulsion system were mounted on the scale model and the latter was fitted with steering gear and a platform linking the two hulls in order to make it operational for live testing. Meanwhile, as thoroughly described in Chapter 7, a simulator model has been built in Matlab® Simulink®, based on the above mentioned characteristic curves. This simulator is intended to replicate with the highest fidelity possible the work of the propulsion system in various operational conditions and environments. It permits to visualize energy fluxes, charge and discharge of the battery in function of the electrical load and production. Several live tests took place to validate the propulsion system. Using similar speed control profiles under live test conditions and in the simulator allowed a careful comparison of the behaviour of the latter and its fine tuning. The results of the last confrontation are exhibited in Chapter 8. This M.Sc. thesis report is closed with the conclusions chapter summarizing the achievements and conclusion of this project and suggesting further developments.

1.4. Literature review

This thesis being partly based on experimental work in a relatively pioneering field, it could not be fundamentally based on previous scientific publications, these being still few in the field.
Hereunder is an overview of the scientific papers, books and websites about projects and experiments whose scopes are to a wider or lesser extent related to the present topic. They are referred to in the relevant sections where they have been of use. Reading and consulting those as well as conducting a comprehensive electric boat market study was of great help when it came to choosing the right technological options in order to design the propulsion system as well as to model it or carry out other specific tasks within the scope of this thesis.

The first two papers of interest to start this thesis were written by Fonseca *et al.* [1] & [2] as they give a strong insight into the whole “Hidrocat” project and all the technological fields it encompasses.

Adamson (2005) [3], Sattler (2000) [4], Weaver *et al.* (2003) [5], Allen *et al.* (1998) [6], Beckhaus *et al.* (2005) [7] and Alleau (2008) [8] all specifically cover the topic of fuel cell use in maritime applications, utilized either to propel a boat or to supply electricity onboard. They describe the type of fuel cell, of use and of system in which they can be implemented for nautical applications, both civil and military. These references are of great interest as they give an overview of similar projects and research conducted so far in this field. They were mainly used for the market study. However, they are very generic and are more of the descriptive type and do not give much insight into the actual propulsion system.

In [9], Wolfe *et al.* (1997) describe the direct control of a solid oxide fuel cell powering a DC motor without buffer batteries. Jiang *et al.* (2003) [18] cover the same subject but in the specific case of a fuel cell powered battery charging station. They propose FC regulation strategies in order to optimize battery charging or powering electrical system. These articles help understand the regulation loop of a hydrogen fuel cell although in the present case, a standard controller is preffered and its regulation will not be modified.

Vergragt *et al.* (1996) [10] contemplate the positive impact of fuel cell use on the environment, depending on the technology and fuel origin.

Wee (2006) [11] glances at the potential fuel cell applications and identifies the most economically viable as buses, recreational vehicles (this could obviously include leisure boats) and light weight vehicles provided high purity hydrogen is produced in sufficient volumes. Thounthong *et al.* (2009) [17] study carefully the energy management of fuel cell/battery/supercapacitor hybrid power source for vehicle applications. They point out that the

fuel cell/battery hybrid source can effectively function to meet the electric vehicle demand and the proposed system has achieved an excellent performance.

In his study, Singhal (2002) [12] sees solid oxide fuel cells as a solution for stationary, mobile, and military applications if a new design proposed in his paper could enter into a mass production phase.

The American Chemical Society (2004) made a comprehensive review of the state-of-the-art, innovative projects and ongoing research in the battery and FC area in [13].

In their exhaustive book [14], Larminie *et al.* (2003) cover all aspects of fuel cell technology known at the publishing time.

Langhor (2004) reviews the different hydrogen storage technologies in his Ph.D thesis [15].

In [16], Teixeira (2009) depicts thoroughly how to characterize a hydrogen fuel cell. He covers the equipment used for testing and monitoring and this discussion inspired the methodology of FC testing for the present project.

Deep information about the hydrogen research and development as well as market is given in reference [19] by Solomon *et al.* (2004) and in [40] by Zittel [1996) while [20a] & [20b] (2004) provide further information about hydrogen and other fuels.

Markvart *et al.* (2003) [23], Messenger *et al.* (2004) [24], Kininger (2003) [25] and Green (2006) [26] are four general references about the photovoltaic theme, from solar radiation to ultimate photovoltaic panel technology.

The modeling and simulation in Simulink® of a Proton Exchange Membrane (PEM) fuel cell solely is covered by Spiegel (2008) [28] whilst Lian Dibo *et al.* (2009) [27] discuss the modeling and simulation of a PEM FC and battery hybrid system. Conclusions include that when the fuel cell can afford the load, only fuel cell will power the load through DC/DC, and charge the battery if necessary; when the load goes exceeding fuel cell's power range, the battery will help to power the load automatically. This has been one of the design foundations of the Hidrocat scale model propulsion system.

Villalva *et al.* (2009) [31] propose an approach to modeling and simulation of photovoltaic panels by finding the parameters of the nonlinear current-voltage equation and adjusting the curve at three points: open circuit, maximum power, and short circuit. Given these three points, which are provided by all commercial PV datasheets, the method finds the best I-V equation for the single-diode photovoltaic.

Rai D. (2004) [32], Karnan *et al.* (2006) [33] regard the dynamic modelling and simulation of brushless direct current (BLDC) motor. This approach treats the dynamic of the BLDC motor exhaustively but as a drawback brings high complexity to the simulator model. Like the dynamic lead-acid battery simulation case, this approach goes far beyond the scope of the present M.Sc. thesis. It is however an interesting direction to follow in the future for further developments of the simulator model.

Reference [35] by HydroComp Inc. (2003) explains the power prediction process as well as optimum propeller design for a catamaran using NavCad™ and [36] by HydroComp Inc. is the help file of NavCad™, a comprehensive source of information guiding the user through multiple steps of the process and helping choose the most appropriate options.

In [37], MacPherson D. (1996) gives instructions for reliable speed prediction while [38] by Falcão de Campos (2007) provides theoretical background and practical guidance to design a propeller.

Alexandre J. (2008) [21] and Falcão A. (2008) [22] thoroughly describe the various parameters influencing solar radiation at the Earth surface and how to take them into account to calculate the effective solar radiation for photovoltaic panels. This could be used in the future to further improve the photovoltaic block of the simulator model. Reference [41] by Mata L. (1981) contains a compilation of solar exposure records in Portugal and other statistics for the last 25 years extremely useful as a reference for the various experiments involving photovoltaic panels and to build the PV block in Simulink®.

Dürr *et al.* (2006) [42] developed a mathematical model describing accurately the behaviour of a lead acid battery under typical discharge conditions. However, it remains to be proven that the author's model is also valid for the charging cycle of a lead acid battery. Additionally this model is currently only valid for the specific battery tested. Ross (2002) [29] and Jackey (2007) [30] both propose modelling solutions to model dynamically lead-acid batteries. Although these dynamic models represent undoubtedly a cutting-edge solution for battery modelling, it goes far beyond the scope of the present M.Sc. thesis. It is however an interesting direction to be followed in the future for further developments of the simulator model.

Latour Th. (2008) [34] recommends the use of the coulometric equation for lead-acid battery simulation. The latter was preferred for its simple, reliable and universal (easily adaptable to different battery types) character.

Huang *et al.* (2010) [39] propose an improved charging control of lead-acid battery with PV panels based on a feedback control system for battery charging after the overcharge point. This research opens the floor to an optimized battery charge controller designed in-house.

Chapter II - Electric Propulsion Boats Market Study

2.1. Scope

This Chapter presents a large scale benchmark of electrically propelled leisure boats, tour boats, ferries and prototypes classified by energy source and with a maximum Length Over All (LOA) of 35 m.

It aims at providing a wide overview of the extent and characteristics of the electric propulsion state-of-the-art on the electric boat market, from standardized in-land small boats to breakthrough round the world concept vessels. Information contained in this study is highly valuable to help take the correct direction when it comes to choosing the technology to be implemented on the Hidrocat and its scale model.

Pushed by strong environmental concerns, the sector of nautical electric propulsion is showing a booming dynamism. This high potential market is expected to grow fast in the coming years as initiatives arise all over the world and an increasing number of end-users show interest for the benefits it can bring while investors see a new niche in it.

By essence, a benchmark of an ever evolving segment cannot be exhaustive. However, on its completion date, November 2009, the present study covers a vast majority of the marketed electric boats. When the boat particulars were found too similar, a choice had been made to avoid redundant information. Special care has been taken at all time to ensure that all significant types of electric boats were included.

Following the benchmark, empirical formulae are proposed in order to define the required capacity of buffer batteries.

2.2. Market study of electrically propelled boats - November 2009

The benchmark herein presented was realized in order to highlight the main present trends in electrical nautical propulsion and to determine what the limits of the offer on nowadays market are. It is the result of intensive research and contact with experts in that field. Only the boats with most relevant and reliable information are hereunder exhibited as it is not always possible to obtain sufficient data. It is also important to note that other types of nautical applications of fuel cell exist but are out of the scope of the present study.

For instance military usage: The new Class 212 and 214 submarines built by Howaldtswerke-Deutsche Werft AG (HDW) in Kiel for various navies around the world are equipped with state-of-the-art specifically designed Siemens electric drive chain (Sinavy(cis)) including a high efficiency (72% total efficiency) hydrogen fuel cell (Siemens Sinavy(cis) PEM BZM 34) and permanent magnet brushless motor of 1700 kW (Siemens Sinavy(cis) Permasyn).

The tables below can be used as an informative tool providing data such as the main boat particulars, propulsion system characteristics and performances. This information collection can orientate a new design in function of the project specifications, based on the market state-of-the-art.

From the below tables, empirical formulae can also be deducted in some cases to design a new electrical propulsion system.

Sources are mainly manufacturer and electric boat association websites: [43] to [55] and the following papers: [3] to [8]

Abbreviations and acronyms can be found in the *Acronyms* section.

2.2.1. Battery powered boats

Table 2.1 - Battery solely powered boats

Name	***Type***	***Hull Type***	***Dimensions [m]***			***People***	***Battery***		***Voltage***	***Motor***	***Range***		***Max Speed***	***Yard***	***Country***
			LOA	***B***	***T***		***Type***	***Capacity [Ah]***	***[V]***	***[kW]***	***[hours]***	***[miles]***	***[knots]***		
Ace	In-land	mono	3.85	1.9	0.4	5	Lead	300	12		7 @ 3.6 kn	NA	3.6	Ruban Bleu	France
Zelec	In-land	mono	5.5	2.1	0.45	8	Lead	540	24	2 x 1	8	NA	5.1	Ruban Bleu	France
Most	In-land	mono	5.9	2.2	NA	10	NA	NA	NA	NA	8	NA	5.2	NA	NA
Voguélec	In-land	catamaran	7	3.4	0.5	17; max 30	Lead	720	36	2 x 3	15	NA	4.1	Ruban Bleu	France
Xperiance 700 Classic	In-land	mono	7	2.4	0.58	12	Lead	460	48	2.4	22 @ 3.1 kn	70	5.2	Ganita	The Netherlands
Odonata	Day-boat	trimaran	8	NA	NA	5	LMP	240	48	2 x 5	8	50 - 100	17 (1 people) 14 (3 people)	E3H	France
Alphena One	Day-yacht, Sailing	mono	8.5	2.4	1.6	6	Gel	NA	36	3.6	4	NA	NA	Alphena Yacht	France

2.2.2. Photovoltaic panels & battery powered boats

Table 2.2 - Photovoltaic panels & battery powered boats

Name	Type	Hull Type	Dimensions [m]			People	Battery		PV	Voltage	Motor	Range	Max Speed	Yard	Country
			LOA	B	T		Type	Capacity [Ah]	[m^2]	[V]	[kW]	[hours]	[knots]		
SunCat 13/12	In-land	Catamaran	3.6	1.7	0.35 - 0.55	2-3	NA	225	ca 3.5	12	NA	NA	3.6 (btry+PV); 2.6 (PV)	Solar Water World	Germany
Aequus	Tour	Mono	7	2.2	NA	7	NA	NA	NA	NA	4.5	5-6	5	Bruno Hervouet, Finot-Conq	France
SunCat 23	Tour & private / In-land & coastal	Catamaran	7	2.5	NA	12	Lead-Gel	4 x 200	6	24	2.8	NA	5 (btry+PV); 3.5 (sp)	Solar Water World	Germany
Terrapin	Canal	Mono	7.3	1.5	NA	ca 4	6 x Lead-Gel	285	ca 1-2	24	2.7	24 (80% btry capacity)	5.5; 3 (cruising)	Norfolk Broads	UK
Aquabus 850T	Dayboat / Fishing	Mono	8.5	2.5	0.48	12	Lead-Gel - No Maintenance	360	5	48	8	NA	6 (cruise)	MW Line	Switzerland
Czeers Mk I	Concept speedboat - Riva-like	Mono	10		NA	4	NA	NA	14	NA	150	NA	30 (btry+PV); 8 (PV)	Czeers Solar Boats	The Netherlands
Aquabus 1050 Standard	Tour	Mono	10.5	2.5	0.76	24	Lead-Gel or AGM (diff versions)	510 - 620 (diff versions)	14	48	8.2	9 (no sun) / 12 + (sun)	7 (btry+PV); 4 (PV)	MW Line	Switzerland
Aquabus C15 Scuba	Diving & Tour	Catamaran	11	4	0.6	30 max	NA	NA	20	48	2x16	7 (no sun) / 9 + (sun)		MW Line	Switzerland
Aquabus C60 Standard	Tour	Catamaran	14	6.6 or 5	1	60; max 75	Lead-Gel	2 x 480	20	48	2x8	8 (no sun) / 12 + (sun)	8-9 (btry+PV); 6 (PV)	MW Line	Switzerland
Sun 21	Cruise yacht	Catamaran	14	6.6	NA	5-6 (long journey)	NA	NA	65	NA	NA	Infinite (24h average); 20h on btry	5-6 (PV only)	MW Line	Switzerland
	First Transatlantic navigation sun powered only; Type MW Line Aquabus C60														
Alstersonne	Ferry	Catamaran	26.53	5.3	NA	100	Gel (6 tons)	2340 (80V) + 420 (12V)	8.2 kW	NA	2 x 12	12 - 16	NA	Zemships	Germany
	Ferry in operation since 2000 on Alster lake, Hamburg														
SunCat 2000	Tour	Catamaran	20 or 27	6.8	NA	120	Lead-Gel	NA	ca 80	NA	2 x 8	10 (no sun) / Infinite (sun)	6.5	Solar Water World	Germany
Planet Solar	Round the world Prototype	Catamaran	31 or 35	15 or 23 (flaps open)	NA	2 skippers; max 200; 50 sailing	NA	NA	470	NA	NA	Infinite (24 h average)	10 (average)	Knierim Yacht Club - Kiel	Germany
	Height: 6 m; Weight: 60 tonnes; Power received by the sun: 103.4 kW; Average engine consumption: 20 kW ; Solar panels efficiency: 22%														

2.2.3. Hydrogen fuel cell powered boats

Table 2.3 - Hydrogen fuel cell powered boats

Name	Type	Hull Type	Dimensions [m]			People	Battery		FC Type	FC Power	H2 Capacity	Storage P	Motor	Range	Max Speed	Yard	Country
			LOA	B	T		Type	Capacity		[kW]		[bars]	[kW]		[knots]		
Hydroxy 300	In-land	Catamaran	7	NA	NA	Max 7	2 x Lead - Gel	200 Ah	PEM	3	76 l	200	2 x 5	12 hours at 4.1 kn on H2 only	6.2 with 7 people	MWLine	Switzerland
	FC & batteries in parallel; batteries are "buffer";@ 4.1 kn, only 1 kW needed; controlled by 2 independent BC9000 bus terminal controllers; battery is not electronically controlled																
Xperiance NX Hydrogen	Canal	Mono	7	2.4	0.5	12	NA	12 kWh	PEM	1.2	4 x 30 l	200	NA	110 miles	NA	Ganita	The Netherlands
Ross Barlow	Canal barge	Mono	20	NA	NA	NA	Lead Acid	NA	PEM	5	2.5 kg	10	NA	NA	NA	NA	UK
	Known as "Protium Project", University of Birmingham; Motor: high torque NdFeB permanent magnet brushed DC; storage in 10 large scale metal hydride cylinders developed by the Birmingham group with Swiss collaborators at EMPA Laboratories in Zurich																
"Canal Boat Amsterdam"	Canal	Mono	22	4.3	1	Max 100	NA	30-50 kWh	PEM	60-70	24 kg in 6 cylinders	35	NA	9 hours at 7.5 kn	8.2	NA	The Netherlands
Alsterwasser	Ferry	Mono	25.56	5.2	1.2	100	NA	360 Ah (7x80V)	PEM	2 x 48 (140V DC)	50 kg	350	100	3 days of use with 50 kg H2	NA	Zemships - SSB Shipyard	Germany
	In operation on the Alster lake, Hamburg since 2008; Fuel Cells PM Basic A50, liquid cooled by Proton motor; Batteries serve as buffer and to "shave" peak loads																

2.2.4. Hydrogen fuel cell sailing yachts

Table 2.4 - Hydrogen fuel cell sailing yachts

		Zéro CO2	***No. 1***	***Yacht XV1***
Hull Type		Mono	Mono	Mono
Energy Source		PV + FC + Wind turbine + Sails	FC + Sails	SP + FC + WM + Sails
Dimensions [m]	***LOA***	11.99	12.26	12.8
	B	4.22	3.76	NA
	T	1.8 to 2.2	1.8 to 2.2	NA
People		8 - 10	12	NA
Battery	***Type***	12V: Gel 400V: LiFePO4	Gel (9 elements)	NA
	Capacity [Ah]	12 V: 288 & 400V: 40	NA	NA
Solar Panels	***[W]***	200	NA	2 x 400
Wind Turbine	***[W]***	300	NA	90
FC Type		PEM	PEM	PEM
FC Power	***[kW]***	35	20	10
H_2 Capacity		10.5 kg (3 x 150 l)	6 kg	17 kg
Storage P	***[bars]***	350	300	NA
Motor	***[kW]***	23	NA	NA
Range	***[hours]***	4 x 24 (daily consumption: 3200 W)	NA	NA
	[miles]	NA	121 @ 8 kn	300+ @ 8 kn
Yard		RM - Yachts & University of Grenoble	Béneteau & MTU	HaveBlue
Country		France	France & Germany	USA
Additional Info		Fuel Cell Genepac developed by Peugeot - Citroën for the automotive sector	Fuel cell technology implemented in a Béneteau First 40.7. Original engine: Diesel 29.4 kW, 130 diesel. MTU is a leading marine diesel engine manufacturer.	Fully autonomous craft. Hydrogen produced on-board: reverse-osmosis water purifier, de-ionizing filter & on-board electrolysis equipment, propulsion propeller produces 500 W when under sails, solar panels,; Debut in 2004 in Ventura, CA, USA

2.2.5. Illustrated results of the market study

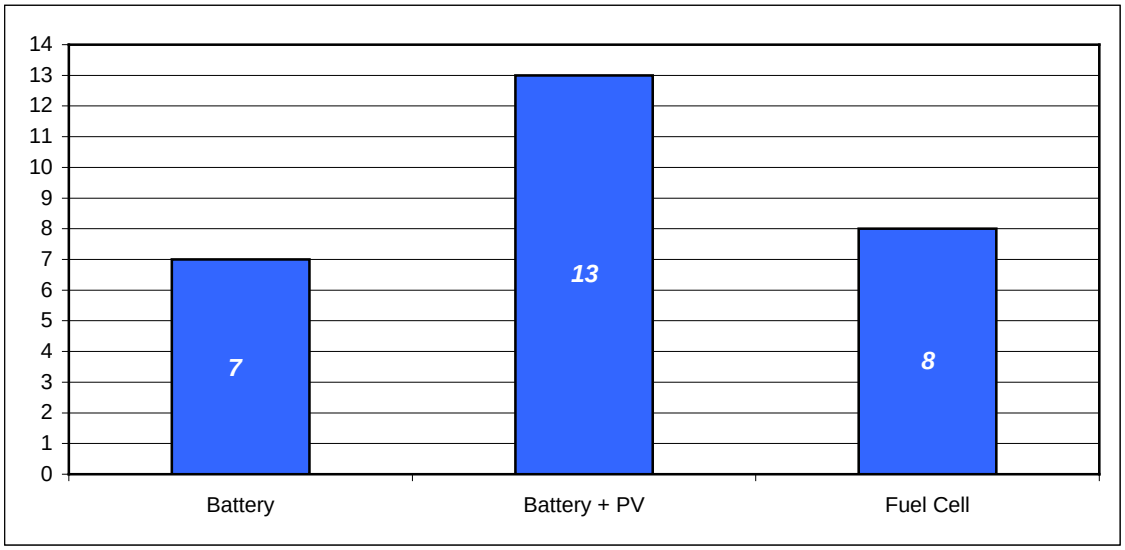

Figure 2.1 - Number of boats in function of the technology used for propulsion.

In this market study, the inventory of 27 boats within the initially specified boundaries was made. As illustrated in *Figure 2.1*, a majority of them is to be found in the Battery + PV panels category. This technology offers on the one hand, greater range / autonomy than batteries only and on the other hand is already mature and well mastered. The “Battery only” category includes mostly small size boats for in-land use. The “Fuel cell” group covers various types of boats, from ferries equipped with powerful hydrogen fuel cells to a sailing boat whose fuel cell is fed with hydrogen produced on board with demineralisation and electrolyse plants.

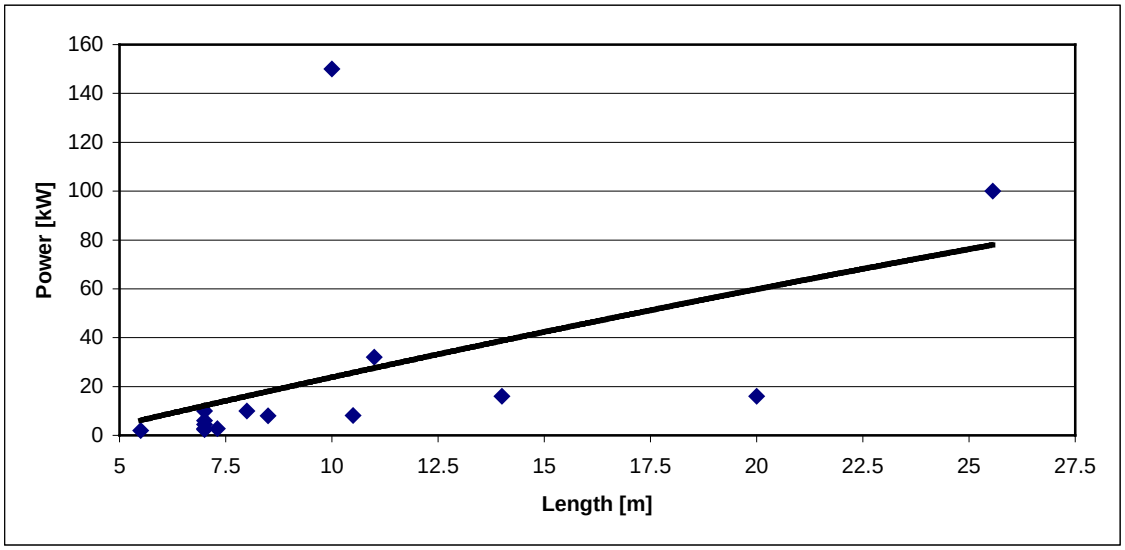

Figure 2.2 - Power of electric motors in function of the length.

It is noticeable that the vast majority of current boats propelled with electrical sources are of limited dimensions and generally low power.

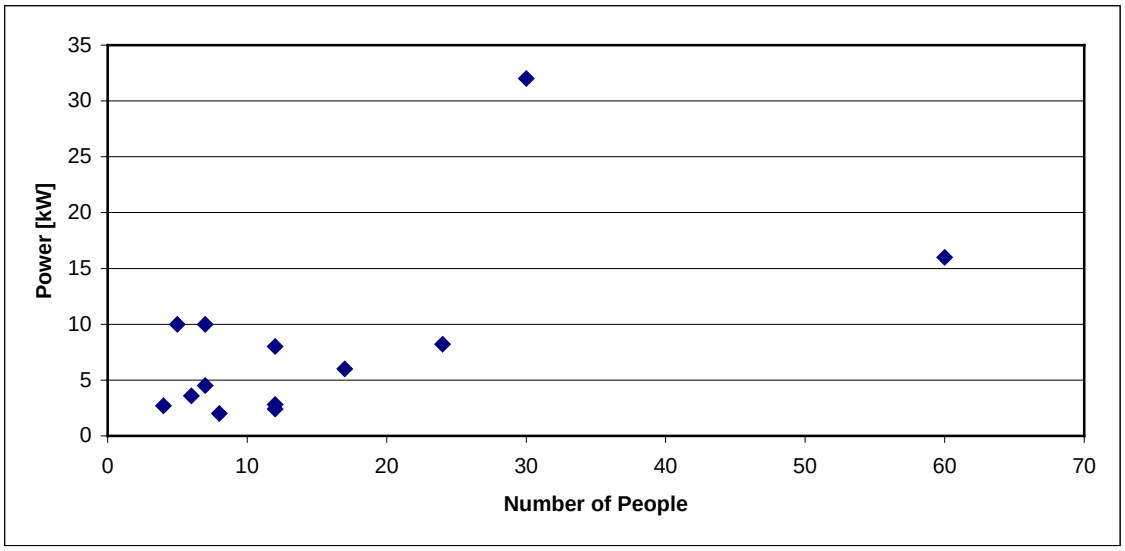

Figure 2.3 - Power of electric motors in function of the number of people allowed onboard.

The extremes have been excluded from *Figure 2.3* in order to exhibit the largest part of the population with greater accuracy.

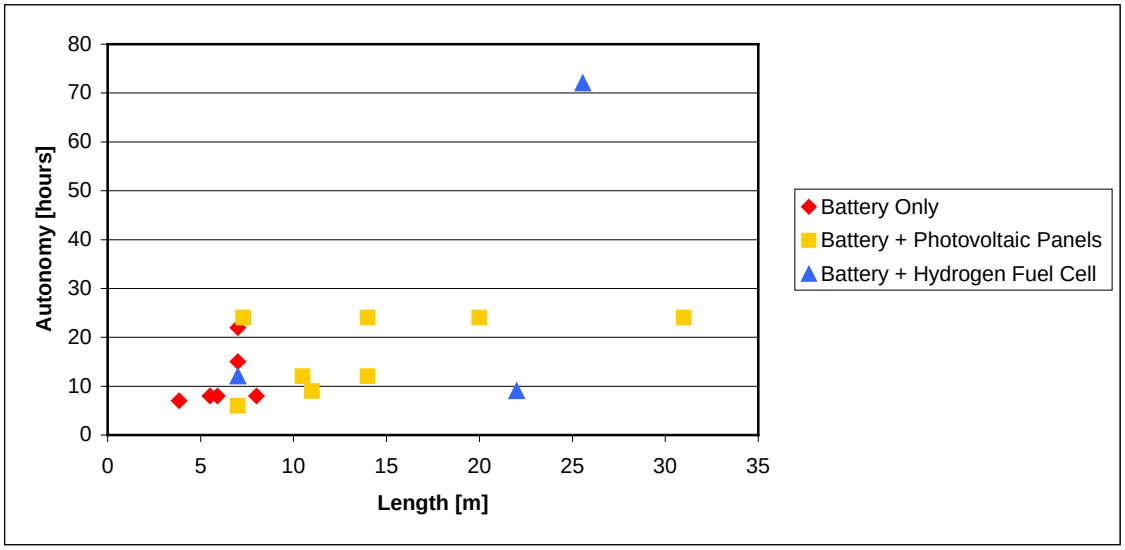

Figure 2.4 - Autonomy in function of the length per type of technology.

In *Figure 2.4*, it is obvious that adding photovoltaic panels to the battery increases dramatically the autonomy. It is important to note that the boats from the “Battery + PV” category with a 24 h autonomy have in fact an infinite energetic autonomy, provided the sun intensity is sufficient during day time.

2.2.6. Empirical formulae for defining buffer battery capacity

Rules for determination of buffer battery capacity and fuel cell power can be deducted from *Tables 2.1 to 2.4* in *1.2. Benchmark of electrically propelled boats - November 2009*:

- Fuel Cell Power: 90% - 110% of motor power (for yachts and ferries whose main power comes from the fuel cell & moderate power)
- Buffer Battery: moderate power (37.5 - 112.5 kW), @ 80V: 3.6 Ah/kW (based on the “Alterwasser” design to be found in *Table 3 - Hydrogen Fuel Cell Powered Boats*)
- Buffer Battery: high power (150 hp +), @ 400V: 0.72 Ah/kW

For other technological choices, a case by case approach is recommended using the information contained in the above mentioned tables.

Chapter III - Hidrocat 1/8 scale model

3.1. General characteristics

The catamaran used to carry out all tests in the scope of the present thesis is a 1/8 scale model based on the drawings of the real 15 metre long Hidrocat.

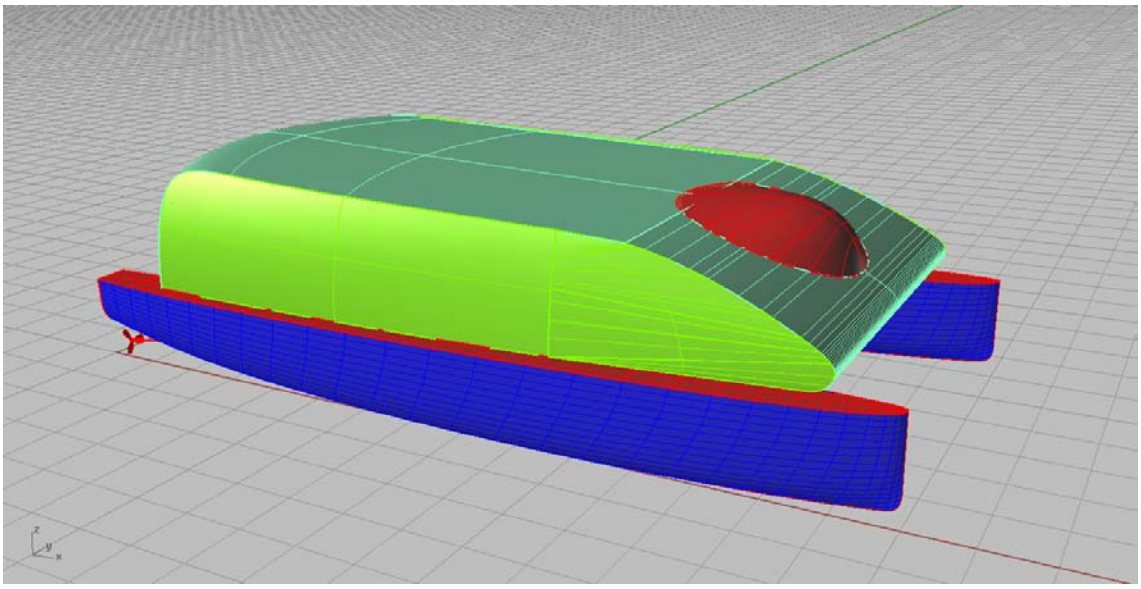

Figure 3.1 - 3-D CAD model of the full scale Hidrocat

It is made of glass fibre - polyester resin composite topped with a polyester-based gelcoat for the hull and of a sandwich material with aluminium reinforcements for the deck.

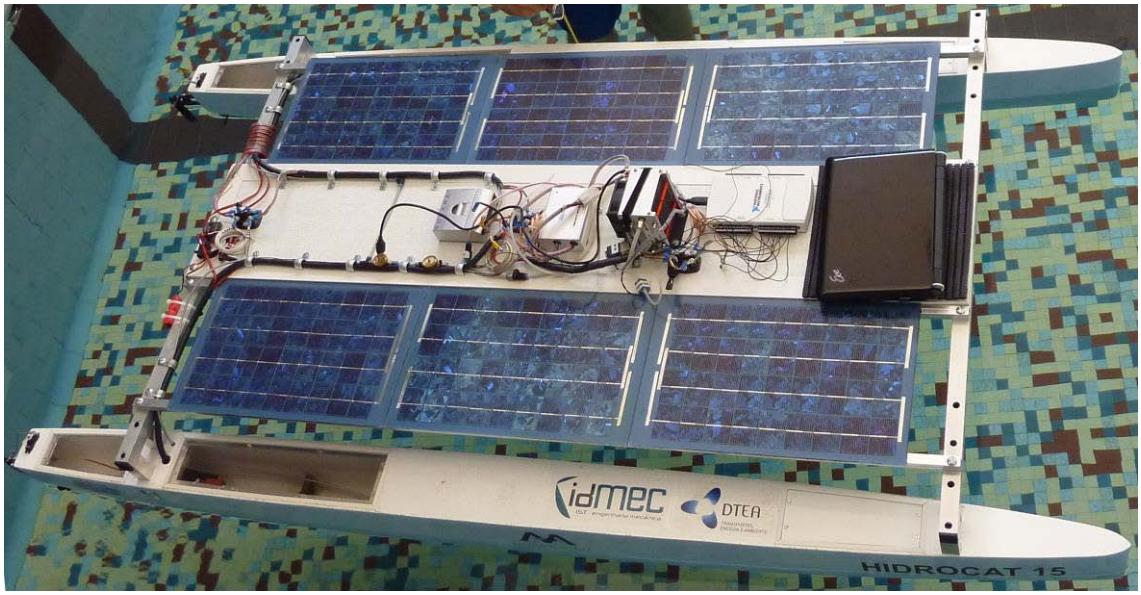

Figure 3.2 - The Hidrocat 1/8 scale model with all its equipment

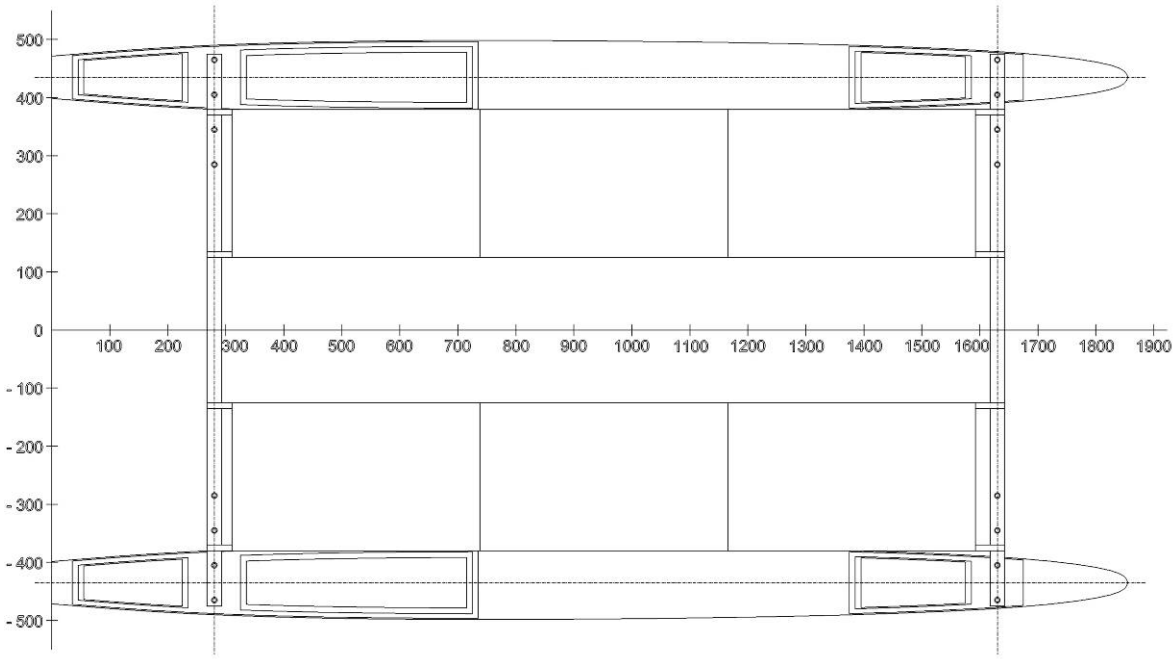

Figure 3.3 - Reference system for the positioning of weights, gravity and buoyancy centres

Scale model main particulars:

- Length between perpendiculars: 1 875 mm
- Beam of each hull: 123 mm
- Total beam: Adjustable: 760 mm to 1000 mm
- Total weight at full load: 27 840 g
- Draft at full load with total beam = 1000 mm:

Table 3.1 - Drafts & coordinates of centres of buoyancy at full load

	Portside [mm]	***Starboard Side [mm]***
Draft Fore	121	124
Draft Amidship	113	115
Draft Aft	106	106
LCB (from APP)	956	960
VCB (from baseline)	74	75

The location of the centre of buoyancy is calculated with Rhino 3D using the above drafts.
As shown in the table below, the starboard hull is about 200 g heavier than the portside one. This difference is due to constructive reasons. It induced a slight difference in draft as indicated in *Table 3.1*.

Table 3.2 - Weight components for calculation of LCG and TCG

Item	***Weight [g]***	***Distance from APP [mm]***	***Distance from Centreline [mm]***	***First Longitudinal Moment [g*mm]***	***First Transversal Moment [g*mm]***
Hull + shaft + motor support SS	3 686	931	-435	3 431 666	-1 603 410
Hull + shaft + motor support PS	3 490	931	435	3 249 190	1 518 150
Set of hatch covers + screws SS	334	674	-435	225 116	-145 290
Set of hatch covers + screws PS	334	674	435	225 116	145 290
Central platform + solar panels	12 000	955	0	11 460 000	0
Metal hydrid canister SS	666	950	-435	632 700	-289 710
Metal hydrid canister PS	666	950	435	632 700	289 710
Fuel cell + regulator + piping + wires + valves	1 269	1 100	0	1 395 900	0
Battery charge regulator Solara 135	161	750	0	120 750	0
Propeller 65 mm diam. SS	5	10	-435	50	-2 175
Propeller 65 mm diam. PS	5	10	435	50	2 175
Motor + wires and connectors SS	66	560	-435	36 960	-28 710
Motor + wires and connectors PS	66	560	435	36 960	28 710
Shaft coupling SS	47	557	-435	26 179	-20 445
Shaft coupling PS	47	557	435	26 179	20 445
NI data acquisition board + wiring	305	1 350	70	411 750	21 350
RC Receiver	25	280	-40	7 000	-1 000
RC 4.8 V battery pack	110	260	-135	28 600	-14 850
Steering servo and transmission bar SS	32	20	-435	640	-13 920
Steering servo and transmission bar PS	32	20	435	640	13 920
Rudder and fixation SS	72	-30	-435	-2 160	-31 320
Rudder and fixation PS	72	-30	435	-2 160	31 320
6 V 4.8 Ah battery SS	850	1 200	-435	1 020 000	-369 750
6 V 4.8 Ah battery PS	850	1 200	435	1 020 000	369 750
Wiring, piping, bolts, nuts, fixing: approx.	1 200	955	0	1 146 000	0
Netbook Asus EeePc 10"	1 450	1 550	0	2 247 500	0
Total:	27 840			27 377 326	-79 760

- LCG: 983 mm
- TCG: - 3 mm

The longitudinal centre of gravity is located about 20 mm fore of the longitudinal centre of buoyancy, which explains the slight trim forward. The difference of trim between portside and starboard is due to the difference of weight of the hulls. By convention, weights on starboard side are positive and those on portside are negative.

3.2. Geometric plan

See *Appendix 3.1 - Geometric plan*

3.3. General arrangement

See *Appendix 3.2 - General arrangement*

3.4. Superstructure design

At the initial stage of the thesis, two bare hulls had already been manufactured. In order to enable the implementation of propulsion equipment and live testing, openings in the decks had to be made and a platform had to be designed and built in order to link the two hulls and to host the solar panels, the fuel cell, remote control equipment and data acquisition equipment.

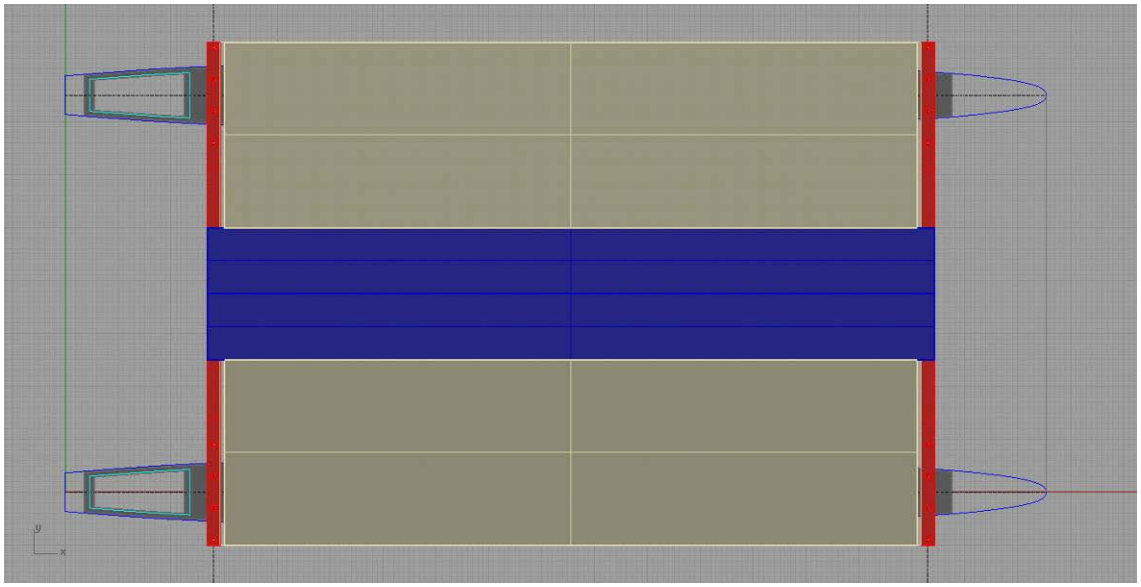

Figure 3.4 - Bird view of the platform of the Hidrocat scale model designed in Rhino 3D

The plate in the centre of the platform, between the rows of solar panels is a honey comb, fibre glass reinforced sandwich panel of 40 mm thickness. It offers high resistance and light weight.
The openings in the deck, sort of “hatches” had to be as wide as possible to allow manual work inside the hull, i.e. usage of composite materials to fix the shafts, installation of transversal bulkheads to hold the motors and mounting the propulsion equipment as well as the steering gear. The turquoise lines in *Figure 3.5* illustrate the openings in the deck. The grey lines are the boundaries of the aluminium plate reinforcements that were to be installed to withstand the stresses induced by the platform from nuts tightening (pure compressive stress in the sandwich panel) as well as for an improved stress redistribution to the entire hull.

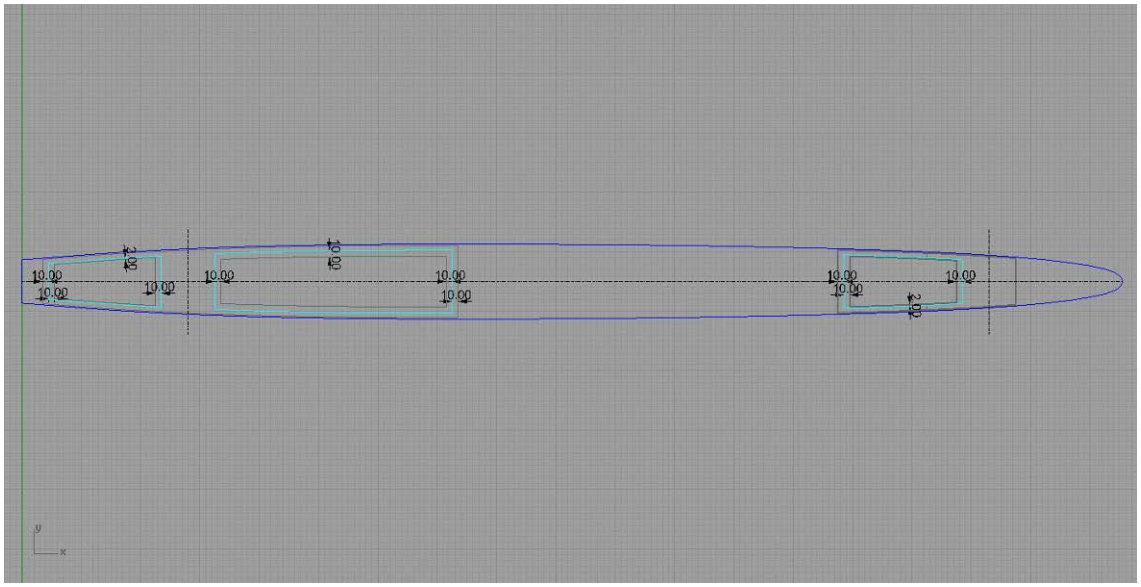

Figure 3.5 - Contours of the hull, deck openings and aluminium reinforcements.

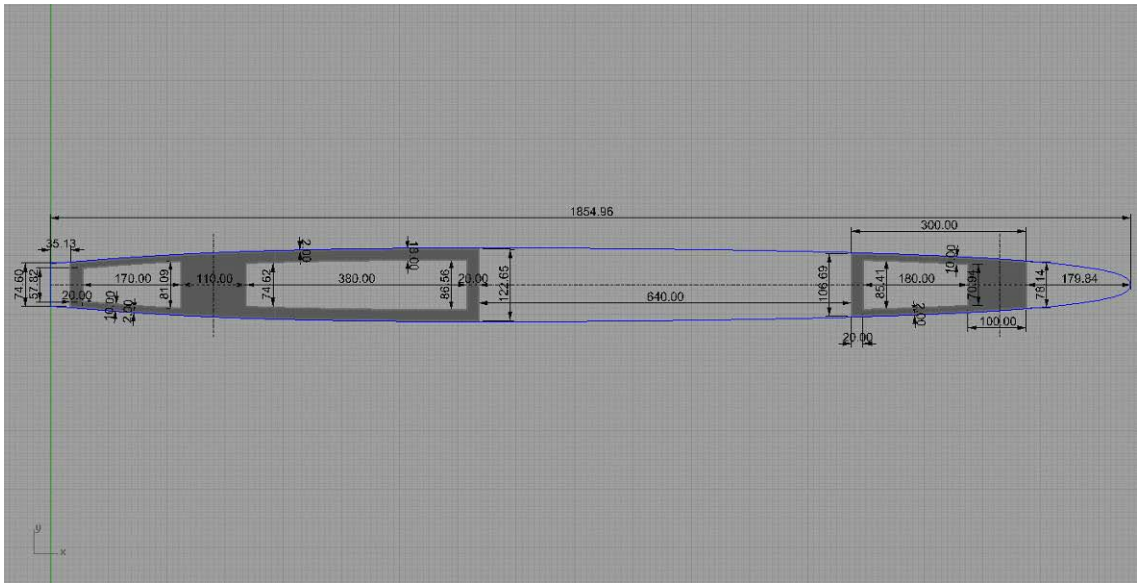

Figure 3.6 - Location and measurements of the aluminium plate reinforcements.

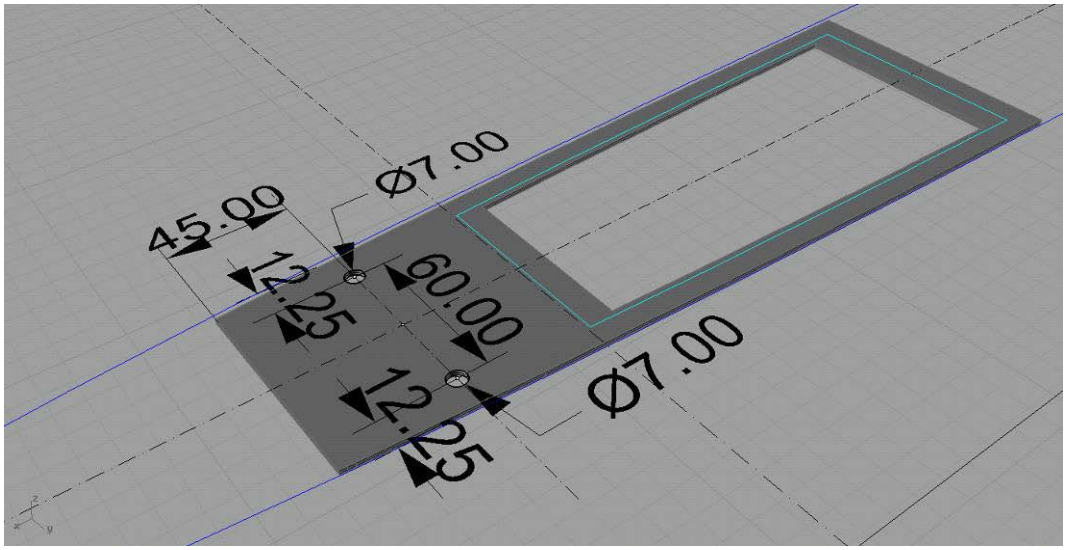

Figure 3.7 - Detail of aluminium plate reinforcement.

The aluminium plates function is also to hold the hatch covers made of polycarbonate plastic plates. Thickness of the plates is 2.5 mm and material is non alloyed standard aluminium.

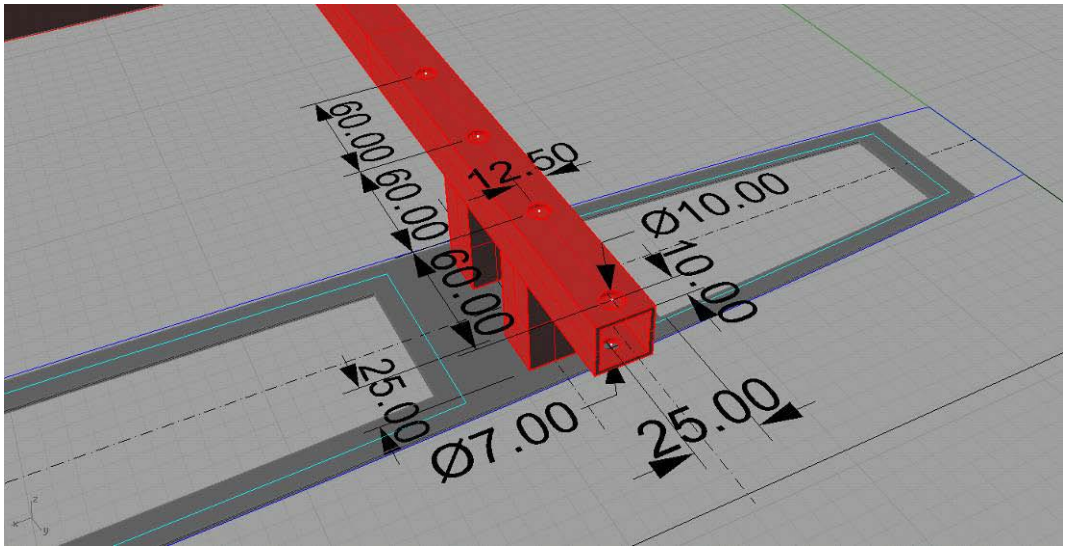

Figure 3.8 - Detail of an aluminium beam linking the two hulls.

The profiles used to make the platform and that are linking the two hulls and supporting the central honey comb plate as well as the two rows of solar panels are non-alloyed standard aluminium 25 mm square profiles. The choice of those was based on resistance requirements, weight, market availability and cost effectiveness.

3.5. Hidrocat scale model finished

See *Appendix 3.3 - Scale model finished*

Chapter IV - Propeller design project

4.1. Important parameters for propeller design

Number of blades:

Following blade area ratio trends, the fewer the blades, the greater the theoretical efficiency. In spite of the desire to provide for more blade area to control cavitation, the selection of the number of blades may occasionally be determined by other factors.
The principal reason for using a different number of blades is to control noise and vibration. The interaction of a blade passing some piece of stern structure or appendage can set up a resonant vibration and can also incite cavitation. In many of these cases the only cure is to revise the number of blades so that the frequency of the passing pulses is changed.

Diameter (as described by the tip-to-tip circle):

In theory, the largest diameter produces the greatest possible efficiency, so the selection of diameter is frequently determined by the available stern opening. However, appropriate tip clearance should be maintained. The amount depends on the application, but is usually somewhere between 10 to 20% of diameter [37].
Diameter also plays an important role on tip cavitation. Since propeller rotation speed (or Revolution Per Minute - RPM) is often not changeable, the diameter may be the only parameter remaining to control tip cavitation.

In general, less blade area increases efficiency, but only slightly. Its principal function is to distribute loads to limit cavitation, so it is best to use as little blade area as possible while retaining enough to reduce blade pressure. If a blade area is too low, however, structural considerations will dictate a thicker, less efficient, blade section. Typical manufacturing limits of blade area ratio are 1.0 for Kaplan ducted propellers and 1.1 for open wheel [36].

Nominal pitch:

Since many propellers (including some of the tested propellers that make up the series) have varying pitch distributions, the nominal pitch is measured at the 0.70 to 0.75 radius.
Face cavitation can become a problem if the vessel is operating with a pitch that is too low. Typical manufacturing limits of p/d ratio are 1.1 for Kaplan ducted propellers and 2.0 for most open wheels.

4.2. Catamaran hydrodynamic resistance calculation with NavCad

In order to design the optimal propeller for the Hidrocat at full scale, use was made of the resistance and power prediction software NavCad 4.23 from HydroComp.

Catamaran resistance is twice the individual hull resistance, plus an added drag due to the interference of the hulls with each other. NavCad predicts this system resistance (hulls and interference) in one of two ways - a catamaran system solution and a modified monohull solution [35].

The catamaran system solution of NavCad directly predicts the total system resistance. The prediction algorithm combines both hull and interference resistances. The modified monohull solution predicts individual hull resistance just as if it were a monohull. NavCad adds interference drag through correlation to catamaran model tests via the aligned prediction feature. With this approach, the effect of hull parameters and spacing can be explicitly evaluated [35].

NavCad has one algorithm for catamarans [Gronnslett, 1991]. The algorithm utilizes a set of curves for residuary resistance. A random collection of full-scale and model tests of high speed displacement catamarans with slender symmetric demi-hulls is the basis of this algorithm.
The method does not take differences in hull separation into account. Differences in interference drag are averaged to produce a generic result. This algorithm exhibits surprisingly good accuracy, however. It is assumed that this is due to two characteristics of these types of vessels. First, the hulls are long and slender operating in a high speed range (Fn from 0.6 to 1.6). A good portion of this resistance will be frictional, which is directly calculated. Second, hull spacing has shown to have the most effect on interference resistance in the lower speed ranges near the principal wave-making hump speed (Fn from 0.3 to 0.7). Above this speed regime, there is little difference in added interference drag due to different hull spacing [Insel, 1991] [35].

The above system solution is inadequate for lower speed ranges and hull types that are not the typical "wave-piercer" or "high-speed displacement catamaran". A modified monohull solution can be used for these situations, and to improve prediction accuracy in general. This approach requires the use of model tests or full-scale trials.
The key to this approach is to work with half of the vessel. In other words, results are shown "per hull". Total resistance will then of course be twice the predicted result.
Residuary resistance coefficients from catamaran model test results are the same for one hull or two [35].

This last approach has been preferred seen the low speed profile of the Hidrocat. In the test report library, a model with similar proportions has been selected and a parent file was filled out with its data for aligned prediction purpose. See *Appendix 4.1 - NavCad model file*.

4.3. Design of the optimal full scale propeller

4.3.1. Determination of Hull Resistance with NavCad

The following parameters are needed to fill in the hull characteristics box in NavCad. They are determined either from the Hidrocat particulars or from Rhino 3D for one hull only.

- Length between PP: 15 m
- Length on WL: 15 m
- Max beam on WL: 0.91 m
- Max molded draft: 0.66 m
- Displacement bare: 4.5 t
- Wetted area: 20.19 m^2
- Maximum section area: 0.43 m^2
- Waterplane area: 10.58 m^2
- Trim by stern: 0 m
- LCB aft of FP: 7.17 m
- Round bilge
- No bulb
- No transom stern immerged
- Bow shape: U-shape
- Stern shape: U-shape
- Loading: Load draft
- Hull type: Displacement
- Method: Basic (only highest speeds (10 - 12 kts) are beyond limit of Fn (by 27.5% for 12 kts) - Not a problem since service speed is between the range and NavCad is able to extrapolate)

The appendages herein considered are the two rudders whose area has been estimated from observations of similar catamarans in dry dock such as the Bahia 46 and Lagoon 440 and the exposed shafts from calculations in Rhino 3D:

- Rudder area: 0,4 m^2 (conservative estimate)
- Rudder drag coefficient: 1,5 (behind stern)
- Exposed shaft area: 0.15 m^2 (conservative estimate from Rhino 3D)
- Exposed shaft drag coefficient: 2 (10^o)

No environment components - i.e. wind, wave and channel - are added to the simulation since the Hidrocat will mostly sail in sheltered / in-land waters.

The hull resistance calculated with NavCad using the modified monohull solution has been confronted to the results of a previous simulation that had been provided by *Fonseca et al. (2009)* in [2] and obtained with a resistance prediction software especially designed for catamarans. As shown below in *Figure 4.1*, the two curves are consistent. Only for the 12 knots speed, a difference of 9% appears. The NavCad values are higher, this may be due to the consideration of appendages and hull roughness. In any cases, this prediction is being more conservative. We can conclude that the results shown below validate the resistance prediction with NavCad and confirm that this model can be use for the design of the optimal propeller.

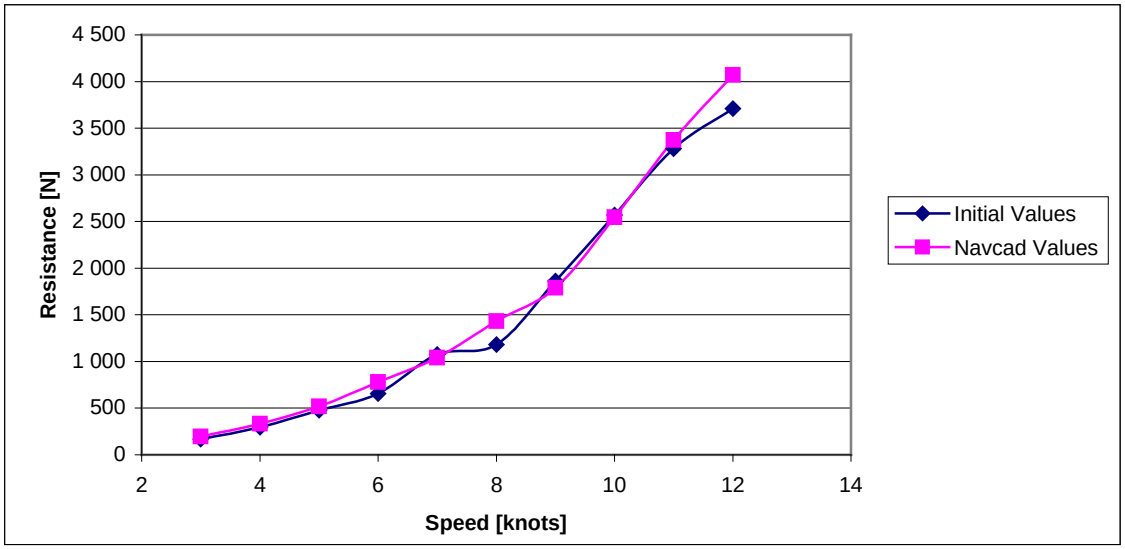

Figure 4.1 - Hidrocat hydrodynamic resistance value comparison

The wake fraction w_s from NavCad is 0.14 as opposed to 0.2 calculated in [2]. The thrust deduction factor *t* obtained with NavCad is 0.1159 compared to 0.1 in [2].
Considering the level of complexity in modelling correctly boats like the Hidrocat due to the absence of fully dedicated software, the values obtained with NavCad are acceptable as they are consistent with previously calculated ones. The full report on the hull resistance is found in *Appendix 4.2 - Hull resistance NavCad report*.

4.3.2. Engine File

In the optimum propeller design process, we will assume that the engine has already been chosen and its characteristics do not change. In the present case and at this stage of the entire Hidrocat project, the selected engines are two Solomon ST74 electric motors of brushless direct current (BLDC) type. Their data sheet is to be found in *Appendix 4.3 - Solomon ST74*

Datasheet. NavCad requires the power curves in order to define optimal characteristics of the propeller for the widest speed range possible and especially for the service speed. According to the data sheet, the following NavCad table was filled in with the engine power curve:

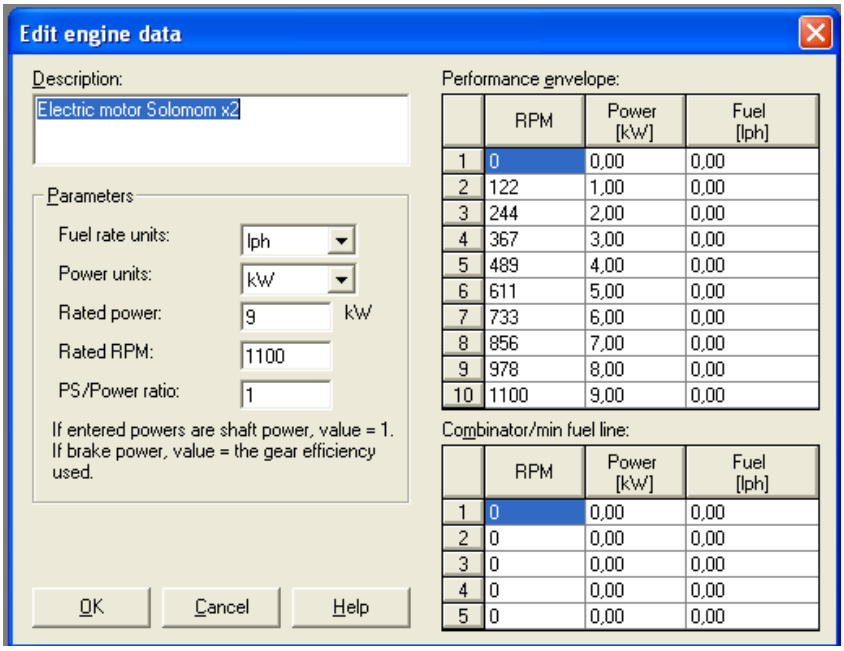

Figure 4.2 - Solomon ST74 BLDC engine file

4.3.3. Initial Constraints

The main constraint in the design of the optimal propeller is the maximum diameter and the latter is function of various parameters determined by the design of the catamaran. Therefore, the 3-dimensional design of the Hidrocat has been consulted to extract the following design characteristics:

- Shaft angle: 9.2º
- Clearance between propeller tip and bottom of the hull: 86 mm
- Shaft length (outside hull): 900 mm
- Propeller diameter: 514 mm

However, since the design of the propulsion system has not yet been fine-tuned, it is reasonable to believe that those factors may vary around the currently set values.
For the present design, it will be assumed that the shaft may be a little longer, as long as the entire propeller remains forward of the transom stern. This would allow greater diameter and consequently lower RPM's and higher efficiency, without narrowing the propeller tip - hull bottom clearance and keeping the same shaft angle.
In fact, in order to stay on the conservative side, the propeller tip - hull bottom clearance will be increased to 100 mm. Typically, this value is comprised between 10% to 20% of the diameter.

New constraints with longer shaft:

- Shaft angle: 9.2º
- Minimum clearance between propeller tip and bottom of the hull: 100 mm
- Maximum allowed shaft length (outside hull) at 9.2º: 1 148 mm
- Maximum propeller diameter: 646 mm

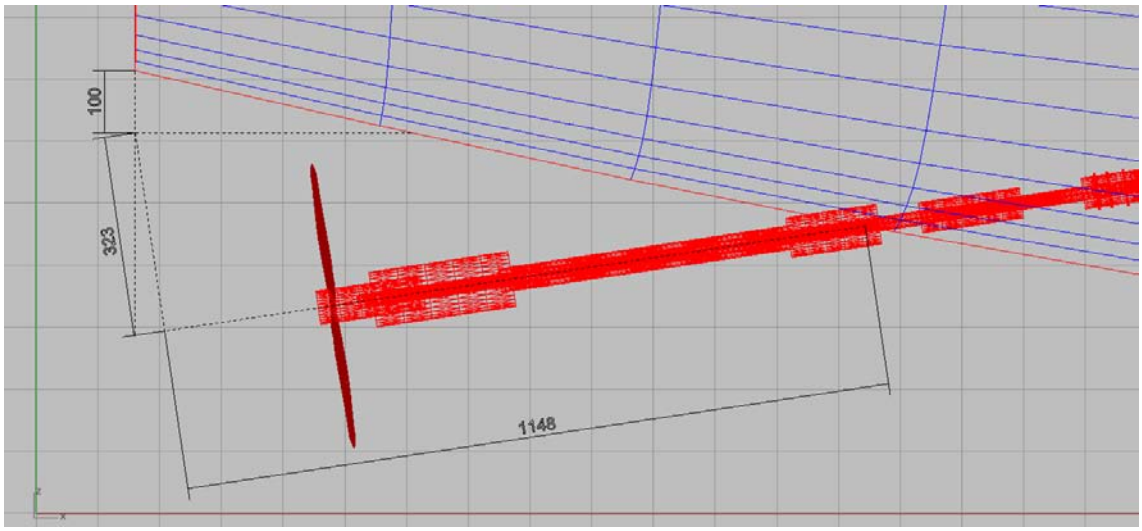

Figure 4.3 - Maximum propeller size calculation from Rhino 3D drawing of Hidrocat

4.3.4. Initial Propeller Characteristics

Based on the above considerations, a series of initial parameters must be input to serve as a base for propeller optimization. Those are chosen as the most favourable acceptable (within pre-defined boundaries, as stated above) parameters. Propulsor initial characteristics:

- Series: B-Series
- Nr. of blades: 3
- Exp. area ratio: 1.1 (1)
- Diameter: 0.64 m
- Pitch: 0.8 m (2)
- Pitch type: CPP (3)
- Scale correlation: B-Series (4)
- Kt multiplier: Standard
- Kq multiplier: Standard
- Blade t/c: 0.02 (5)
- Roughness: 30 μm (6)
- Propeller cup: 0
- Cavitation breakdown: Yes

(1) In general, less blade area increases efficiency, but only slightly. Its principal function is to distribute loads to limit cavitation, so it is best to use as little blade area as possible while retaining enough to reduce blade pressure. If a blade area is too low, however, structural considerations will dictate a thicker, less efficient, blade section. Typical manufacturing limits of blade area ratio are 1.0 for Kaplan ducted propellers and 1.1 for open wheel [36].

$$DAR = PAR / (1.067 - 0.229 * pitch/diameter) \text{ [36]} \quad \text{(Eq. 4.1)}$$

$$EAR = 0.34 * DAR * (2.75 + (DAR / num\_blades) \text{ [36]} \quad \text{(Eq. 4.2)}$$

(2) Nominal pitch of the propeller. Typical manufacturing limits of P/D (Pitch/Diameter) ratio are 1.1 for Kaplan ducted propellers and 2.0 for most open wheels. However, B-Series propellers have been developed for p/d ratio between 0.5 and 1.4 [36].

(3) Either fixed-pitch (FPP) or controllable pitch (CPP). Two different “Analysis types” can be run with CPP propellers for shaft power applications, with an additional analysis available for system analysis. These are, 1) Fixed RPM (the pitch will vary, but RPM is fixed), 2) Max. efficiency (the pitch and RPM both vary to find the combination that produces the maximum propeller open-water efficiency), and 3) Combinator (the pitch and RPM vary along the established engine file Combinator line) [36].

(4) It has been found that the full ITTC-78 correction more closely correlates to real-world experience for the large, slower rotating propellers found on merchant or military vessels, while the original B-series or equivalent profile corrections are more suitable for small craft propellers [36].

(5) The thickness-to-chord ratio t/c at 0.75 of the propeller radius has been calculated using the below formula with an EAR of 1.1:

$$t/c = (0.0185 - 0.00125 * num\_blades) * num\_blades / (2.073 * EAR) \text{ [36]} \quad \text{(Eq. 4.3)}$$

(6) The standard ITTC new propeller roughness value is 30 microns [36].

In order to calculate the resistance, the most suitable method is “displacement/semi-displacement”, as recommended by the NavCad “Method Expert”.

At a further stage, it is possible to select three systems with different characteristics. In this case, three different diameters namely: 0.60 m, 0.62 m and 0.64 m have been selected. The pitch is the variable parameter. At first, the EAR was also left variable for optimization. After a series of computation, the output for this parameter was 0.3 for all three systems. This value is generally the smallest acceptable but it was resulting in unacceptable cavitation values.

Consequently, this parameter has been chosen manual and values have been increased until reaching cavitation values within an acceptable range.

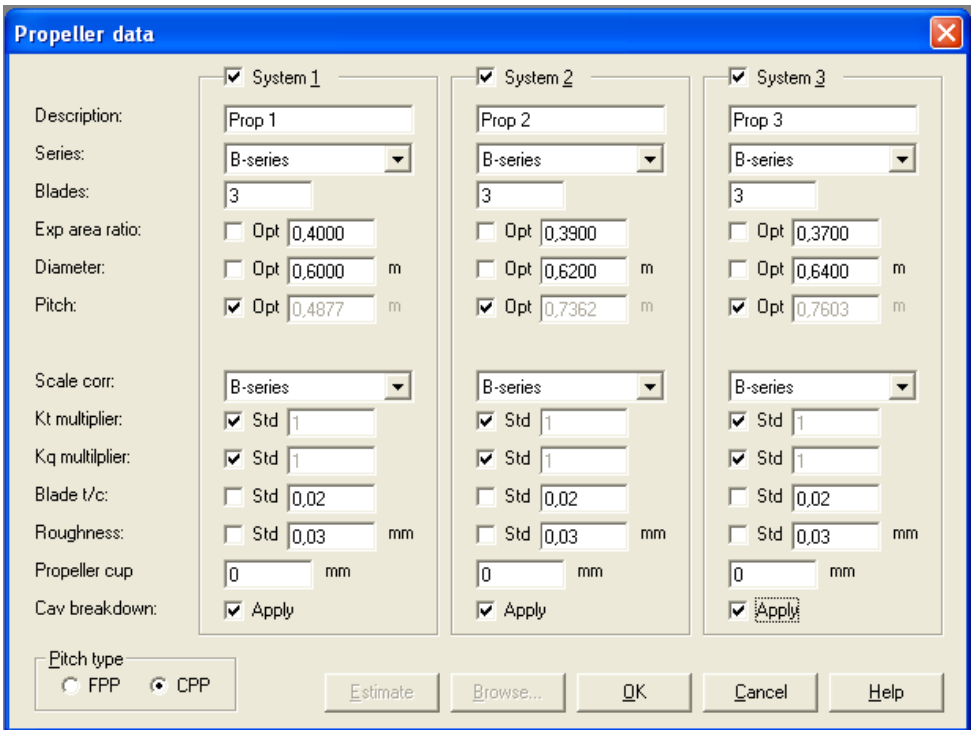

Figure 4.4 - The three selected propeller systems

4.3.5. Optimal Propeller

The optimal propeller for the Hidrocat, given her hull and motors characteristics, resulting from the design and optimization process has the following parameters:

- Series: B-Series
- Nr. of blades: 3
- Exp. area ratio: 0.37
- Diameter: 0.64 m
- Pitch: 0.76 m
- Blade t/c: 0.02
- Propeller cup: No

The reduction gear ratio had to be adapted to match the profile of each of the three tested systems, the objective being that at maximum propeller RPM, the motor would rotate at a speed close to its maximum RPM in order to provide its maximum power. In the optimal system (nr. 3) scenario, the gear ratio was 2.2. The full report on the optimized propeller is found in *Appendix 4.4 - Optimized propeller NavCad report*.

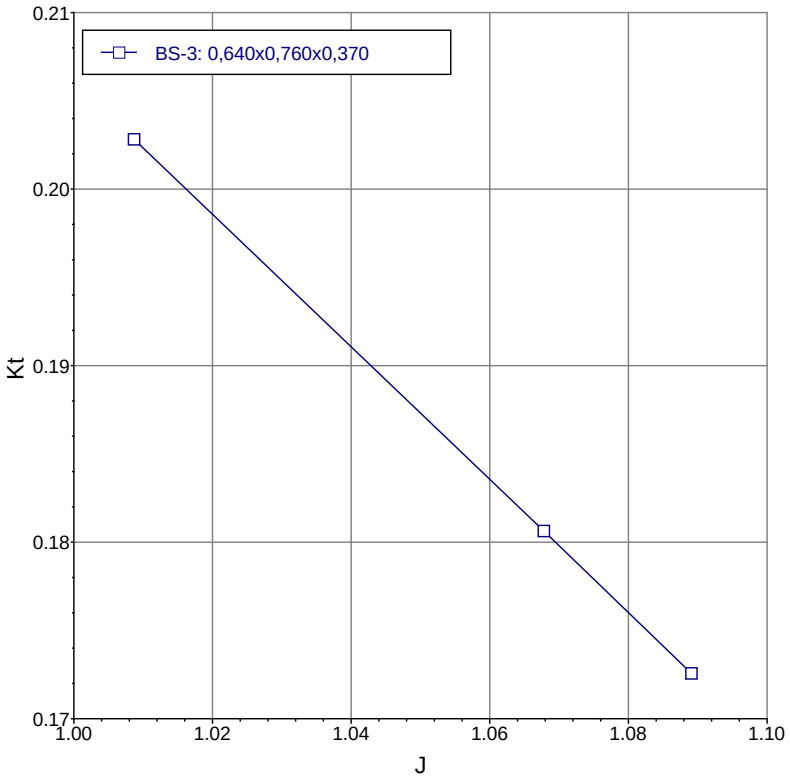

Figure 4.5 - Thrust Coefficient in function of the advance coefficient for the Hidrocat optimized propeller

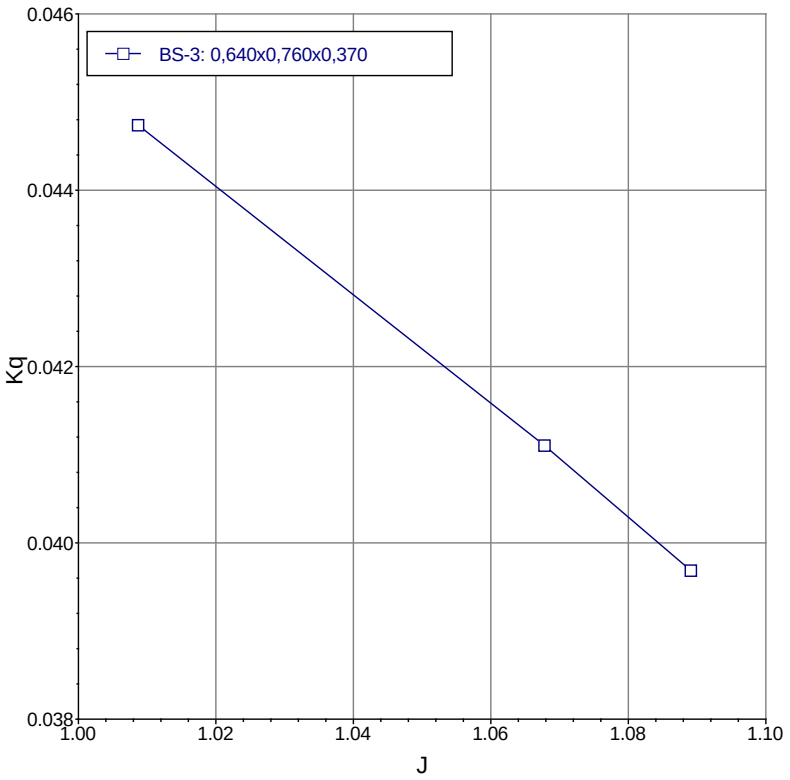

Figure 4.6 - Torque Coefficient in function of the advance coefficient for the Hidrocat optimized propeller

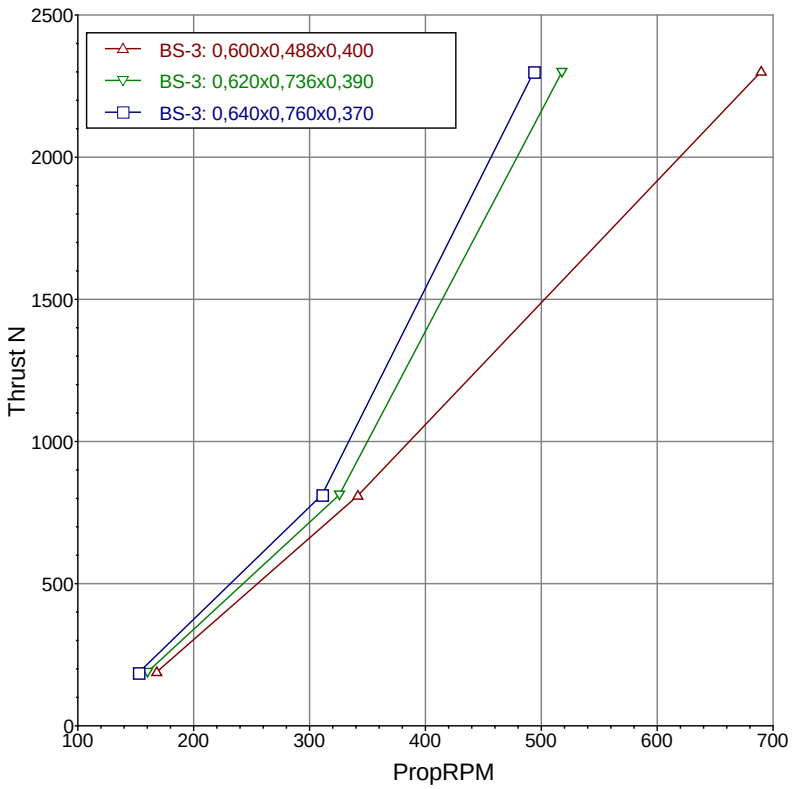

Figure 4.7 - Thrust in function of propeller RPM for the three systems

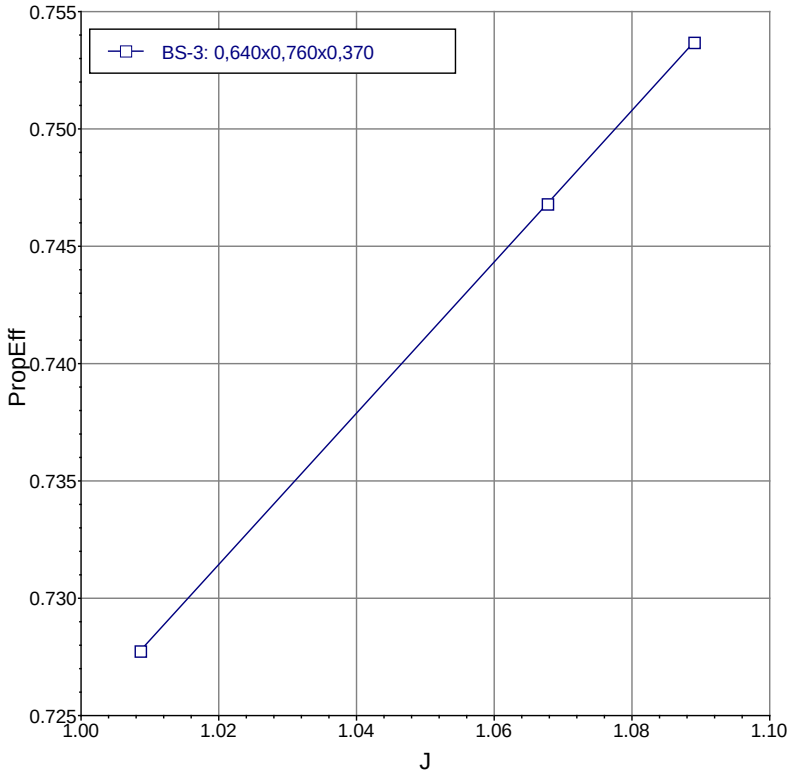

Figure 4.8 - Efficiency in function of the advance coefficient for the Hidrocat optimized propeller

4.4. Downscaling of the optimal full scale propeller for use in the simulator

The propellers used on the scale model were found on the radio-control model market since manufacturing tailor-made ones would have resulted too costly and time consuming. They were picked after browsing radio control equipment catalogues based on power, speed and pitch parameters. The selected propellers come from the Graupner range and have 65 mm diameter which is approximately in-line with the optimized full scale propeller, taking into account the scale factor. The propellers have opposite pitches as one of the propellers is rotating clockwise and the other counter clockwise

Figure 4.9 - Propeller used on the Hidrocat 1:8 scale model

However, for the computer-based simulator, the characteristics of the propellers are based on the optimized ones. The thrust coefficient Kt and torque coefficient Kq are non-dimensional. The parameter that will change is the advance coefficient J since it is dependent upon the advance speed, the RPM and the diameter of the scale model propeller.

$$J = V_a / (n.D) \qquad \text{(Eq. 4.4)}$$

In order to determine the advance speed from the model speed, the wake fraction of the model w_m is required. Kt and Kq are kept as such (see *figures 4.5* and *4.6* above) as the Reynolds number of the full scale Hidrocat and the scale model are close [38].

Since the flow around the ship is turbulent and the flow around the model is laminar, it is not possible to use the ITTC statistical formula to determine w_m. Other alternatives exist, such as using formulae based on the width of the flow in the wake and the velocity profile in this area. However, NavCad does not provide this data and it was consequently not possible to carry out accurate calculations of the model wake fraction. As a result, the wake fraction that will be selected for further use, e.i. in the propulsion system simulator, is the same as the ship wake fraction in [2], that is $w_m = w_s = 0.2$.

Chapter V - Propulsion system description

5.1. Process description

The first step prior to dimensioning the various components of the propulsion system of the Hidrocat scale model is the determination of its hull resistance. The necessary force to overcome the hull resistance up to a preliminarily set speed will define the required motor power. Subsequently and in accordance with the operation scheme of the scale model, battery capacity and fuel cell and photovoltaic panel power can be calculated.

5.2. Calculation of the Hidrocat scale model hull resistance

The full scale Hidrocat hull resistance data calculated by way of specific catamaran resistance prediction software has been provided by Pr. Fonseca [2]. The difference between hydrodynamic resistance and total resistance lies in the wind resistance. See table below:

Table 5.1 - Full scale Hidrocat hull resistance

Speed	***Hydrodynamic Resistance***	***Total Resistance***
[knots]	***Rh [N]***	***Rt [N]***
1	19.49	21.02
2	81.13	87.24
3	168.91	182.67
4	295.61	320.08
5	479.16	517.40
6	655.85	710.91
7	1 076.15	1 151.09
8	1 181.41	1 279.30
9	1 863.36	1 987.25
10	2 568.69	2 721.64
11	3 281.08	3 466.15
12	3 710.48	3 930.73

All formulae used in the below process were found in [38]

In order to obtain the resistance of the model, the speed has been scaled down to find the equivalent model speed and various parameters have been calculated for the ship and then converted into model parameters as follow (for fresh water at 15ºC):

$$V_m = \frac{V_s}{\sqrt{\alpha}} \qquad \text{(Eq. 5.1)}$$

- Ship Total Resistance Coefficient C_{Ts} :

$$C_{Ts} = \frac{R_{Ts}}{(0.5 \times \rho_{SW} \times V_S^2 \times A_W)} \quad \text{(Eq. 5.2)}$$

- Ship Frictional Resistance Coefficient C_{Fs} :

$$C_{Fs} = \frac{0.075}{[\log(\mathrm{Re}_s \times 10^8) - 2]^2} \quad \text{(Eq. 5.3)}$$

- Wave Resistance Coefficient C_{Ws} (where R_{Ws} was known from the ship resistance computation):

$$C_{Ws} = \frac{R_{Ws}}{(0.5 \times \rho_{FW} \times V_S^2 \times A_W)} \quad \text{(Eq. 5.4)}$$

- Correlation Coefficient Ca, using the Holtrop formula:

$$Ca = 0.006 \times (LWL + 100)^{-0.16} - 0.00205 \quad \text{(Eq. 5.5)}$$

- Form factor *(1+k)* = 1.151 determined by finding out the ordinate at x = 0 of the $\frac{C_{Ts}}{C_{Fs}} = fn\ (\frac{Fn^4}{C_{Fs}})$ curve.

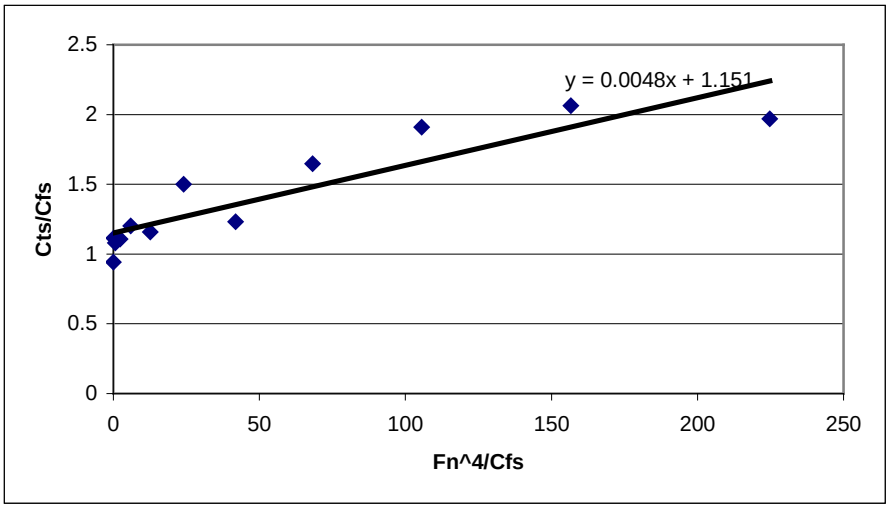

Figure 5.1 - $\frac{C_{Ts}}{C_{Fs}} = fn\ (\frac{Fn^4}{C_{Fs}})$ *for determination of the form factor.*

- Model Reynolds Number Re_s :

$$\mathrm{Re}_m = \frac{V_m \times LWL_m}{\nu_{FW}} \qquad \text{(Eq. 5.6)}$$

- Model Frictional Resistance Coefficient C_{Fm}:

$$C_{Fm} = \frac{0.075}{[\log(\mathrm{Re}_m \times 10^8) - 2]^2} \qquad \text{(Eq. 5.7)}$$

- Model Total Resistance Coefficient C_{Tm} (where $C_{Wm} = C_{Ws}$):

$$C_{Tm} = (1+k) \times C_{Fm} + C_{Wm} + Ca \qquad \text{(Eq. 5.8)}$$

- Model Total Resistance R_{Tm} :

$$R_{Tm} = C_{Tm} \times (0.5 \times \rho_{FW} \times V_m{}^2 \times A_W) \qquad \text{(Eq. 5.9)}$$

- Model Effective Power P_{Em} :

$$P_{Em} = R_{Tm} \times V_m \qquad \text{(Eq. 5.10)}$$

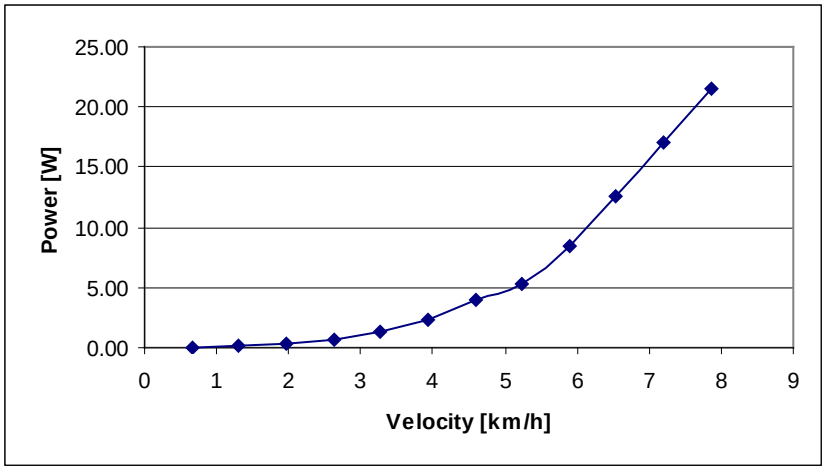

Figure 5.2 - Effective power versus Model velocity

The effective power will have to be incremented in function of the efficiency of the motors and propellers used.

5.3. Electric motors

5.3.1. Power

The maximum effective power required to reach the scale model top speed, i.e. 2.18 $m.s^{-1}$, is 21.6 W. However, this value does not account for the various efficiencies. A larger draft on the model in comparison with the full scale Hidrocat is also expectable since it will have to bear multiple monitoring instruments resulting in a surplus of weight.
Therefore, it is important to affect the effective power with the following coefficients:

- $\eta_{motor} = 70\%$ (data sheet)
- $\eta_{propeller} = 40\%$ (retailer estimate)
- *draft margin* = 30% (conservative margin)

Total required power = 110 W → Min. 55 W per motor

This figure may seem very distant from the original one but on the one hand it is important to guarantee that the top speed can be reached and on the other hand, the motor power consumption must be sufficient to create visible variations in the battery state of charge and to facilitate the monitoring of energy fluxes.

5.3.2. Technology

There are two basic technological options:

- Conventional DC brushed motors
- Brush-less DC motors (BLDC)

Seen the obvious technological advantage of BLDC motors over conventional brushed ones, both in terms of power/weight ratio and for their efficiency, it is highly probable that the full scale Hidrocat will be equipped with BLDC motors. It is also the trend of the market, as shown in the market study in *Chapter II - Electric Propulsion Boats Market Study*.
It makes then all sense to replicate the future choices on-board the scale model since the latter serves as a laboratory to experiment and validate technological choices before going full scale.
Below follow general considerations about this type of motors.

The Brushless DC (BLDC) motor is the ideal choice for applications that require high reliability, high efficiency, and high power-to-volume ratio. Generally speaking, a BLDC motor is considered to be a high performance motor that is capable of providing large amounts of torque over a vast speed range. BLDC motors are a derivative of the most commonly used DC motor,

the brushed DC motor, and they share the same torque and speed performance curve characteristics. The major difference between BLDC and brushed DC motors is the use of brushes. BLDC motors do not have brushes (hence the name "brushless DC") and must be electronically commutated [33].

A BLDC motor is highly reliable since it does not have any brushes to wear out and replace. When operated in rated conditions, the life expectancy of a BLDC motor is over 10,000 hours. Although a BLDC motor may cost more than a brushless motor, it will often more than pay for itself in the amount of work time saved [60].

In the present case, the motors were found in the “Model Motors AXI” range. Since the electrical circuit main voltage will be 12 V, the motors must be able to function with this voltage.
The model best approaching the power and voltage requirements is the Outrunner 2212/34 Gold Line.

Here are a few characteristics of this motor:

Table 5.2 - AXI 2212/34 Gold Line main characteristics

Max Voltage	V	16
RPM/V	-	710
Max. Efficiency	%	78
Max. Efficiency Current	A	4 - 8 (> 72 %)
Max. Power at 12 V	W	96
Current Capacity	A	10 (60 s)
Dimensions (Diam. x L)	mm	27.7 x 30
Weight with cables	g	57

Figure 5.3 - AXI 2212/34 Gold Line

5.4. Battery

5.4.1. Technology

As an introduction to the technological aspect of batteries, the below table exhibits the energy density of usual battery technologies:

Table 5.3 - Energy density of four different battery types [20b]; [42]

BatteryType	***Wh/kg***	***Wh/dm3***
Lead-acid	41	100
NiMH	95	300
NiCad	39	140
Lithium-ion	150 - 250	230

5.4.1.1. Lithium-ion

Today's state-of-the-art in batteries is the Lithium-ion (Li-ion) technology with the highest specific energy density available on the market. This technology also allows re-charge to 80% of the battery capacity in a short period of time. These batteries are widely used in mobile appliances and for more heavy duty applications such as electric or hybrid vehicles [20b]. The main drawbacks of Li-ion technology are its cost and specific charging process requiring accurate monitoring of the state of charge (SOC). This last requirement was prohibitive in the present case since no standard Li-ion battery charge controllers for use with PV panels are available on the market.

5.4.1.2. Nickel-metal hydrid

Nickel-metal hydrid (NiMH) is a common type of battery for portable appliances and in all-electric vehicles. Whilst this technology also attains high level of performance at a lower cost than the lithium-ion technology its energy density, is 1 to 2.5 times lower than the Li-ion battery. The NiMH charging process, such as the Li-ion one is complex and requires temperature or voltage monitoring. Hence this technology is unsuitable for the present application.

5.4.1.2. Lead-acid

Lead acid batteries are still the most common devices to store and deliver electricity in the range from 5V to 24V DC. A low price, high availability and ease of manufacture account for the wide use of the lead acid battery in many designs, sizes, and system voltages [42]. Despite having a very low energy density and a low energy-to-volume ratio, their ability to supply high surge currents means that the cells maintain a relatively large power-to-weight ratio [20b]. These features, along with their low cost, make them attractive for use in this scale model.

5.4.2. Capacity

The battery has two main functions within this electrical circuit:

- Guarantee a minimal autonomy according to the testing requirements
- Act as a buffer to supply power when the power sources are unable to meet the demand from the motors and to level current peaks

However, additional criteria are to be considered in order to dimension correctly the battery stack:

- The allowed discharge rate (C-rate)
- The duration of current peaks
- Depth of discharge

Depending on the battery technology, the allowed discharge rate, i.e. the maximum energy made available by the battery over a period of time may vary. Most lead-acid portable batteries have a discharge rate of 1 C meaning that if the battery capacity is 1000 mAh, at 1 C, the battery will supply 1000 mAh during 1 hour. At 0.5 C, it would supply 500 mAh during 2 hours and at 2 C, it would supply 2000 mAh during 30 minutes.
Nevertheless, even if the discharge rate given by the manufacturer may be in most cases 1 C, the battery is in fact capable of much quicker and non-damaging discharge if the latter does not last long enough to increase the battery temperature to unacceptable levels.

The cycle life of a sealed lead-acid battery is directly related to the discharge depth. The typical number of discharge/charge cycles at 25°C with respect to the depth of discharge is [39]:

- 150 - 200 cycles with 100% depth of discharge (full discharge)
- 400 - 500 cycles with 50% depth of discharge (partial discharge)
- 1000 and more cycles with 30% depth of discharge (shallow discharge)

In order to determine the required capacity, one can establish a minimal autonomy threshold to allow execution of tests and data acquisition with the scale model without any external source of power other than an initially charged battery.

For 1 hour operation at mid-power (55 W) with full discharge, the minimal battery capacity has to be:

$$Minimal\ Battery\ Capacity = \frac{Power}{Voltage} = 4.5\ \ Ah \qquad \text{(Eq. 5.11)}$$

This would require a discharge rate of 1 C which is acceptable for a sealed lead-acid battery.

As mentioned above, the battery stack will in fact not work as a sole power supplier. As exhibited in *Figure 5.10 - Propulsion system scheme*, the fuel cell and the photovoltaic panels are connected in parallel at the battery terminal. The battery becomes then a buffer when the demand from the motors exceeds the power supply from the two above mentioned power sources. The battery will also cut off damaging current peaks. While dwelling on float-charge, an external load can be connected to a lead-acid battery. In such a case, the battery acts as a buffer. During off-peak periods, the batteries get fully charged. On peak traffic times, the load exceeds the net supply provided by the rectifier (charger) and the battery supplies the extra energy. A car battery works in a similar way [39].

5.4.3. Charge

There are three stages in acid-lead battery charge:

- *Bulk charge* maintains a constant current as the battery voltage increases up to the point at which 'gassing' occurs − typically 14.4 volts. Above this voltage the electrolyte begins to break down into hydrogen and oxygen gases, causing loss of electrolyte. This varies according to the type of battery and is normally set by a switch by the user.
- *Absorption charge* maintains the voltage close to the gassing point, and the charge current drops off as the state of charge rises, until the battery is fully charged.
- *Float charge* keeps the battery topped up and compensates for the battery self-discharge. This float voltage is typically 13.5 V [20b].

5.5. Fuel cell

5.5.1. Definition

A fuel cell is an electrochemical cell that converts a source fuel into an electrical current, heat and reaction products. It generates electricity inside a cell through reactions between a fuel and an oxidant, triggered in the presence of an electrolyte. The reactants flow into the cell, and the reaction products flow out of it, while the electrolyte remains within it. Fuel cells can operate continuously as long as the necessary reactant and oxidant flows are maintained.
Fuel cells are different from conventional electrochemical cell batteries in that they consume reactant from an external source, which must be replenished – a thermodynamically open system. By contrast, batteries store electrical energy chemically and hence represent a thermodynamically closed system [14].

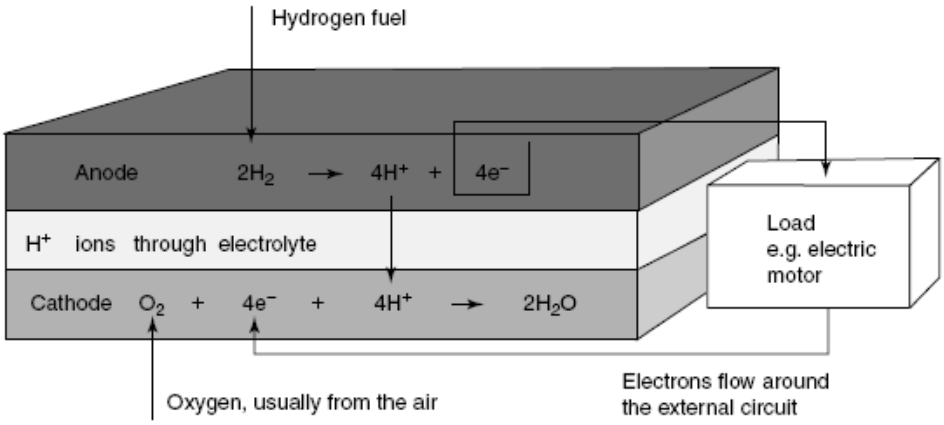

Figure 5.4 - Basic hydrogen fuel cell electro-chemical reaction scheme [14]

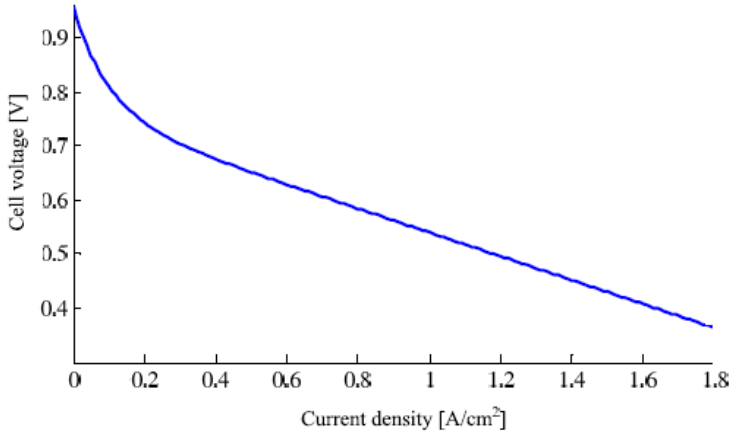

Figure 5.5 - Hydrogen fuel cell typical current-tension curve [34]

In the specific case of a hydrogen fuel cell, the work principle is rather simple and starts with the oxidation of hydrogen in presence of oxygen (*Eq. 5.12*). Hydrogen (in gaseous form) enters by the anode and air enters through the cathode where water is produced (see *Fig. 5.12*). Thanks to a polymer membrane, only protons (H^+) can reach the cathode side. Hence the name Proton Exchange Membrane (PEM) characterizes this type of fuel cells. This proton transfer drags some water. The electrons are exchanged by an external circuit and imply the circulation of an electrical current. The stack current I_{stack} (*Eq. 5.13*) is proportional to the hydrogen molar flow ($\dot{m}_{H_2}$) and the Faraday constant (F) [20a]; [58].

$$\begin{aligned} 2\mathrm{H_2} &\Rightarrow 4\mathrm{H^+} + 4\mathrm{e^-} \\ \mathrm{O_2} + 4\mathrm{H^+} + 4\mathrm{e^-} &\Rightarrow 2\mathrm{H_2O} \\ \hline 2\mathrm{H_2} + \mathrm{O_2} &\Rightarrow 2\mathrm{H_2O} \end{aligned} \qquad \text{(Eq. 5.12)}$$

$$I_{\mathrm{stack}} = \frac{\dot{m}_{\mathrm{H_2}} 2F}{N_{\mathrm{cell}} M_{\mathrm{H_2}}} \qquad \text{(Eq. 5.13)}$$

5.5.2. Fuel cell selection

The main criteria for fuel cell selection were:

- Compactness
- Lightweight
- High Efficiency
- Power output close to max. motor power

In order to meet the above requirements, a hydrogen fuel cell had to be selected since this technology is the most efficient available nowadays.
The Horizon H-100 Proton Exchange Membrane (PEM) hydrogen fuel cell has been chosen as it offers characteristics perfectly matching the above requirements.

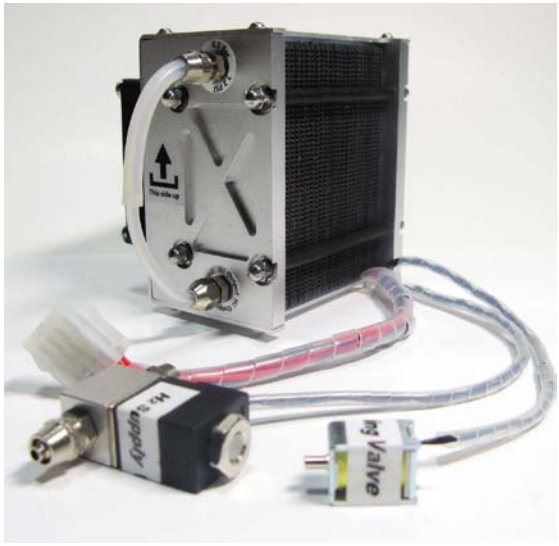

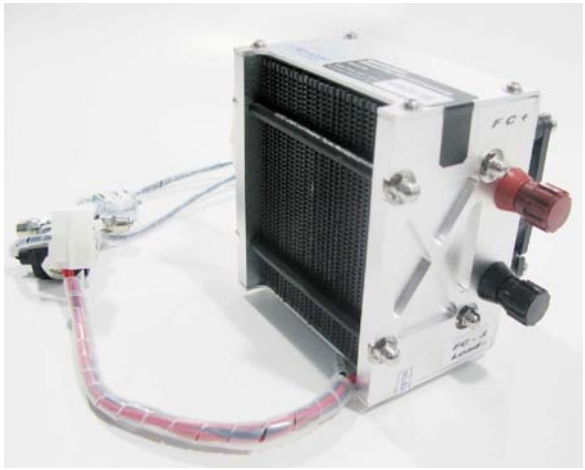

Figures 5.6 & 5.7 - Side views of the H-100 Horizon PEM hydrogen fuel cell

H-100 Horizon PEM hydrogen fuel cell main characteristics are exhibited in *Table 5.4*:

Table 5.4 - Horizon H-100 PEM hydrogen fuel cell main characteristics

Parameter	***Horizon H-100 PEM***	***Unit***
Type of fuel cell	PEM	
Number of cells	21	
Rated power	100	W
Rated performance	14 V@7.2 A	
Output voltage range	13 - 23	V
Weight (with fan & casing)	0.95	kg
Size	143 x 109 x 94	mm
Reactants	Hydrogen and air	
Rated H2 consumption	1.4	l/min
Hydrogen pressure	0.4-0.45	bar

Controller weight	0.4	kg
Hydrogen supply valve voltage	12	V
Purging valve voltage	12	V
Blower voltage	12	V
Ambient temperature	5-35	°C
Max stack temperature	65	°C
Hydrogen purity	99.999% dry H_2	
Humidification	Self-humidified	
Cooling	Air (integrated cooling fan)	
Start up time	Immediate	
Efficiency of system	40% @ 14 V	

5.5.3. Fuel storage capacity

The amount of hydrogen embarked is a determinant of the autonomy of the scale model. There are different ways of storing pure hydrogen [15]:

- Compressed hydrogen (usually ranging from 200 bars to 700 bars)
- Liquefaction
- Chemical absorption in metal hydrides

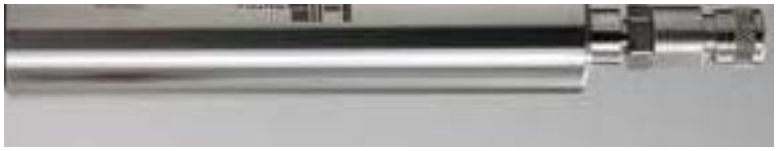

Figure 5.8 - H Bank Technology HB-SC-0050-Q 50 litre metal hydride hydrogen canister

Despite having the highest energy/weight ratio (120 MJ/kg or 33.3 kWh/kg - LHV) of all current fuels [20a], the main issue with hydrogen storage remains its poor energy/volume ratio (0.01005 MJ/l at atmospheric pressure - LHV) [20a]. See *Table 5.5* below:

Table 5.5 - Energy density of hydrogen in function of storage mode [40]

Form of Storage	***Energy density by weight*** [kWh/kg]	***Energy density by volume*** [kWh/l]
gas (20 MPa)	33.3	0.53
gas (24,8 MPa)	33.3	0.64
gas (30 MPa)	33.3	0.75
liquid (-253°C)	33.3	2.36
metal hydride	0.58	3.18

From the above table, it is obvious that for a small scale project like the present one, the only realistic way of storing hydrogen on board is using metal hydride canisters. In order to limit the weight of equipment on-board, 2 small 50 l canisters of 650 g. each were selected.

The model is HB-SC-0050-Q made by H Bank Technology Inc. (see *Figure 5.8*) and the specifications are shown in *Table 5.6*:

Table 5.6 - HB-SC-0050-Q Metal hydride canister main characteristics

Parameter	***HB-SC-0050-Q***	***Unit***
Hydrogen Storage Capacity	50 ± 5%	dm^3
Hydrogen Charge Pressure	25 - 35 (25ºC)	bar
Hydrogen Discharge Pressure	>1 to ≤10 (25ºC)	bar
Hydrogen Discharge Purity	≥ 99.9999	%
Hydrogen Discharge Flow Rate	≤ 0.2 (25ºC)	%
Environmental Temperature	50 - 60	ºC
Heat Exchange Method	Air Convection/Water Bath	
Dimension	32 (diameter) x 200 (length)	mm
Total Weight	< 650	g

The 2 metal hydride canisters contain together approximately 100 standard litres of hydrogen. The latter carry around 100 x 0.01005 MJ/l = 1.005 MJ = 0.2792 kWh (hydrogen LHV).
With a fuel cell efficiency of about 40%, this is equivalent to 0.1117 kWh usable to propel the model or recharge its battery. At 12 V, this is the equivalent of 9.3 Ah, i.e. twice the capacity of the battery. This means that, ideally, the fuel cell is able to recharge fully the battery 2 times with 100 litres of hydrogen stored in the two metal canisters.

5.6. Photovoltaic panels

Since solar radiation can be considered as “cost-free”, it should be used as much as materially possible to limit the use of other sources of energy. In this case, installing solar panels will allow energy consumption cuts from hydrogen canisters and pre-charged battery. The area occupied by photovoltaic panels on-board the Hidrocat scale model, just like on-board the full scale Hidrocat, is hence defined by the area available to host them and by weight limitation. The type of solar panels used for this application is regular photovoltaic array protected by a glass panel on one side and supported by a thick silicone-type film. There was space and weight allowance for 6 Solarex SX10M photovoltaic panels. Their characteristics are as follow:

Table 5.7 - Solarex SX10M photovoltaic panel main characteristics

Parameters	***Value***	***Unit***
At 1000 Wm-2 - 25ºC:		
P_{MAX}	10	W
V_{OC}	21.0	V
I_{SC}	0.65	A
V_{PMAX}	16.8	V
I_{PMAX}	0.59	A
At 800 Wm-2 - 47ºC:		
P_{MAX}	7.1	W
I_{PMAX}	0.48	A

Those solar panels are connected in parallel to keep the voltage equal to the voltage of a single unit while the current is summed up.

5.7. Battery charge controller

The battery charge controller plays an essential role within this propulsion system. It regulates the energy coming from the PV panels and the fuel cell in accordance with the battery SOC, the power drawn from the battery by the motors.

For an optimal energy management, the ideal solution would have been to work with a tailor-made system, including an independent battery SOC-meter and two charge controllers, one of them optimized for photovoltaic panels and the other for the fuel cell. However this development being beyond the scope of the present project, decision was made to implement an existing battery charge controller designed for solar panels. The main function of the latter is to lower the input voltage (coming in principle from the solar panels) to an acceptable level in order to optimize the battery charging. In fact, this voltage threshold and the output current vary according to the battery SOC. The battery charge controller monitors the SOC (or in this case, the apparent SOC since the battery is used as a buffer) and adapts its output accordingly always aiming at an optimal, hence as fast as possible, charge of the battery.
The selected model is a Solara® SR170CX.

Table 5.8 - Solara® SR170CX battery charge controller main characteristics

Parameters	***Value***	***Unit***
Nominal Voltage	12	V
Absorption Voltage	14.4	V
Bulk Voltage	14.8	V
Float Voltage	13.7	V
Input Voltage Cut	11.0 - 12.2	V
Load Re-connect Voltage	12.8	V
Max PV panel Current	10 (25ºC)	A
Environmental Temperature	-25 to 50	ºC
Self-Consumption	6	mA
Dimension	92 x 93 x 38	mm
Total Weight	175	g

Figure 5.9 - Solara® SR170CX battery charge controller

5.8. Radio Control Equipment

The radio control equipment is regular R/C model gear with one channel for each motor and one for the steering gear. Each motor is controlled by an independent speed controller with opposite connection schemes in order to make the motors rotate in opposite directions (since the propellers are inverted in order to avoid a natural sway motion.

- R/C emitter-receiver: Futaba FF6 2.4 GHz (6 channels)
- BLDC Motor speed controllers (x2): Graupner 7221 25A/h
- Servos (x2): HS81 3 kg

It is important to note that the receiver and the servos are fed by an independent 4.8 V 2000 mAh NiMH battery and hence are not using power from the main circuit.

5.9. Complete propulsion system

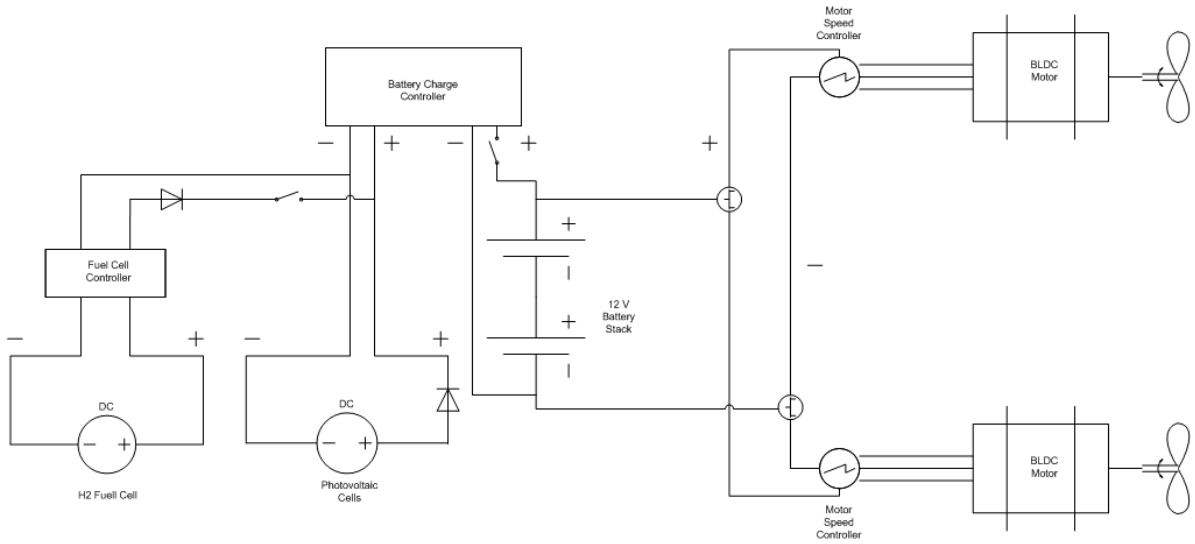

Figure 5.10 - Propulsion system scheme

The electrical circuit main voltage is 12V. This choice is dictated by the abundance of components available on the market for this generalized voltage.

On the left lower side of the above schematic are represented the FC and the PV. The fuel cell power terminals are connected to the FC controller and the latter is connected to the battery charge controller in parallel with the PV terminals. In order to prevent potentially damaging reversed currents flowing from the PV to the fuel cell and vice versa, diodes (up to 6 A maximum current) are mounted in series on the positive polarity cable of both components. According to the manufacturer recommendations, the FC shall not be connected to an electrical load at start up and shut down, therefore, a switch allows disconnection of the FC during these phases. The battery charge controller is connected to the battery terminal. The battery stack is composed of two 6 V batteries connected in series. This choice was dictated by data acquisition board voltage limitation (max. 10 V). This way, the battery voltage is split in two and monitored voltages shall never exceed 7 V. A switch between the battery stack and the battery charge controller enables battery disconnection when not in use to avoid accelerated self discharge (when the FC and PV are not supplying power, the battery charge controller voltmeter and LCD screens are fed by the battery).

The motor speed controllers are connected in parallel with the battery stack and to one BLDC motor each through three wires. They are controlled independently by radio via a multi-channel receiver.

5.10. Energy balance assessment

The below table exhibits the theoretical autonomy of the propulsion system in various operational conditions. It is based on the theoretical efficiencies and consumptions. For the FC, it accounts for the total amount of energy contained in the embarked hydrogen.

Table 5.9 - Propulsion system theoretical autonomy in various operational conditions

Motors	***Battery initial SOC***	***PV***	***FC***	***Autonomy at 100%***
100% = 110 Wh	100% = 54 Wh	100% = 60 Wh	100% = 111.6 Wh	3h 19 min
			0% = 0 Wh	1h 05 min
		50% = 30 Wh	100% = 111.6 Wh	2h 04 min
			0% = 0 Wh	40 min
		0% = 0 Wh	100% = 111.6 Wh	1h 30 min
			0% = 0 Wh	29 min
	50% = 27 Wh	100% = 60 Wh	100% = 111.6 Wh	2h 46 min
			0% = 0 Wh	32 min
		50% = 30 Wh	100% = 111.6 Wh	1h 44 min
			0% = 0 Wh	20 min
		0% = 0 Wh	100% = 111.6 Wh	1h 16 min
			0% = 0 Wh	15 min
	0% = 0 Wh	100% = 60 Wh	100% = 111.6 Wh	2h 14 min
			0% = 0 Wh	-
		50% = 30 Wh	100% = 111.6 Wh	1h 24 min
			0% = 0 Wh	-
		0% = 0 Wh	100% = 111.6 Wh	1h 01 min
			0% = 0 Wh	-
Motors	***Battery initial SOC***	***PV***	***FC***	***Autonomy at 50%***
50% = 55 Wh	100% = 54 Wh	100% = 60 Wh	100% = 111.6 Wh	Infinite
			0% = 0 Wh	Infinite
		50% = 30 Wh	100% = 111.6 Wh	6h 37 min
			0% = 0 Wh	2h 10 min
		0% = 0 Wh	100% = 111.6 Wh	3h 01 min
			0% = 0 Wh	59 min
	50% = 27 Wh	100% = 60 Wh	100% = 111.6 Wh	Infinite
			0% = 0 Wh	Infinite
		50% = 30 Wh	100% = 111.6 Wh	5h 33 min
			0% = 0 Wh	1h 05 min
		0% = 0 Wh	100% = 111.6 Wh	2h 31 min
			0% = 0 Wh	29 min
	0% = 0 Wh	100% = 60 Wh	100% = 111.6 Wh	Infinite
			0% = 0 Wh	Infinite
		50% = 30 Wh	100% = 111.6 Wh	4h 28 min
			0% = 0 Wh	-
		0% = 0 Wh	100% = 111.6 Wh	2h 02min
			0% = 0 Wh	-

5.11. Sankey diagram of the complete propulsion system efficiency

Sankey diagrams are a specific type of flow diagram, in which the width of the arrows is shown proportionally to the flow quantity. They are particularly suitable to illustrate the efficiency of a system or process.

Beckhaus P. *et al.* (2005) [7] provide an example of a Sankey diagram of an LPG fuel cell installed on board a sailing yacht. They do not include the propulsive part in the power balance though.

The Sankey diagram of the complete propulsion system is depicted in *Figure 5.11* below.

Table 5.10 - Parameters used for the Sankey diagram of the complete propulsion system

Location	Lisbon (38º N)
Month	July
Time	13:00
Temperature	30ºC
Relative Humidity	50%
Sky Conditions	Clear
Solar Radiation	900 W. m^{-2}
PV Area	0.6 m^2
PV Efficiency η_{PV}	10%
FC Voltage	14.8 V
FC Efficiency η_{FC}	38%
DC Motor Efficiency η_{MOTOR}	70%
PV Efficiency $\eta_{PROPELLER}$	40%
PV Efficiency $\eta_{TRANSMISSION}$	98%

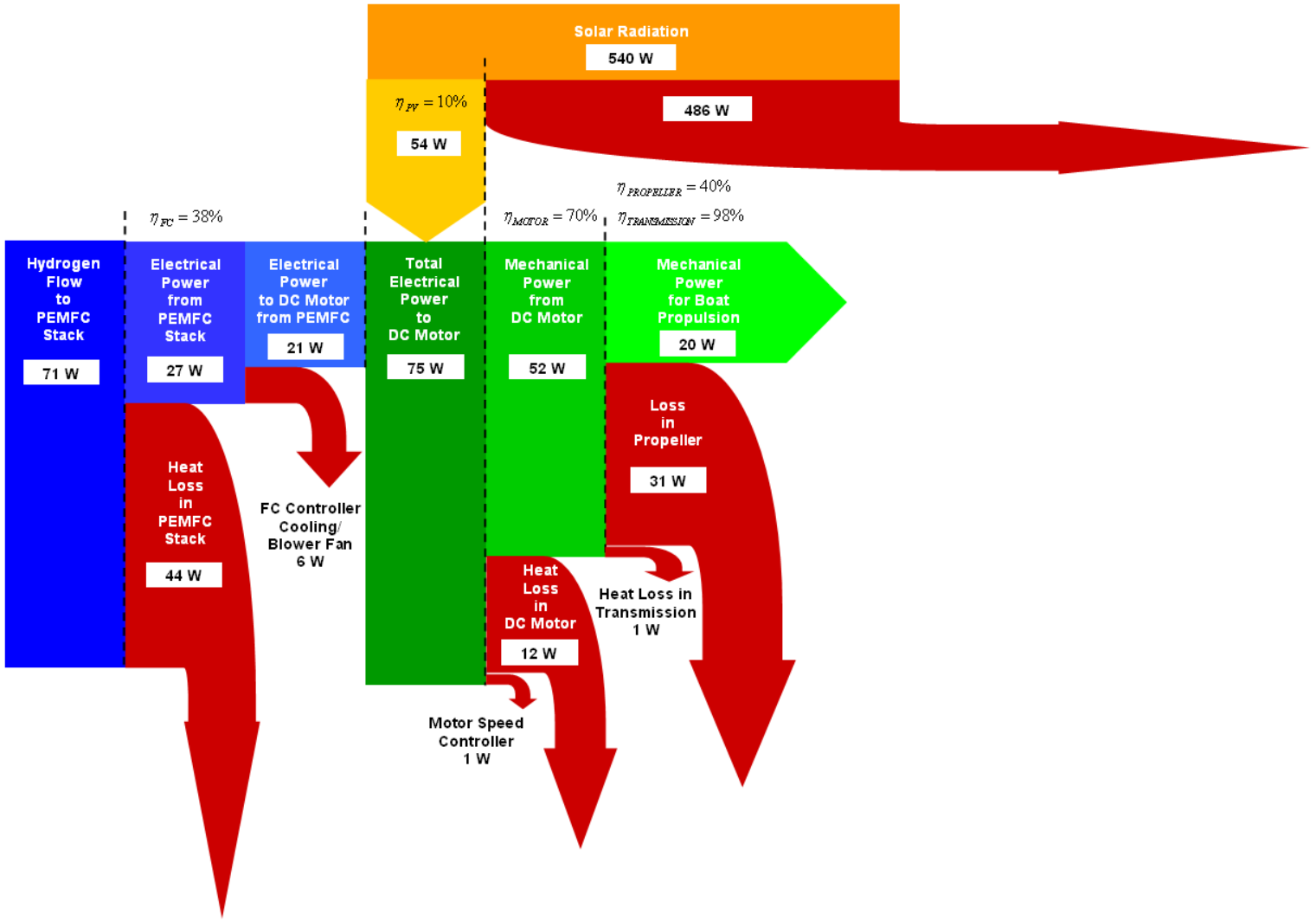

Figure 5.11 - Sankey diagram of the complete propulsion system efficiency

Chapter VI - Propulsion system component testing in laboratory

6.1. Introduction

The entire propulsion system and its components are described in *Chapter V - Propulsion System Description* where the manufacturer data is exhibited for each of the main components. However, in order to be able to correctly model the propulsion system and foresee the actual energy consumption / production, it is important to carry out meticulous laboratory testing and characterization of the main components as their output and characteristic curves may sometimes substantially differ from theoretical data provided by the manufacturer. This chapter describes the testing procedures and results of the hydrogen fuel cell, photovoltaic panels and battery charge controller. It also covers the data acquisition topic.

6.2. Hydrogen fuel cell

6.2.1. Test description

The hydrogen fuel cell has been tested and characterized in different atmospheric conditions (different temperatures: 25ºC - 30ºC - 35ºC and RH: 25% - 50% - 85%) obtained with the system depicted in *Figure 6.2* by increasing the electrical load - with 30 seconds steps - in order to draw its characteristic current - voltage curve for each atmospheric condition.
As suggested in [16], the electrical load is made of pairs of light bulbs connected in parallel (see *Figure 6.1* below). The advantage of using light bulbs versus other electrical resistance is their electrical power dissipation ability and the visual control they offer which is helpful at an experimental stage. The electrical load being made of pairs of 12 V bulbs in serial, it can withstand a voltage of about 24 - 26 V which is safe since the maximum voltage output given by the manufacturer is 23 V. The load is made as follows:

- (2 x 1.2 W)
- (2 x 3 W) x 2
- (2 x 5 W) x 17

Figure 6.1 - Electrical load used for fuel cell testing

6.2.2. Testing material

- Voltmeter (1): The FC voltage was measured at the electrical load terminals by means of a multimeter. Type: UNI-T UT60C - Reading definition: 0.01 V - Range: 0 - 20 V
- Ammeter (2): The current drained to the electrical load was measured by means of a Hall-effect ammeter (clamp meter). Type: British Standard Tester BS62 - Reading definition: 0.01 A Range: 0 - 20 A
- Hydrogen flow meter (3): The hydrogen inlet flow was controlled and measured by a gravitational flow meter. Type: Key Instruments, MR3000 3A01 - Reading definition: 0.125 Range: 0.1-1.2 l/min - Relative error: ± 4%
  Note: this flow meter needs to be calibrated for the appropriate fluid. See calibration for hydrogen in *Appendix 6.1 - Flow meter calibration for hydrogen*.
- Stove (4): To achieve the desired temperatures and humidity levels, a stove was used to insulate the testing environment from the outside atmosphere. Temperature thresholds were reached by using the resistance heater of the stove.
- Humidifier (5): Humidification was realized by adjusting an air flow passing through water and spreading water micro-droplets into the environment. When combined with higher temperatures, this technique did not suffice and was then combined with humidified foam.
- Thermometer - Hygrometer (6): Temperature and RH were constantly monitored with a thermo and hygrometer linked to a climate probe enclosed inside the stove. The temperature was punctually double checked using a traditional mercury-like thermometer located inside the stove. Type: Rotronic HygroLog-D - Reading definition: 0.1ºC & 0.1% RH
- Gas detector (7): Potential hydrogen leaks were monitored using a gas detector Testo 316-1. Accuracy: > 200 ppm

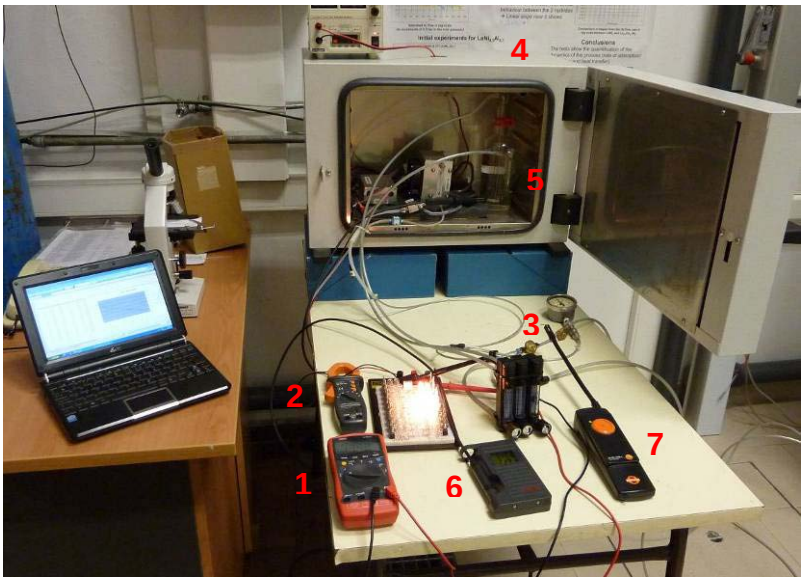

Figure 6.2 - Fuel cell testing equipment

Since both the temperature and the humidity are perturbed by the fuel cell itself and the thermal inertia of the stove, tests in each of the 9 conditions were to be carried out quickly to avoid to wide variations. For all tests, a variation of +/- 1ºC around the target temperature was observed and +/- 1% RH for 25% and 50% RH and +/- 2% for 85% RH.
The perturbations are due to important heat and water vapour release by the FC at high power rates. These phenomena can be compensated by reacting quickly on the humidifier flow-meter as well as on another room temperature air inlet flow meter.
Obviously, the daily atmospheric conditions had also a strong influence and the test campaign had to be split since the first day was too dry to achieve 85% RH.
When a fuel cell is tested at different moments in time, it is important to ensure that its output remains even since a non-operated fuel cell tends to see its output drop over time. Consequently, the fuel cell was operated for some time until it reached the same open circuit voltage as previously prior to launching the second test campaign at higher relative humidity.
No change in cell behaviour was noticed due to previous tests i.e. consistent output in the same testing conditions.

6.2.3. Efficiency calculation

In order to calculate the overall efficiency of the fuel cell, a simple yet accurate and reliable method was used. The latter consists of comparing the energy absorbed, the input energy, and the electrical energy produced, the output energy.
The below expression compares the energy contained in the hydrogen consumed by the fuel cell with the electrical power produced, this energy is taken instantaneously, i.e., independently of the time, it can be considered as power.

$$Overall\ Efficiency_{FuelCell}\ [\%] = \frac{Electrical\ Output\ [W]}{Energy/\mathrm{s}\ [Js^{-1}]} \qquad \text{(Eq. 6.1)}$$

$$Energy/s\ [J.s^{-1}] = \frac{H_2 Flow\ [mole.\min^{-1}]}{60} \times H_2 LHV[kJ.mole^{-1}] \times 10^3 \qquad \text{(Eq. 6.2)}$$

Hydrogen LHV, assuming the water vapour remains in this state = 241.8 kJ.mole^{-1}

$$H_2 Flow\ [mole.\min^{-1}] = H_2 Flow\ [l.\min^{-1}] \times n\ [mole.l^{-1}] \qquad \text{(Eq. 6.3)}$$

Using the ideal gas law to find the number of moles per litre:

$$pV = nRT \qquad \text{(Eq. 6.4)}$$

p = 101 325 Pa (atmospheric pressure) + 45 000 Pa (H_2 inlet pressure) = 146 325 Pa

V = 1 dm^3

R = 8.314472 $J.K^{-1}.mol^{-1}$

T = 293.15 K (Room temperature)

→ n = 0.060033541 moles

6.2.4. Testing results

As an example, in *Table 6.1* hereinunder are exhibited the measurements and calculations of the 30ºC - 85% RH test:

Table 6.1 - Fuel cell test result at 30ºC - 85% RH

Load	***Voltage***	***Current***	***Power***	***H2 Flow***	***H2 Flow***	***H2 Purge***	***Energy/sec***	***Efficiency***
[W]	***[V]***	***[A]***	***[W]***	***[l/min]***	***[mole/min]***	***[mole/min]***	***[J/s]***	***[%]***
0	18.18	0.00	0.00	0.03	0.0017	0.0295	6.7693	0.00
2.4	17.50	0.14	2.45	0.03	0.0017	0.0294	6.7693	36.19
8.4	16.70	0.34	5.68	0.06	0.0037	0.0293	14.9689	37.93
14.4	16.25	0.53	8.61	0.10	0.0057	0.0292	23.1230	37.25
24.4	15.75	0.78	12.29	0.16	0.0098	0.0290	39.2949	31.26
34.4	15.45	1.00	15.45	0.20	0.0117	0.0288	47.3126	32.66
44.4	15.05	1.30	19.57	0.26	0.0157	0.0286	63.2116	30.95
54.4	14.80	1.56	23.09	0.33	0.0196	0.0284	78.9287	29.25
64.4	14.55	1.83	26.63	0.33	0.0196	0.0282	78.9287	33.73
74.4	14.30	2.08	29.74	0.39	0.0234	0.0281	94.4639	31.49
84.4	14.12	2.30	32.48	0.39	0.0234	0.0279	94.4639	34.38
94.4	13.93	2.55	35.52	0.45	0.0272	0.0277	109.8172	32.35
104.4	13.78	2.78	38.31	0.49	0.0291	0.0276	117.4256	32.62
114.4	13.61	2.98	40.56	0.52	0.0310	0.0274	124.9885	32.45
124.4	13.45	3.22	43.31	0.58	0.0347	0.0268	139.9780	30.94
134.4	13.27	3.46	45.91	0.64	0.0384	0.0260	154.7856	29.66
144.4	13.10	3.66	47.95	0.70	0.0420	0.0253	169.4112	28.30
154.4	12.90	3.92	50.57	0.76	0.0456	0.0244	183.8550	27.50
164.4	12.75	4.14	52.79	0.76	0.0456	0.0237	183.8550	28.71
174.4	12.60	4.33	54.56	0.76	0.0456	0.0230	183.8550	29.67
184.4	12.48	4.51	56.28	0.82	0.0492	0.0224	198.1169	28.41

Figure 6.3 below shows the voltage-current and power-current curves of the 30ºC - 85% RH test.

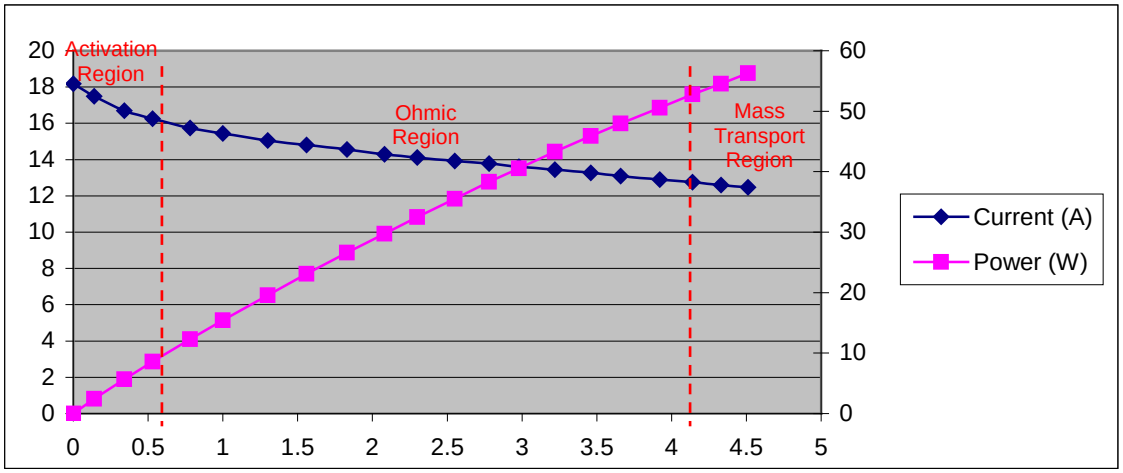

Figure 6.3 - FC voltage-current and power-current characteristic curves at 30ºC - 85% RH

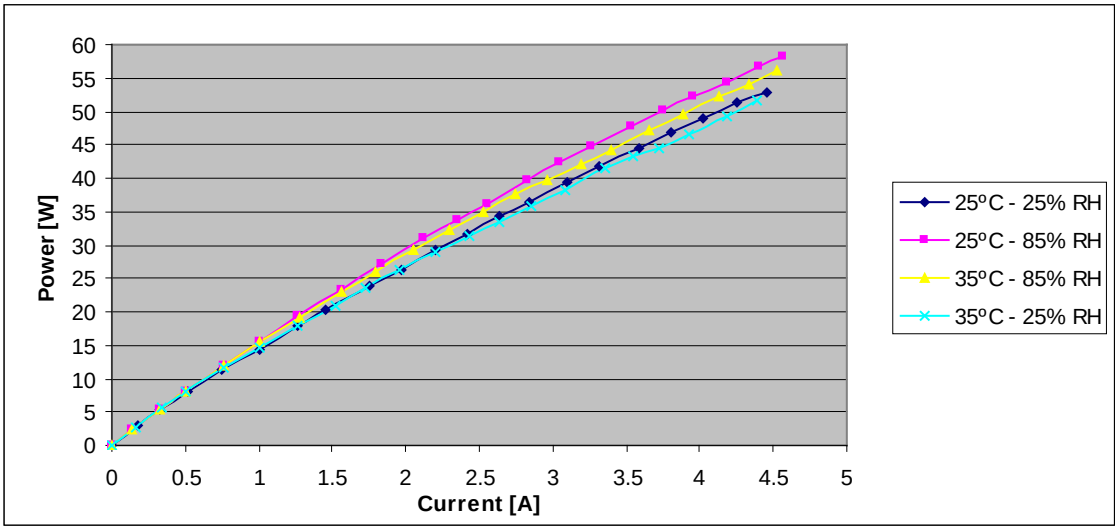

Figure 6.4 - Hydrogen fuel cell power-current curves for different temperatures and RH

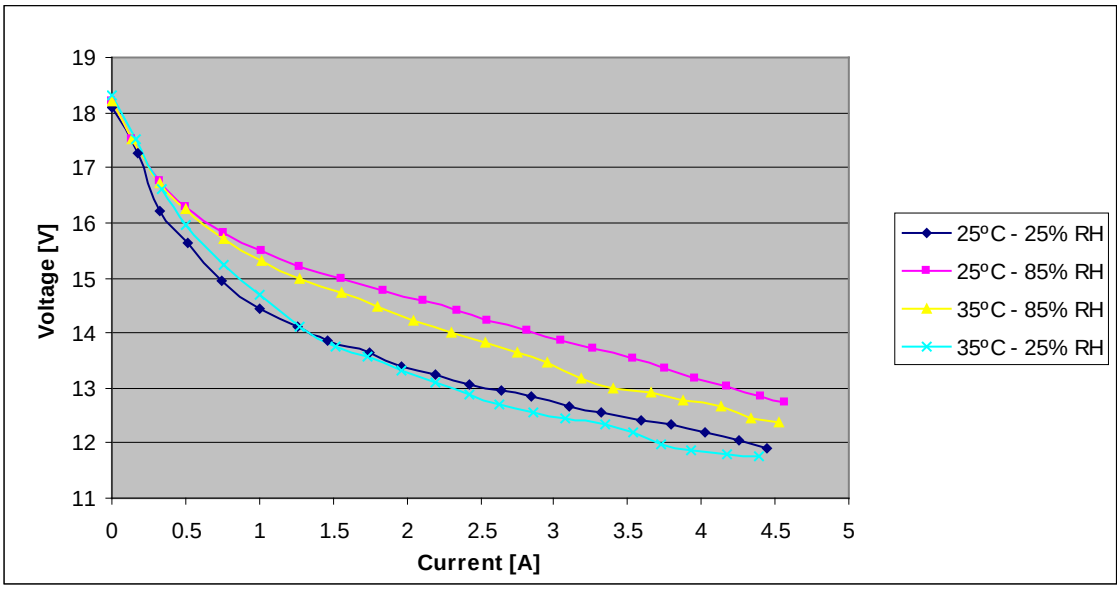

Figure 6.5 - Hydrogen fuel cell current-voltage curves for different temperatures and RH

6.2.5. Discussion

The hydrogen fuel cell test campaign allowed drawing current-voltage characteristic curves for 9 different atmospheric conditions. These curves will be implemented in the propulsion system simulator to model the fuel cell in different conditions of operation. They also highlight some behavioural trends. The most obvious output difference is due to humidity variation:

- Output difference due to HR variation from 25% to 85% @ 25ºC: 8.90%
- Output difference due to HR variation from 25% to 85% @ 30ºC: 8.15%
- Output difference due to HR variation from 25% to 85% @ 35ºC: 7.79%

The output variation due to temperature change is slighter:

- Output difference due to temp. variation from 25ºC to 35ºC @ 25% RH: - 2.51%
- Output difference due to temp. variation from 25ºC to 35ºC @ 50% RH: - 1.99%
- Output difference due to temp. variation from 25ºC to 35ºC @ 85% RH: - 3.68%

The fuel cell output increases with HR and decreases with temperature rise, all tests consistently confirm this behaviour.

6.3. Photovoltaic panels

Two samples of the 6 photovoltaic (PV) panels described in *Chapter V - Propulsion System Description* have been tested with a variable electrical load (same type as the one used for the fuel cell) in order to define its characteristic voltage-current curve.
The power output of a solar panel depends on the resistance of the electrical load to which it is connected. In an open circuit (OC) situation (infinite resistance) the voltage of the solar panel will be high, but no current will flow and therefore no power is generated. In a short circuit (SC) situation (zero resistance) current flows, but with zero voltage and so again no power is generated. These results all follow from Ohm's Law which gives the relationships between voltage, current, resistance, and power [23].

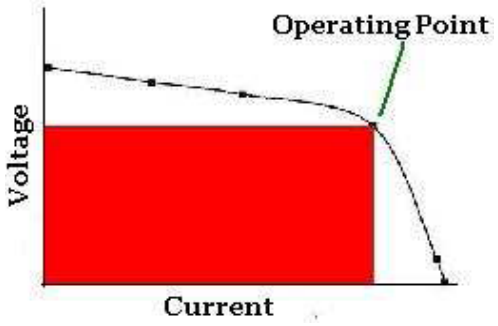

Figure 6.6 - Photovoltaic panel characteristic curve and typical operating point [24]

The curve depicted in *Figure 6.6* is typically of all PV panels. The operating point for the PV is the mid-point of the bend in the curve. This is the point at which the solar panel generates its peak power output. Since power is given by multiplying voltage and current, the rectangle with the largest area which can be drawn under the plotted curve has its upper right hand corner at the operating point. It is impossible to fit a rectangle with a larger area under the curve [24].

6.3.1. Test description

Two tests have been carried out in Lisbon (latitude 38º 43' N), at 1 PM on sunny and clear sky days:

- June 10 with approximately 50º tilt angle, panel facing South
- June 15 panel in horizontal position

The electrical load was made as follows:

- (2 x 1.2W) x 2
- (2 x 3 W) x 8

The test starts with open circuit to obtain the maximum voltage point. Progressively the pairs of bulbs are switched on until the light intensity diminishes dramatically. At this point and for a short instant a short circuit is made between the two solar panel terminals to obtain the current peak [25]. Two different panels have been tested 3 times each and in the 2 different testing conditions: optimal panel inclination (around 50º tilt angle) and horizontal panel (0º tilt angle). Variations in the results obtained from either panel were within the range of result variations obtained with the same panel along the 3 tests. Hence, it can be concluded that these results are reliable and that they may be extrapolated to the 6 panels composing the Hidrocat scale model solar energy system.

6.3.2. Testing material

The voltage and current were monitored and acquired continuously using a data acquisition board from National Instruments. See *6.5. Data acquisition equipment*

6.3.3. Results

The results exhibited below are an average of the total 6 tests carried out in each panel position. Odd coordinates, obviously due to measurement issues, have been removed intentionally. Solar radiation levels in Lisbon at that period of the year is estimated at 900 $W.m^2$ (see *Appendix 6.2 - Solar radiation in Lisbon [41]*)

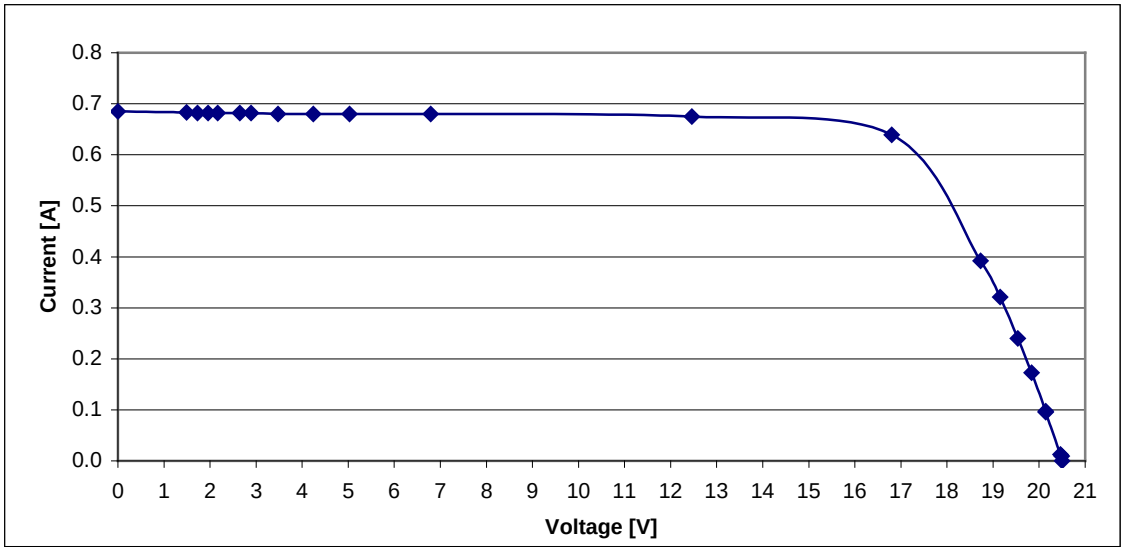

Figure 6.7 - Solarex SX10M PV panel current-voltage characteristic curve at 50º tilt angle

The maximum power obtained from this first test is 10.7 W (around 16 V) which is above the manufacturer data (10W). The open circuit voltage is 20.5 V and the short circuit current 0.685 A.

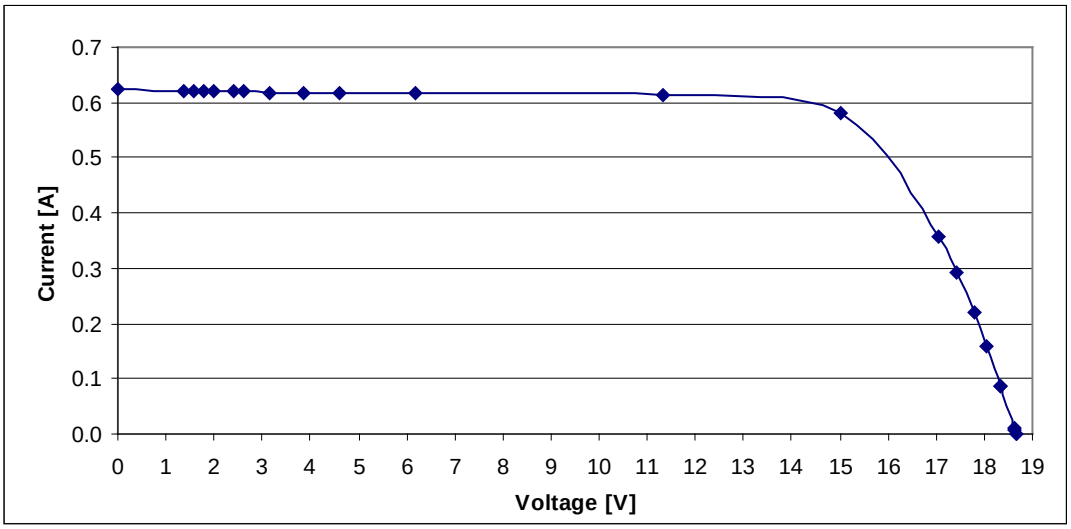

Figure 6.8 - Solarex SX10M PV panel current-voltage characteristic curve at 0º tilt angle

The maximum power obtained with the horizontal panel is 8.7 W (around 15 V).

6.4. Battery charge controller

The aim of the battery charge controller testing was to verify the manufacturer data as for voltage thresholds and to determine current intensities in function of the battery SOC. Different operation conditions were tested in order to characterize its behaviour and be able to model it.
The tests were carried out as follows: A 5 A max power supply was connected to the input terminals of the battery charge controller to simulate the power source - photovoltaic panels and/or fuel cell. At the output terminals was connected a sealed lead-acid 12 V 4.5 Ah battery.
Tests have been carried out with different initial battery states of charge. After each change in the battery charge status on the charge controller LCD screen, the battery was disconnected and left at rest for 10 minutes in order to let the SOC stabilize.
The material used to measure voltage and current was the same as in *6.2.2. Testing material*.

6.4.1. Test results

Table 6.2 - Solara SR170CX charge current and voltage thresholds

SR170CX Status	***Battery Stabilized Volt. [V]***	***Max Output Volt. [V]***	***Max Output Cur. [A]***
Low battery	< 11.60	14.8	5
< 10%	11.80 - 12.00	14.8	5
10% - 35%	12.00 - 12.30	14.8- 14.5	3 - 2.3
35% - 60%	12.30 - 12.60	14.3	0.9 - 0.5
60% - 80%	12.60 - 12.85	14.3	0.5 - 0.3
> 80%	> 12.85	13.9 - 13.6	0.25 - 0.15

Obviously, the output voltage is dependent on the input. The output can never outrange the input. Thus, the input voltage must be at least equal to the output voltages exhibited in *Table 6.2* to allow the battery charge regulator to work according to its specifications. The load connection voltage ranged from 12.82 V to 12.97 V input voltage.

6.5. Data acquisition equipment

6.5.1. Data acquisition board features

In order to keep records of measurements as well as to monitor the propulsion system remotely, a data acquisition board National Instrument NI USB 6211 in conjunction with the LabVIEW 8.5 software from National Instrument were utilized.

- Maximum voltage range: -10 V to 10 V
- Maximum voltage range accuracy: 2.69 mV
- Acquisition analogue channels: 8
- Resolution: 16 bits
- Sample rate: 250 kS/s

6.5.2. Overcoming the limitations

This type of data acquisition board is not designed for directly measuring currents and voltages are limited to +/- 10 V. Therefore, measurements had to be adapted to those limitations:

- Current: measured by means of calibrated cables, using Ohm's Law (see calibration in *Appendix 6.3 - Cable calibration for current measurement*)
- Fuel cell voltage: the total voltage was divided into 3 sub-voltages measured by groups of 7 cells (around 6 V each group in OC)
- Photovoltaic panels voltage: the total voltage was divided into 4 sub-voltages measured at both ends of each photovoltaic cell line (around 5 V each line in OC)
- Battery voltage: instead of using one single 12 V battery, a pair of 6 V batteries connected in series were used and voltage was sampled on one of them and doubled subsequently.

6.5.3. Examples of LabVIEW 8.5. data acquisition platform

For the complete propulsion system, the battery, PV panels and FC voltages and battery, PV panels, FC and motor currents (through calibrated cables) can be monitored in real time on the front panel of the data acquisition platform created in LabVIEW 8.5 (see *Figure 6.9* hereunder). This panel displays a meter, a numeric indicator and a graph for each measurement. The data is stored in an excel file.

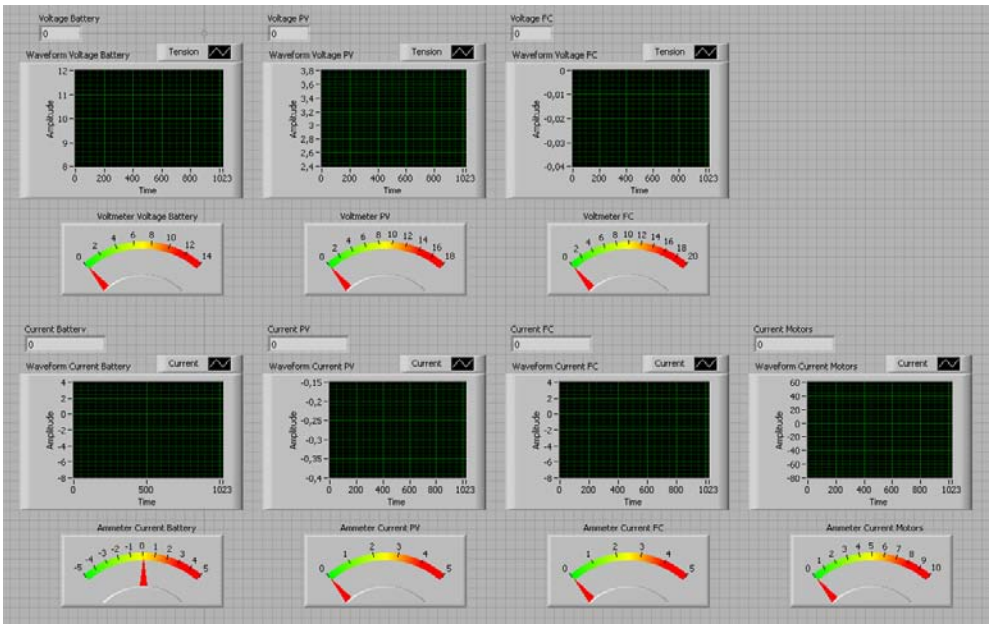

Figure 6.9 - Front panel of the data acquisition interface for the entire propulsion system.

For the PV panel characterization, the voltage of the 4 individual cell lines and the total current are monitored as shown in *Figure 6.10*.

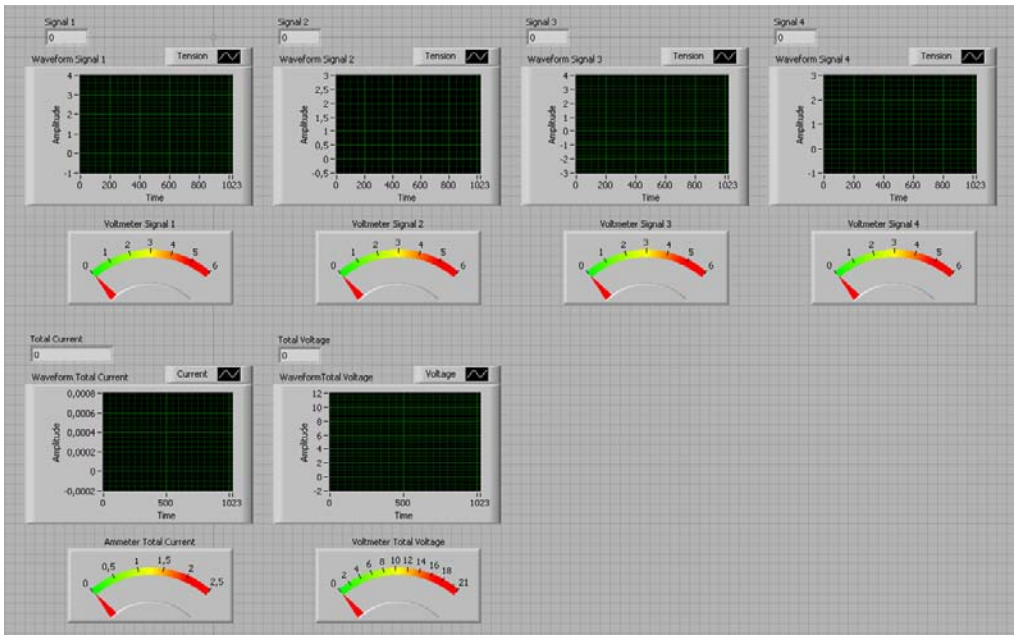

Figure 6.10 - Front panel of the data acquisition interface for a photovoltaic panel.

Chapter VII - Propulsion system modelling

7.1. Propulsion system model overview

A computer-based model of the Hidrocat scale model propulsion system has been designed in Matlab® Simulink®.
The aim of creating this model is to simulate the actual propulsion system with high fidelity and hence understand better how the propulsion system and its energy fluxes work.
This virtual model provides also a flexible environment for system fine tuning, optimization and validation as well as making autonomy prediction in function of the operation scheme and the environmental conditions.

Contrary to usual dynamic models of BLDC motor [32], lead acid battery [29], [30], PEM fuel cell [27], [28] or photovoltaic panels [31] that are very generic and offer tuning possibilities by adjusting various parameters, this model has been built based on experimental testing of the various components of the propulsion system. It is consequently expected to match actual working of each component even further since it is not based on actual testing results and not on theoretical data (except for the motor).

Those results have been implemented within the computer-based model using a Simulink® tool called “look-up tables” that allow the system to interpolate and extrapolate from experimental data. This way, the model also works dynamically but only using curves extracted from real life testing. The architecture of the model is also valid and will be applicable to the full scale Hidrocat propulsion system. Only the characteristic curves of the propulsion system components will have to be replaced by the relevant ones.

Each component is modelled individually in a so-called “block” and is connected to the others through the “In” and “Out” ports to form the complete model. Some blocks have specific parameters that can be adjusted by double clicking on it, e.g. the solar radiation for the PV or the relative humidity and temperature for the FC.

The principal input of the system is the boat “throttle” that is either a constant voltage level or an adjustable voltage profile. The outputs include among other values, the consumed current, produced power, battery SOC, motor RPM, boat speed. Some outputs are capital for the whole system to work as they are used as inputs in other blocks and other outputs are only informative and their signals are shown with scopes or displays.

The following sections describe each block individually and the complete model including all of them with all their inter-connections.

7.2. Motor

Inputs

- "In1" Motor Voltage [V]: the input voltage is the trigger of the entire circuit. Varying from 0 to 7 V, it determines the motor RPM through a theoretical voltage/rpm linear ratio given by the manufacturer.
- "In2" Required Torque [Nm]: this input is indirectly generated by the input Motor Voltage which is translated into RPM and then sent to the propulsion parameter blocks that will calculate the torque necessary to reach such rotation speed depending on hydrodynamic and propulsive characteristics. The Required Torque allows current calculation

Outputs

- "Out1" Motor Current [A]: the actual current consumed by one motor. It is the theoretical current increased by the motor efficiency. Together with the voltage, it determines the power consumption of the motor. This current is drained from the batteries.
- "Out2" Mechanical Power [W]: the actual shaft power for one motor. Calculated from the torque divided by rotations per second.
- "Out3" Electrical Power [W]: the electrical power consumed by one motor. It results from the product of the motor current and voltage.
- "Out4" Motor Efficiency [%]: varies according to the motor theoretical current following manufacturer data.
- "Out5" Motor RPM [min^{-1}]: this shaft rotation speed output is used to determine the required torque in the propulsion parameters block.

Block description

Due to the specific equipment required and the complexity of testing small BLDC motors, no actual tests have been carried out and this block is based on two characteristic curves provided by the manufacturer: RPM-Voltage and Current-Efficiency. This block models a single motor and its controller and is multiplied by 2 to account for the 2 motors outside the block.

In1 is restricted between 0 and 7 V since the motors are not supposed - for this application - to rotate faster than 5000 RPM. The input voltage is converted in RPM with a gain of 710 RPM/V. The Motor RPM is the output "Out2".
In1 is also used to determine the self consumption of the motor speed controller which varies with the speed of the motor and consequently the input voltage. This consumption is calculated through a linear relation Input Voltage-Consumed Current.

In2 is divided by 2 to account only for the torque of a single motor. The shaft applied torque = equivalent motor torque:

$$Motor\,Torque\ [Nm] = \frac{Power\,[W] \times 60}{RPM\ [\min^{-1}] \times 2 \times \Pi} \qquad \text{(Eq. 7.1)}$$

From the *Eq. 7.1,* the mechanical power is calculated and is the output “Out5”.
This mechanical power when divided by the voltage gives the ideal current (with an ideal efficiency of 100%). This ideal current is used in a loop to determine the motor efficiency (based on the manufacturer data). This loop iterates until equilibrium is reached and motor efficiency is determined (output “Out4”).

The ideal current, when divided by the efficiency gives the real motor current. The latter is summed up with the motor speed controller current consumption and gives the output “Out1”.

The electrical power is obtained from the product of the motor voltage and its real current (output “Out3”). The ratio between the mechanical power and the electrical power is the motor efficiency.

As opposed to a dynamic model, the present motor block does not simulate current peaks at motor start or when the shaft is blocked. However, since the motor shaft is linked to a small propeller, the current peaks at start are limited (very low friction in the transmission line and low torque from the propeller to overcome).

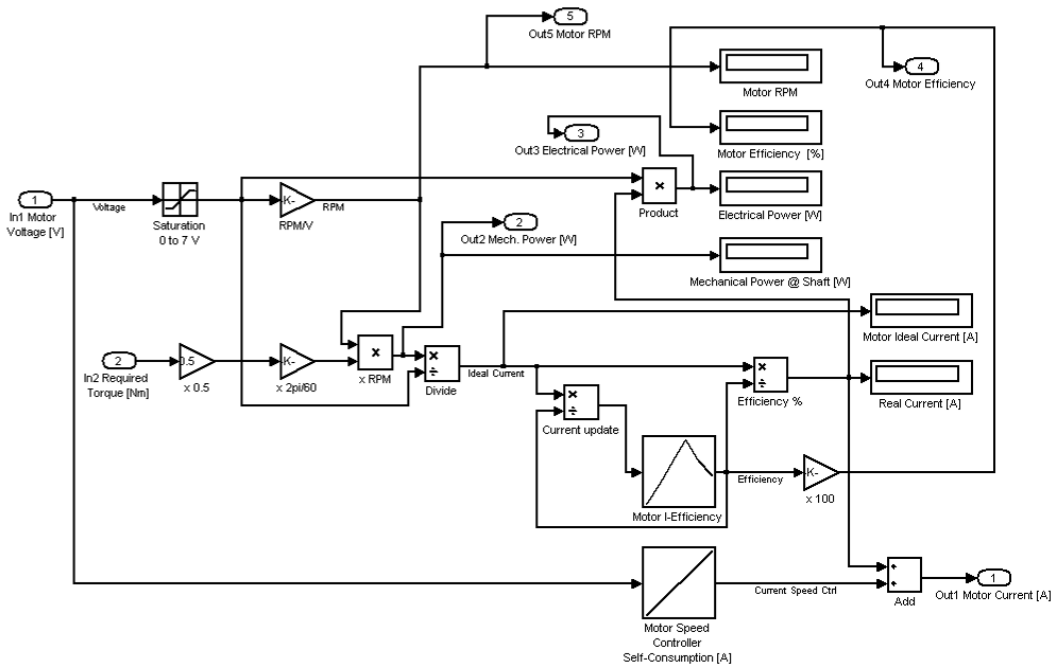

Figure 7.1 - BLDC motor block

7.3. Battery

M. Dürr et al. (2005) [42] developed a mathematical model describing accurately the behaviour of a lead acid battery under typical discharge conditions. However, it remains to be proven that the author's model is also valid for the charging cycle of a lead acid battery. Additionally this model is currently only valid for the specific battery tested. For the above reason, the coulometric equation used by Th. Latour (2008) [34] was preferred for its universal nature.

Inputs

- "In1" Current Drawn from Batteries [A]: current consumed by the motors and their speed controllers, the battery charge controller, the fuel cell controller and the fuel cell cooling fan.

Outputs

- "Out1" State of Charge [%]: SOC in percentage of the battery 4.5 Ah total capacity.
- "Out2" Battery Voltage [V]: Varying from 11.5 V to 13 V and proportional to the SOC.

Adjustable parameters

- Initial State of Charge [%]: the battery SOC at the beginning of the simulation, from 0 to 100 %.

Block description

The most common way to estimate the state of charge is the coulometric equation (*Eq. 7.2)*. It simply integrates the electrical current over the time of utilization. An initial SOC must be known.

$$SOC(t) = SOC_0 + \frac{1}{Q_{bat}} \int_{t_0}^{t} i_{bat}(t)dt \qquad \text{(Eq. 7.2)}$$

The battery block depicted in *Figure 7.2* is a simple translation of the E*q. 7.2*. The current drawn from the batteries (In1) is turned positive through a sign inverter and integrated over time of utilization resulting in the battery charging intensity in Coulombs (A.s). This electrical charge is divided by the battery capacity (Q_{bat}) in Ah and subtracted to the initial state of charge (SOC_0). The sign convention is that when the input current In1 is negative, current is drawn from the batteries and hence lowers the SOC. Contrarily, when positive, it recharges the battery and increases the SOC.

The SOC resulting from this subtraction/addition is kept between 0.01 and 1 by means of a saturation element and is multiplied by 100 to express it in percentage (Out1).

In order to obtain the battery voltage (Out2), the SOC is multiplied by 1.5 in order to represent the battery voltage variation (1.5 V amplitude) and is added to the minimum battery voltage 11.5 V.

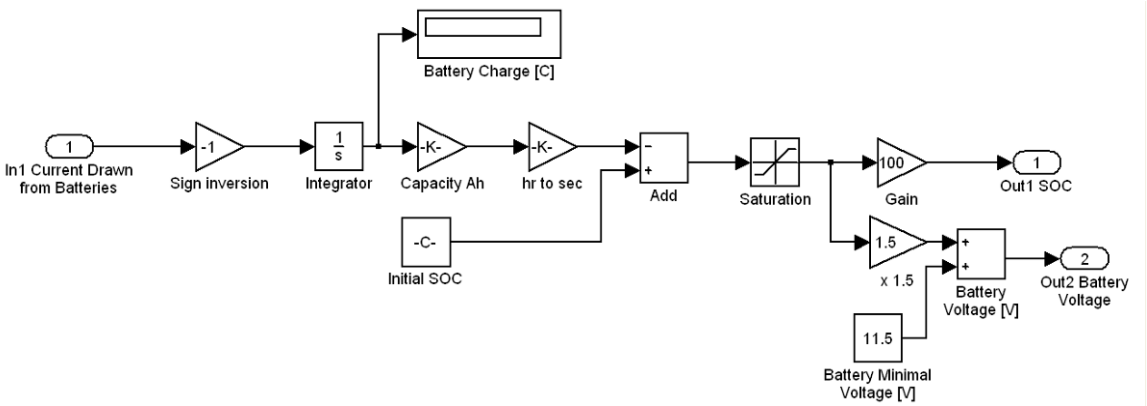

Figure 7.2 - Sealed lead-acid battery block

7.4. Fuel Cell

Inputs

- "In1" Voltage to Fuel Cell [V]: voltage coming from the battery charge controller. This voltage will define the current the fuel cell is able to produce depending on the atmospheric conditions.

Outputs

- "Out1" Fuel Cell Current [A]: current produced by the fuel cell.
- "Out2" Fuel Cell Power [W]: useful power produced by the fuel cell, i.e. the product of the fuel cell voltage and the fuel cell current.
- "Out3" Fuel Cell Controller Current [A]: current consumed by the fuel cell controller and cooling fan.

Adjustable parameters

- Temperature [ºC]: the output of the fuel cell as been sampled at 25, 30 and 35ºC. However, temperatures inside and outside this interval are also valid entries since the look up table interpolates and extrapolates linearly.
- Relative Humidity [%]: the output of the fuel cell as been sampled at 25, 50 and 85 % RH. However, RH inside and outside this interval are also valid entries since the look up table interpolates and extrapolates linearly.

Block description

The core of the fuel cell simulation model is the three-dimensional look up table that summarizes the results of the entire fuel cell testing campaign. This table is a 3 entry table (three types of breaking points): temperature, RH and voltage. The test results (an example is exhibited in *Table 6.1 - Fuel cell test result at 30ºC - 85% RH*) have been obtained by increasing progressively an electrical load. However, the increase steps in voltage and current were not even. For best efficiency, look-up table should have regular break points. Therefore, the test results have been standardized, implying pre-interpolation, to provide a current value for each increase of 0.5 V and in each of the 9 testing conditions.

In1 is the voltage level required by the battery charge controller. This voltage is incremented by 0.45 V that corresponds to the voltage drop induced by the inverted current protection diode.
In order to avoid negative currents, a saturation element is introduced and prevents from inputs higher than 18.3 V which is the tested voltage of open circuit (current is nil).

This voltage is one entry of the lookup table, the temperature and RH are the two others. The output of the lookup table is the corresponding current.

The consumption of the fan increases with a temperature rise (more cooling power required). This consumption in function of the temperature has also been determined during the test campaign and the results are used in a 1-D linear interpolation lookup table using the temperature as sole input.

This current is the output Out3. Both for practical reason and to match reality, it is assumed that the fuel cell output is neutral, i.e. that it always produces at least the current consumed by its controller.

Out2 informs about the power output of the fuel cell, hence it is the product of the current produced by the fuel cell and it voltage.

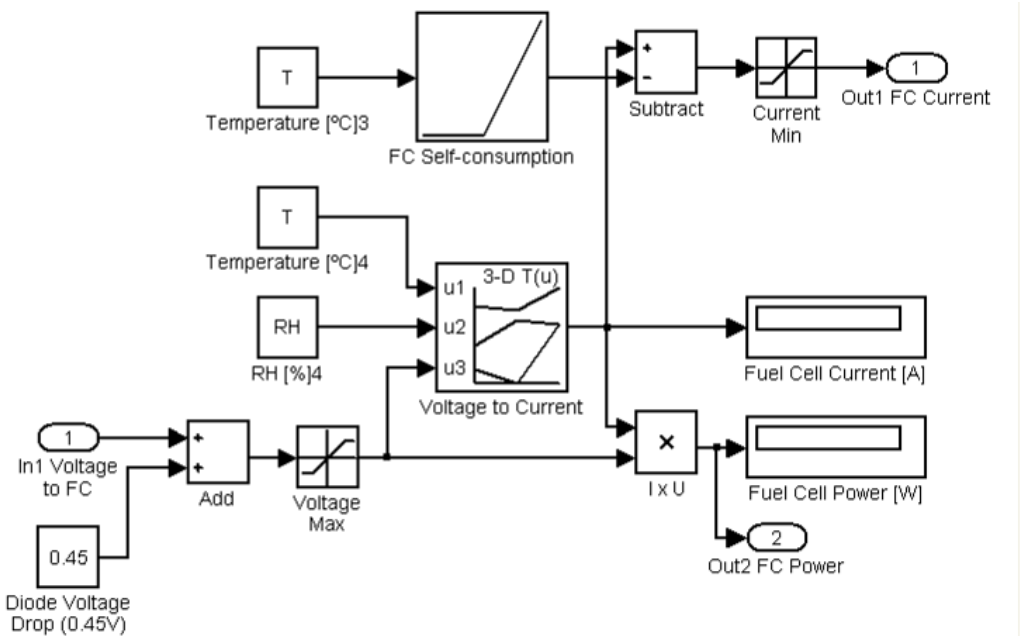

Figure 7.3 - PEM hydrogen fuel cell block

7.5. Photovoltaic panel

Inputs

- "In1" Voltage to Photovoltaic Panel [V]: voltage coming from the battery charge controller. This voltage will define the current the photovoltaic panel is able to produce depending on the solar radiation.

Outputs

- "Out1" Photovoltaic Panel Current [A]: current produced by the photovoltaic panel
- "Out2" Photovoltaic Panel Power [W]: power produced by the photovoltaic panel, i.e. the product of the fuel cell voltage and the fuel cell current.

Adjustable parameters

- Solar Radiation [$W.m^{-2}$]: Between 0 and 1000. The output of the PV panel has been tested (as described in *6.3.1. Test conditions*) for a radiation of 900 $W.m^{-2}$. Based on theoretical output current/solar radiation relation provided by the manufacturer, a linear relation was established between the solar radiation and the current produced under the form of a coefficient affecting the current value.

Block description

In1 is the voltage level required by the battery charge controller. This voltage is incremented by 0.45 V that corresponds to the voltage drop induced by the inverted current protection diode.
In order to avoid negative currents, a saturation element is introduced and prevents from inputs higher than 18.655 V which is the open circuit voltage (current is nil) measured while testing the PV. This voltage is the entry of the 1-D lookup table that performs linear interpolation of input values using the specified table. In Villalva M. *et al.* [31] propose to model and simulate PV panels by finding the parameters of the nonlinear I-V equation and adjusting the curve at three points: open circuit, maximum power, and short circuit. In this case, in order to match better the real output of the PV, the characteristic I-V curve has been found by experimentation and the data is used in the lookup table. Extrapolation is performed outside the table boundaries.
The current value from the lookup table is affected by a Solar Radiation Coefficient. Since the output of the PV panel has been tested (as described in *6.3.1. Test conditions*) for a radiation of 900 $W.m^{-2}$, this SR Coefficient is 1 for 900 $W.m^{-2}$ and varies linearly from 0 to 1.087 when SR varies from 0 to 1000 $W.m^{-2}$. The 6 PV panels being connected in parallel, the total current of the array is the sum of the currents produced by each PV panel individually, hence in this case the current from the lookup table affected by the SR coefficient is multiplied by 6 (Out1).

The product of the PV voltage and current the total electrical power produced by the 6 PV panels (Out2).

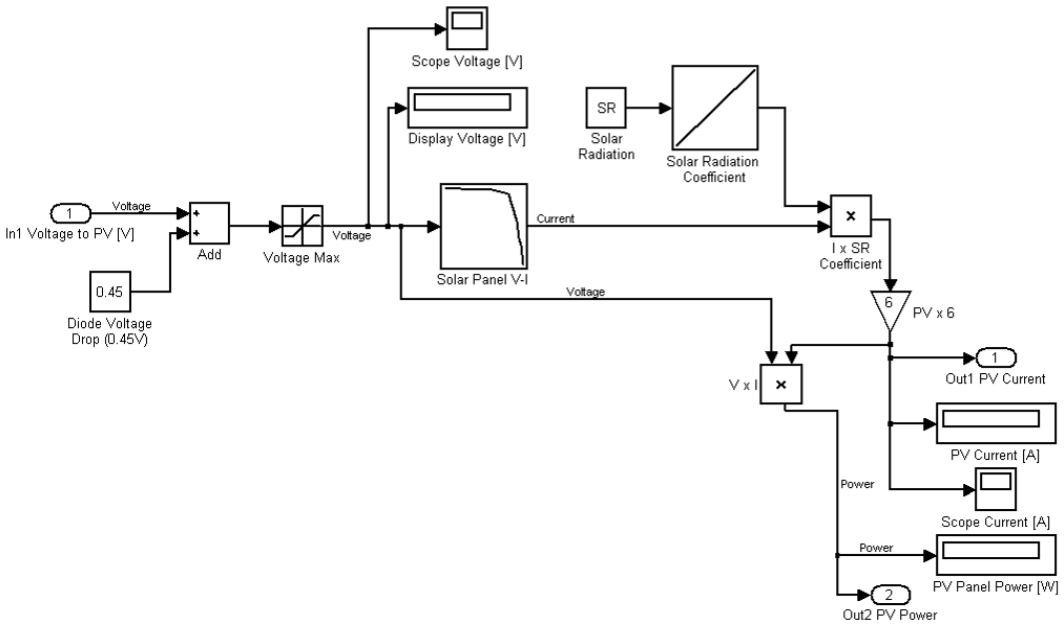

Figure 7.4 - Photovoltaic panel block

7.6. Battery charge controller

Inputs

- "In1" Fuel Cell Current [A]: equal to the fuel cell "Out1", i.e. current produced by the fuel cell.
- "In2" Photovoltaic Current [A]: equal to the photovoltaic panel "Out1", i.e. current produced by the 6 PV connected in parallel.
- "In3" Battery State Of Charge [%]: equal to the battery "Out1", i.e. the instantaneous battery SOC

Outputs

- "Out1" Fuel Cell Voltage [V]: the minimal voltage threshold the FC shall reach while current is drawn. This voltage defines the maximum current the FC can produce via the relevant current-voltage curve (determined by the atmospheric conditions).
- "Out2" Photovoltaic Voltage [V]: the minimal voltage threshold the PV shall reach while current is drawn. This voltage defines the maximum current the PV can produce via the relevant current-voltage curve (affected by a solar radiation coefficient).
- "Out3" Battery Current [A]: current produced by FC and PV available for battery charging or motor power supply.

Block description

B. J. Huang et al. (2010) [43] propose an improved charging control of lead-acid battery with PV panels based on a feedback control system for battery charging after the overcharge point. Nonetheless, this is beyond the scope of the present thesis and the simulation hereunder describes the behaviour of the Solara® SR170CX.

In1 and In2 do not really form part of this block. However, since FC and PV are materially connected together at the battery charge controller, it is logical to sum these currents up within this block. A saturation component ensures that the current always remains greater than zero.
The rest of the block is symmetric for both the PV and the FC. Consequently, only one branch will be herein described.

As explained in *5.7. Battery Charge Controller*, the battery charge controller adjusts its voltage output according to the battery SOC (by way of monitoring the battery voltage). Since this component can only limit a voltage to a maximum level (no lifting up), input voltage must be ≥ output voltage. There are 3 output voltage thresholds, as exhibited in *Table 6.2 - Solara SR170CX charge current and voltage thresholds* and these correspond to the minimum input voltages from the PV and FC. This behaviour is modelled by mean of a lookup table that outputs 3 different voltage thresholds in function of the battery SOC:

- 14.8 V: 0 - 35 % SOC
- 14.5 V: 35 - 80 % SOC
- 13.7 V: 80 - 100 % SOC

The SOC is used as an input of another lookup table whose function is to zero progressively the current produced by the FC and PV when the SOC reaches 98% (this value has been chosen arbitrarily) by way of increasing linearly the input voltage of the FC and PV to their OC voltages (FC: 18.3 V; PV: 18.655 V). The SOC is input to a relay that allows its output to switch between two specified values (in this case 0 and 1). When the relay is on, it remains on until the input drops below the value of the switch off point (98 % SOC) parameter. When the relay is off, it remains off until the input exceeds the value of the switch on point (100% SOC) parameter. The block accepts one input and generates one output. Voltage resulting from the SOC-voltage lookup table and voltage-to-zero FC and PV currents are connected to a two-way switch triggered by the relay output. When the SOC is below 98 %, the switch connects to the SOC-voltage lookup table and when greater 98 %, it connects to the voltage-to-zero-current lookup tables. The signals going through the switches are Out1 and Out2.

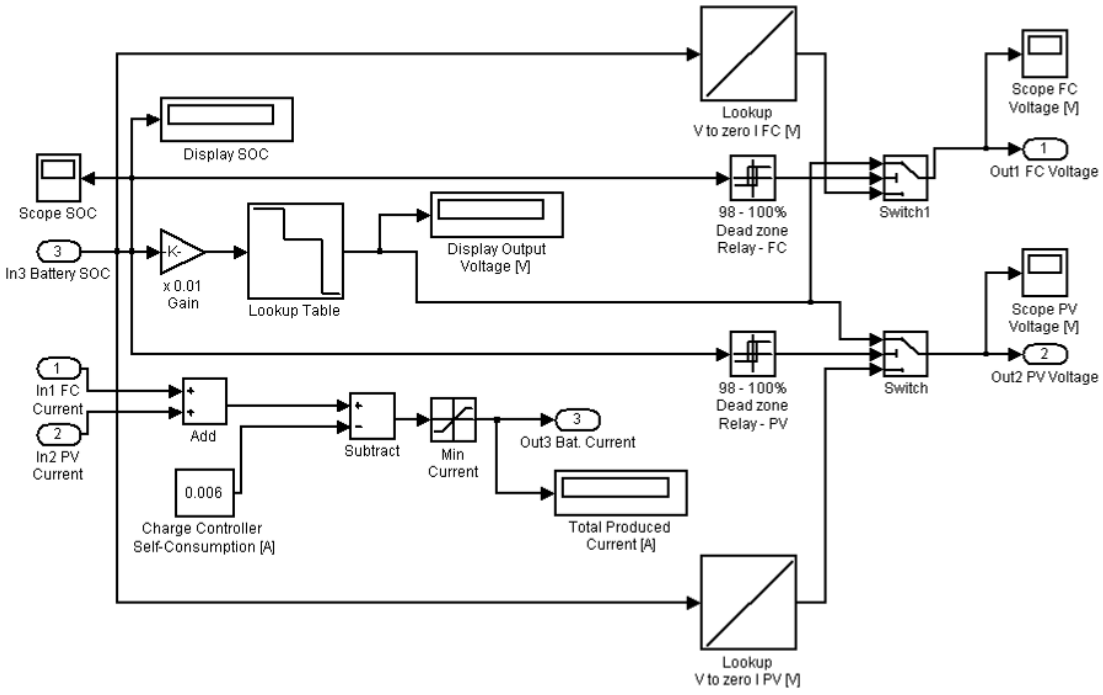

Figure 7.5 - Battery charge controller block

7.7. Propulsion parameters

Inputs

- "In1" Motor RPM [min^{-1}]: equal to the motor "Out5", the motor shaft rotation speed

Outputs

- "Out1" Torque [Nm]: the resistant torque induced by the propeller rotating at a given speed in a specific water density
- "Out2" Thrust [N]: the thrust required to reach a particular speed
- "Out3" Speed [$m.s^{-1}$]: Hidrocat scale model speed

Adjustable parameters

- Water Density [$kg.m^3$]
- Propeller Diameter [m]

Block description

This block is fundamentally a graphical translation of the mathematical expressions of the advance coefficient J, the thrust coefficient K_T and the torque coefficient K_Q the two last ones being reverted and used to determine the thrust T and the torque Q [38].

$$J = \frac{V_a}{n.D} \quad \text{(Eq. 7.3)}$$

$$T = K_T.\rho.n^2.D^4 \quad \text{(Eq. 7.4)}$$

$$Q = K_Q.\rho.n^2.D^5 \quad \text{(Eq. 7.5)}$$

The RPM is converted into boat speed V (output Out3) by means of a lookup table whose values are based on testing carried out in a swimming pool. The speed of the boat has been calculated from the time necessary to cover a certain distance and the RPM estimated from the throttle position (associated error: approximately 10%).
Once the boat speed is determined, the advance speed V_a is obtained from the expression (Eq. 7.6) were w_m is the wake fraction = 0.2 (see *4.2. Downscaling of the Optimal Full Scale Propeller for Use in the Simulator*) [38].

$$V_a = V \times (1 - w_m) \quad \text{(Eq. 7.6)}$$

J is calculated with the *Eq. 7.3* and K_T and K_Q are obtained from 1-D lookup tables whose data is the outcome of the optimal propeller design process in NavCad (see *figures 4.5 & 4.6*). The K_T - J and K_Q - J curves are taken as such since they are adimensional.
However, in order to refine the match between experimental results and simulation model output, an adjusting coefficient of 4.4 had to be applied to J before it is used as an input value in the lookup table. This may be due to lack of accuracy of the RPM - speed correlation, to the phenomenon of cavitation that is not taken into account and most important, to the fact that the propellers used on the Hidrocat scale model have different characteristics from the optimized full scale ones from which the K_T - J and K_Q - J curves are taken.
Nevertheless, corrections and fine-tuning of theoretical models are often necessary to reach a sufficient fidelity of the simulation.

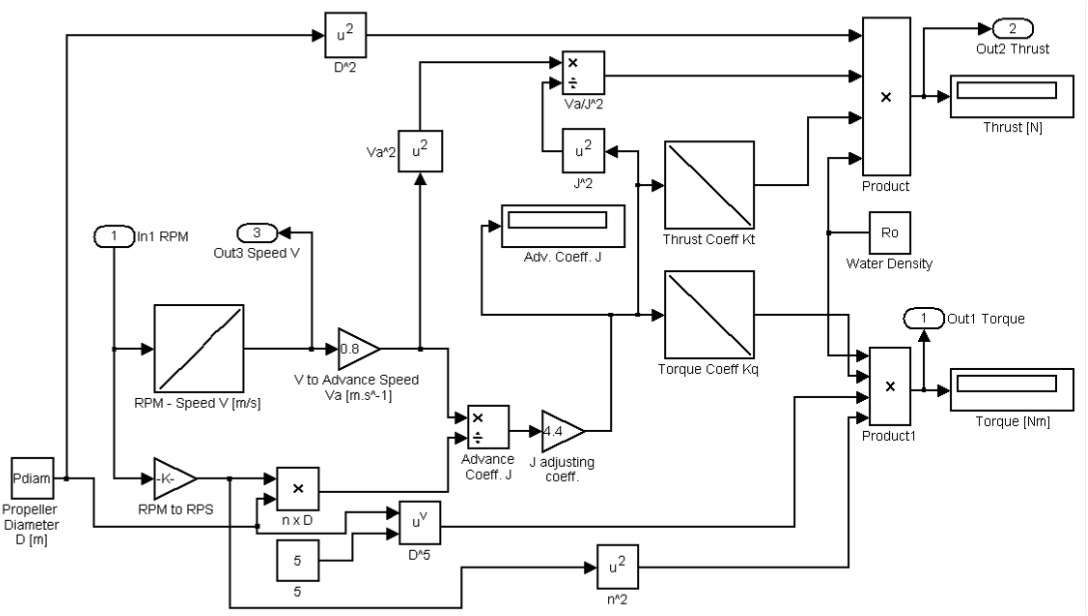

Figure 7.6 - Propulsion parameters block

7.8. Complete propulsion system model

The *Figure 7.8* below depicts the connections between the various blocks described above.
The system input is the speed controller, an electrical throttle that controls the motor speed by modifying their input voltage. Two options are left to the user, either a constant input voltage or a programmable input scheme using a signal builder that could represent a sailing pattern. In order to validate this simulation model, live tests have been carried out following a strict motor voltage pattern. This experiment has been confronted to the outputs of the simulation model. This subject is covered by *Chapter VIII - Comparison between experimental data and simulation model*. The *Figure 7.7* below illustrates a voltage input profile over time:

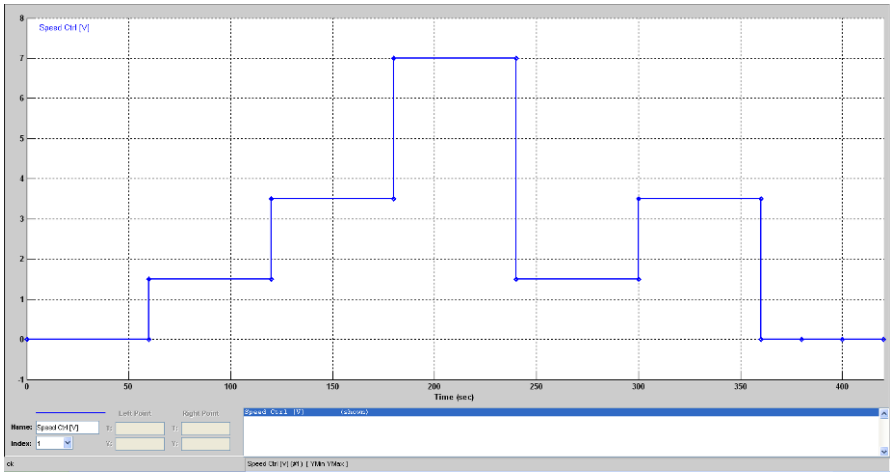

Figure 7.7 - Speed control via voltage profile for replication of the live test with the Simulink® model simulator

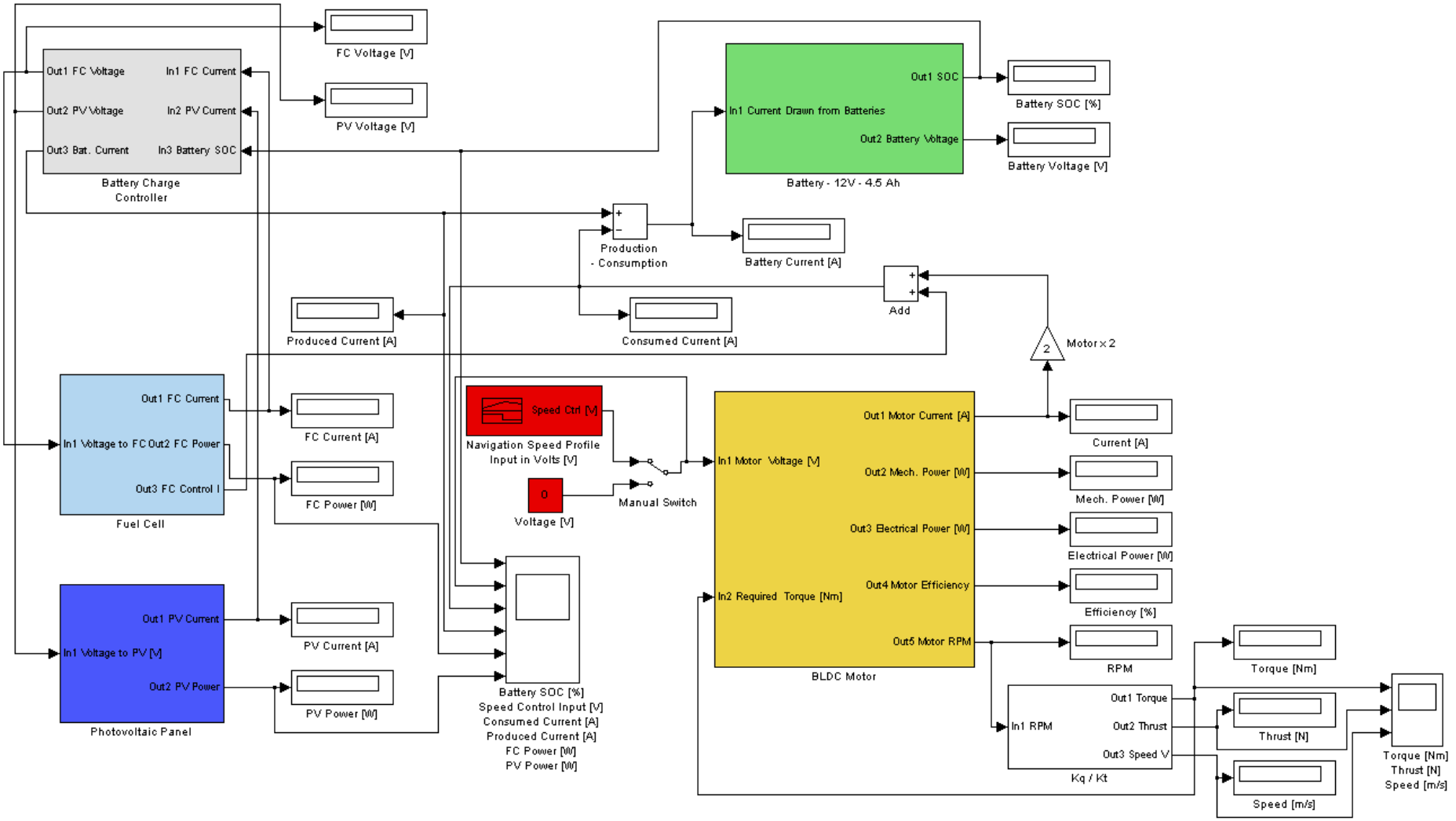

Figure 7.8 - Complete propulsion system model with its different blocks interlinked

The current required by the motor is multiplied by 2 to account for the 2 motors. The sum of this current and the FC controller current form the consumed current. The produced current is the Out3 of the battery charge controller and is the current available to charge the battery stack and to feed the motors. Produced and consumed currents are summed and the result is the input of the battery block. If this result is negative, it will draw current from the battery stack and hence lower its SOC and vice versa.

Most outputs are visually accessible with displays and 2 main scopes record and show the evolution of the signals over the simulation period. See *Appendix 7.1 - Scope simulation signal record*.

The first scope exhibits electrical parameters:

- Battery SOC [%] (Battery Out1)
- Speed Control Input [V]
- Consumed current [A] (2 x Motor Out1)
- Produced current [A] (Battery Charge Controller Out3)
- FC Power [W] (Fuel Cell Out2)
- PV Panel Power [W] (Photovoltaic PanelOut2)

The second scope exhibits mechanical parameters:

- Torque [Nm] (Propulsion Parameters Out1)
- Thrust [N] (Propulsion Parameters Out2)
- Speed [$m.s^{-1}$] (Propulsion Parameters Out3)

Chapter VIII - Comparison between experimental data and simulation model

8.1. Introduction

A comprehensive propulsion system simulation model has been built to allow computer-based simulations of the behaviour of such system in various operational and atmospheric conditions.
In order to validate this model, 2 live tests with 2 different initial battery SOC's (100% and 75%) have been carried out and their results are confronted with those from the simulation model, results are discussed, the errors are quantified and their potential causes are assessed.
Tests and simulations were based on a possible sailing speed profile, in which the motor speed command varies along the test duration according to the *Figure 8.1*.

Table 8.1 - Simulation power and voltage profiles

Time Interval	***Power***	***Voltage***
[min]	***-***	***[V]***
0 to 1	0	0
1 to 2	Minimum	1.1
2 to 3	Medium	2
3 to 4	Maximum	4
4 to 5	Minimum	1.1
5 to 6	Medium	2
6 to 7	0	0

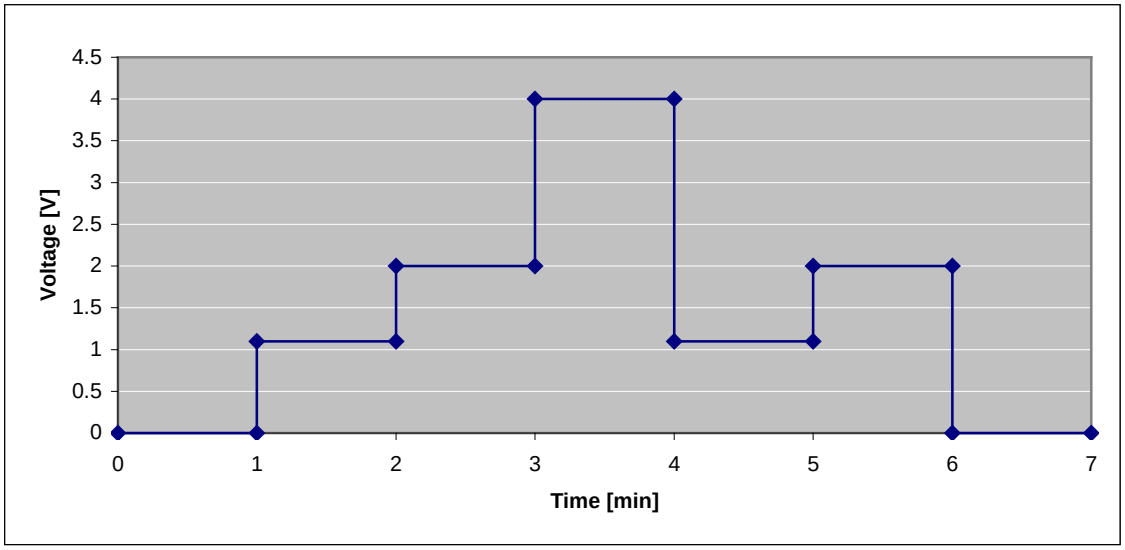

Figure 8.1 - Motor input voltage profile

8.2. Live test conditions

Environment:

- Location: Lisbon
- Date: 30.07.2010
- Time: 13:35 - 14:00
- Temperature: 28ºC
- RH: 55%
- Solar radiation: 850 $W.m^{-2}$ (estimate based on [41])

Data acquisition equipment:

- Data acquisition board: NI USB 6211
- Software: LabVIEW 8.5
- Channels: 3
- Type of measurement: Referenced single-ended

Since the IST swimming pool facilities which used to be the usual testing environment for the Hidrocat scale model does not let enough solar radiation in, these 2 live tests took place outside, using a single motor and the propeller being immersed in a box of water.
The atmospheric conditions were measured prior to launching the test.
The motor control followed a strict 7 minute profile depicted in *Figure 8.2*. The throttle level has been translated into motor input voltage by way of measuring the motor RPM corresponding to a certain throttle position on the radio control and by converting these RPM's into voltage using the RPM/volt curve provided by the motor manufacturer.

The motor control profile of the simulation model is an exact replica of the live test one.

In order to measure currents with the data acquisition board, use must be made of calibrated cables (as explained previously) in which the voltage drop due to Joules effect is measured and subsequently converted into current. However, since these voltage drops are of very low amplitude, the associated error can become substantial.
In order to avoid these uncertainties, the data acquisition board was used only to measure voltages whereas currents were measured manually at each throttle position change using an ammeter.

8.3. 100% SOC test

The stabilized voltage of the batteries prior to start the first live test of the propulsion system was measured at 12.94 V, which can be considered as fully charged battery voltage. It is difficult to state with high accuracy what is the temporary maximum voltage at the battery terminals but one can reasonably assume that the latter is higher than the stabilized voltage. Consequently, despite the battery SOC being close to 100%, the battery charge controller may top this voltage further (float voltage), as we will see in the results exhibited in *Figure 8.2* below.

8.3.1. Live testing and simulation outcome comparison, discussion and error assessment

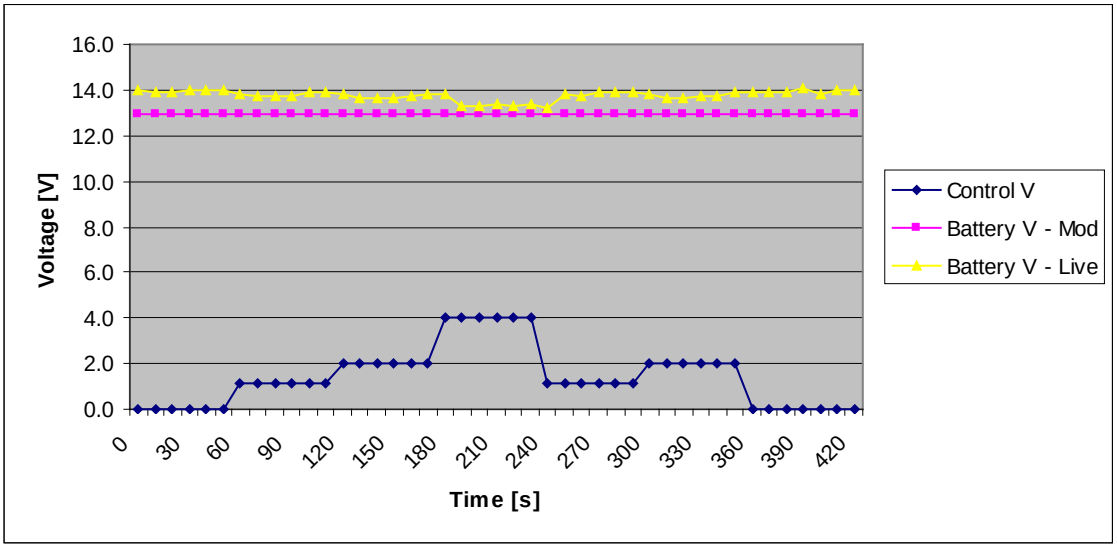

Figure 8.2 - 100% SOC Motor control voltage; Battery voltage - Model & Live test

The main difference between the experimental data and the simulation output is that the voltage measured at the battery terminals is not stabilized. Hence, it is difficult to compare those 2 voltage levels. The battery voltage obtained from the simulation increases from beginning to end of simulation by 0.04 V (from 12.94 V to 12.98 V) while the fluctuating voltage measured in the live test increased on average by 0.5 V but it is highly dependent on the power supply from the FC and PV. It is noticeable that the experimental battery voltage is consistently higher than the model voltage but depends on the load from the motors since the higher the load, the more current drawn by the motors and the less current charging the battery.
This behaviour illustrates the “buffer” role of the battery. The model does only provide stabilized V values, neglecting this instantaneous buffer behaviour.

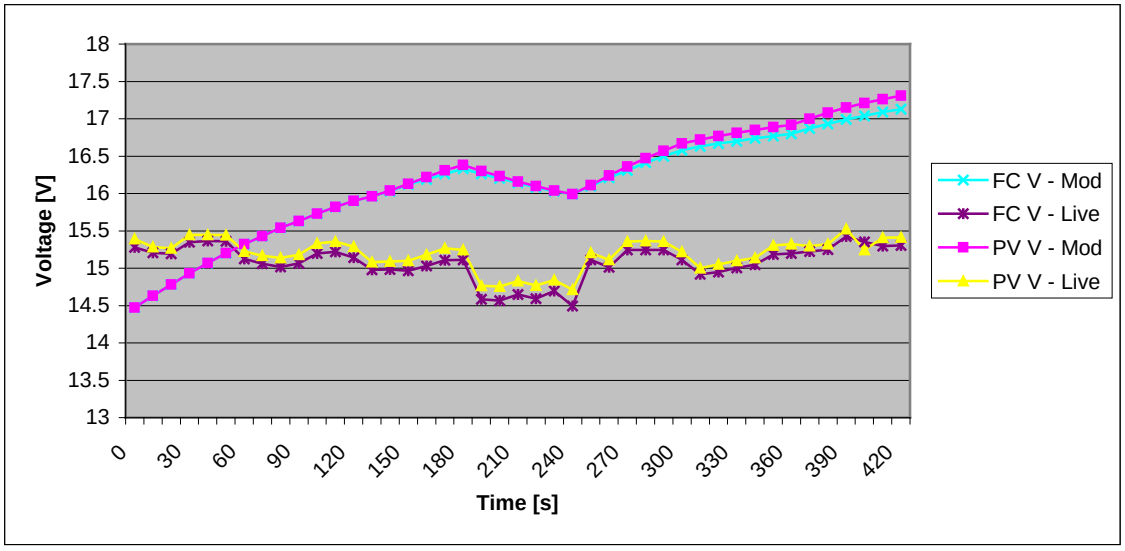

Figure 8.3 - 100% SOC FC voltage - Model & Live test; PV panel voltage - Model & Live test

Since the initial battery SOC was above the last battery charge controller step (at 80% SOC), the behaviour of the latter was simulated with characteristic curves progressively zeroing the current by increasing the input voltage of PV and FC to their open circuit voltages. As shown in *Figure 8.3*, when the electrical load is higher (control voltage = 4 V and motor current = 2.59 V), the battery SOC slightly decreases which originates a slight drop in FC and PV voltage, resulting in an increased current production in order to compensate the SOC drop. Same behaviour is observed with the live test. However, the voltage threshold is consistently lower. This can be seen as an attempt of the charge controller to charge the battery momentarily beyond 100% SOC and hence need for higher currents causing lower voltage levels at PV and FC. It is interesting to note that the PV voltage remains consistently above the FC voltage. The definition of the data acquisition board being of 2.69 mV (see *6.5.1. Data acquisition board features*), this difference cannot be explained by measurement errors. This difference, varying between 0.06 V and 0.1 V may be explained by the internal resistance in the FC controller inducing a voltage drop.

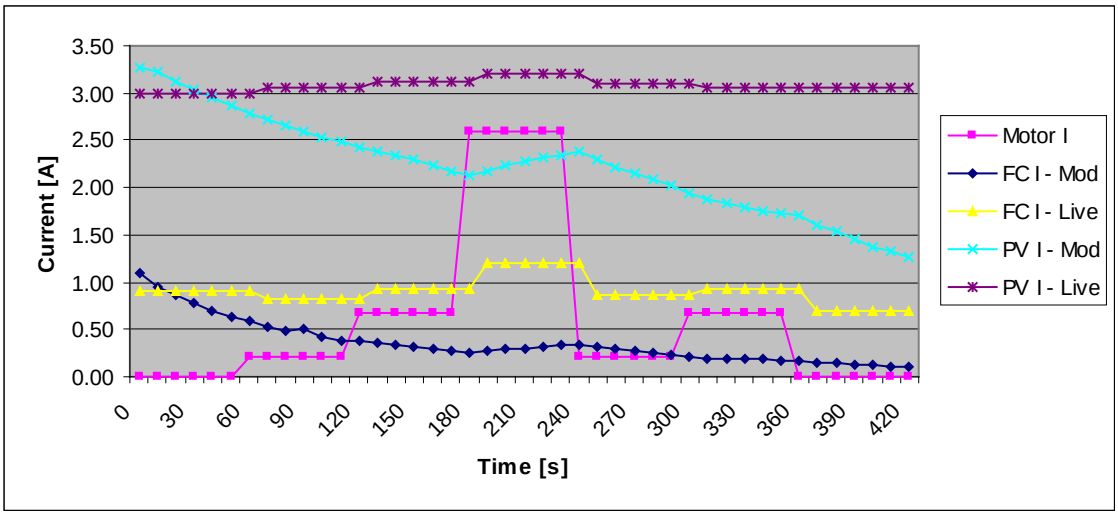

Figure 8.4 - 100% SOC FC current - Model & Live test; PV panel current - Model & Live test

Currents obtained experimentally follow the same behaviour as the voltages, showing dependency on the electrical load. Similarly, the current simulation follows the same trend as the voltage simulation. This is logical as currents are dependent on voltage level at the battery charge controller. From the *Figure 8.4*, it can be easily observed and concluded that the battery charge controller is not optimized for working with fuel cells. This is due to the difference in characteristic curves between FC and PV. PV panels have generally their highest output around 15 V and see their voltage drop dramatically beyond this point when the current increases (see *6.3. Photovoltaic panels*), whereas fuel cells have different curves with their instability zone appearing at much lower voltages (around 11 - 11.5 V) and giving their highest output just before this zone. The FC is in this case under-exploited. This scenario is actually positive as long as the solar energy suffices to supply enough energy to motors and to recharge batteries.

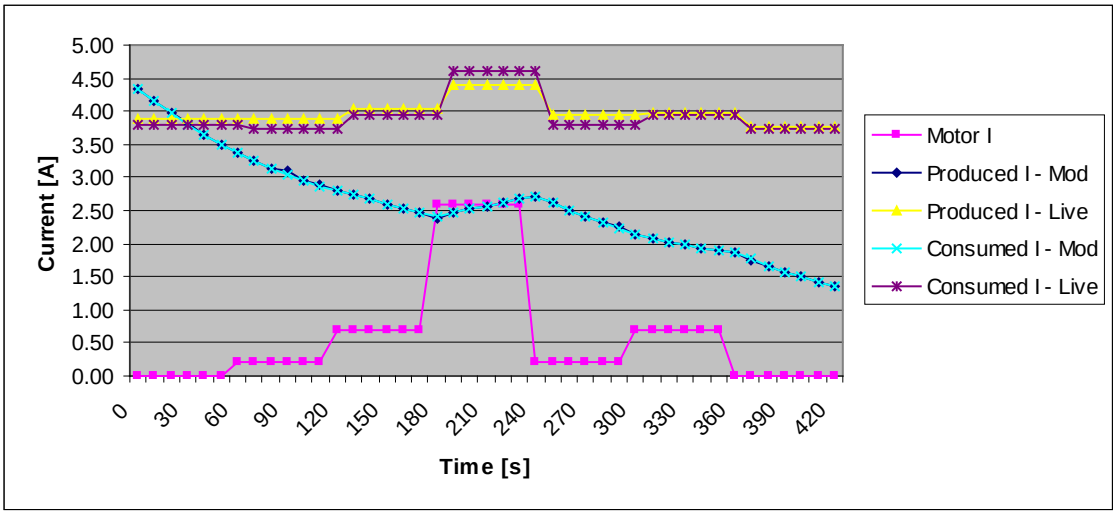

Figure 8.5 - 100% SOC Motor current; Produced & consumed current - Model & Live test

Simulation model produced currents and voltages match perfectly whereas experimental ones show some difference (maximum = 0.2 A). This gap can be explained by the single measurement of currents during the 60 second interval between each input voltage change. If the current of the motors for instance had a short peak at the moment of that punctual measurement, it may originate an error that will be then spread over the 60 second interval. See *Figure 8.5*.

8.4. 75% SOC test

Prior to start the second test, the battery stabilized voltage was 12.63 V which corresponds to 75% SOC. The choice of this particular SOC was dictated by the change in charging state, from absorption charge to float charge, it allows to observe along this 7 minute test / simulation.

8.4.1. Live testing and simulation outcome comparison and discussion and error assessment

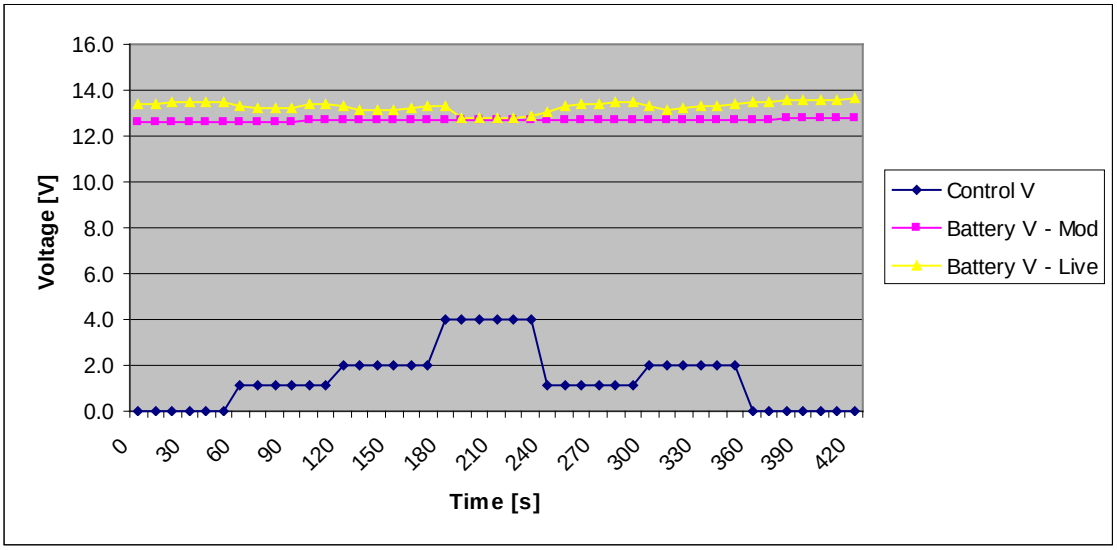

Figure 8.6 - 75% SOC Motor control voltage; Battery voltage - Model & Live test

As illustrated in *Figure 8.6*, the battery voltage given by the model increases from 12.63 V to 12.75 V relatively linearly (showing limited inflexions at control voltage changes and increasing at a slower pace when electrical load increases), whereas the live test battery voltage increases from 13.41 V to 13.63 V showing stronger variations in its slope related to electrical load steps. This behaviour is comparable to the first test (100% SOC) but the gap between simulated battery voltage and experimental data is reduced. This voltage difference can be explained by the buffer behaviour of the battery and the fact that the voltage measured at its terminal is not the battery stabilized voltage.

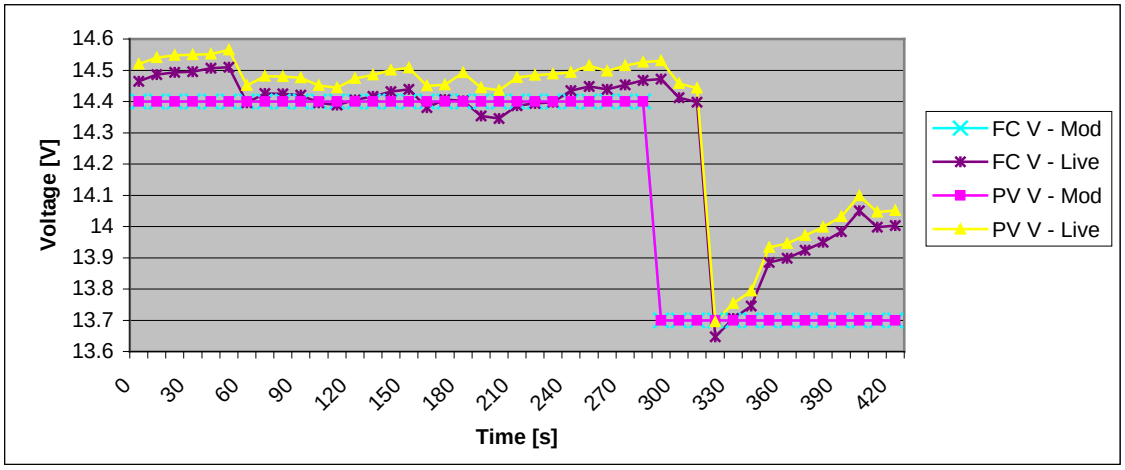

Figure 8.7 - 75% SOC FC voltage - Model & Live test; PV panel voltage - Model & Live test

At time 0 and for approximately the first 5 minutes, the battery charge controller is on absorption charge mode with a theoretical voltage at 14.4 V. This state lasts until 290 s with the model and 320 s in the live test, as depicted in *Figure 8.7*. This difference can be reasonably explained by the fact that the initial SOC was not exactly the same on both sides. Nonetheless, the behaviour similarity is obvious. After the voltage drop due to charge stage switch, the voltage of the real charge controller tends to increase as the SOC increases while in the simulation, the latter remains constant until reaching 80%. The experimental PV voltage remains between 0.05 V and 0.09 V above FC voltage, slightly closer than in the first test.

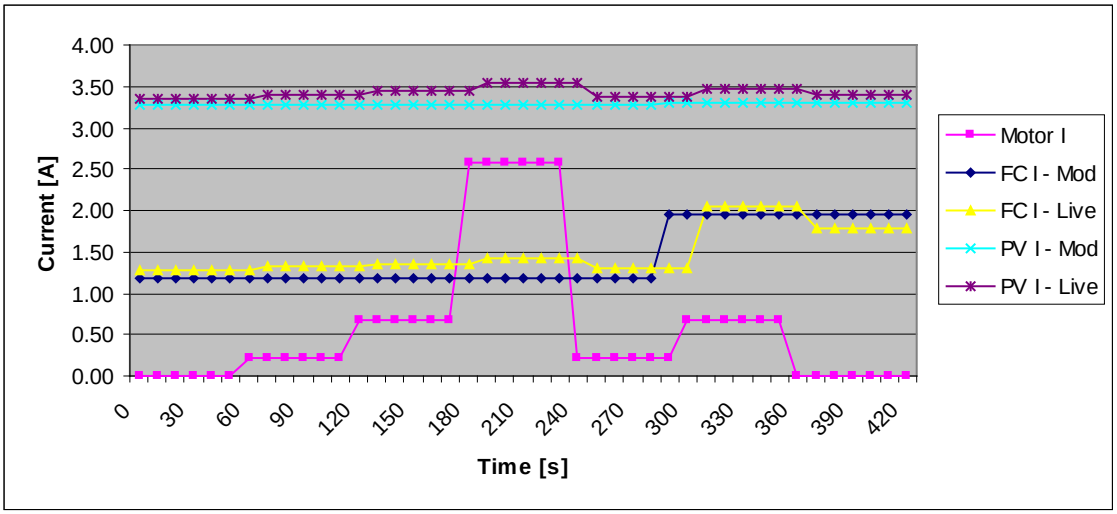

Figure 8.8 - 75% SOC FC current - Model & Live test; PV panel current - Model & Live test

Figure 8.8 shows that the current simulation is substantially closer to the reality in this scenario (between 0.1 V and 0.17 V difference). It is noticeable that the FC reacts much stronger to the voltage sudden change than the solar panel (the current-voltage characteristic curve of PV is close to horizontal around 14V).

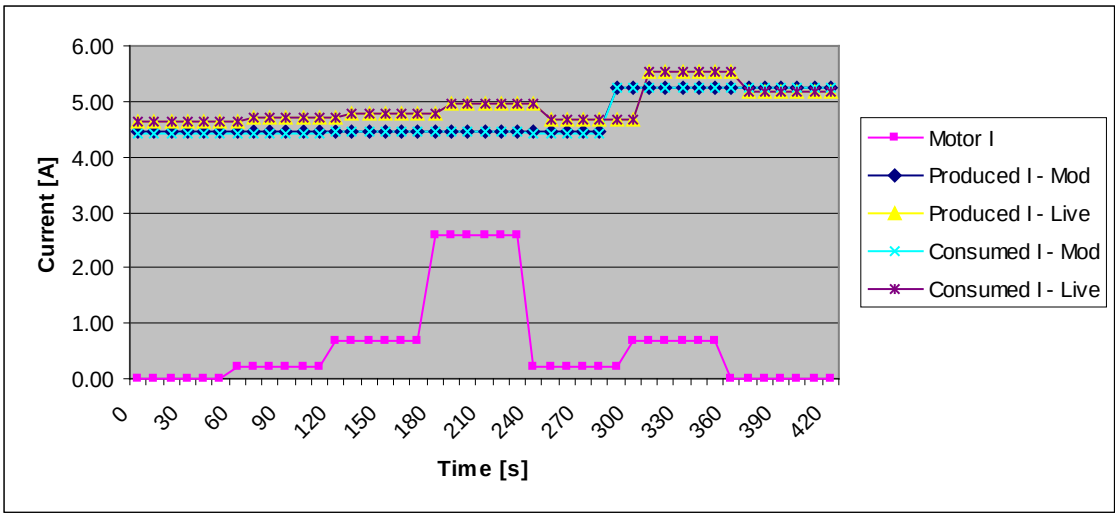

Figure 8.9 - 75% SOC Motor current; Produced & consumed current - Model & Live test

As it can be observed in *Figure 8.9*, the behaviour of the produced and consumed currents is consistent with the current curves exhibited in *Figure 8.8*. There were less measurement errors in this test as the produced and consumed current curves are almost perfectly superposed (maximum difference: 0.1 V from 250 s to 300 s).

8.5. Error cause assessment

- Bollard pull conditions: In the live test the propeller rotates in a small box filled with water and the boat speed is zero, there is water recirculation and turbulences. The K_T/J and K_Q/J curves used in the model are not depicting the reality of the test.
- Manual current measurement: Since substantial uncertainties have been observed while measuring currents by way of calibrated cables and data acquisition board, it has been decided to measure them using an ammeter. The drawback of this method is that practically wise, currents can only be measured once at each 60 second step of the simulation and this measurement can potentially occur during a short current peak, propagating the error over the entire 60 s step.
- It is very complex to simulate the battery instantaneous voltage with the model since the latter depends on the float voltage of the battery charge controller and on the electrical load. However, this value is not critical since it does not provide information about the energy produced and consumed by the system which is the most relevant information such simulator can provide.
- The battery charge controller, despite its relatively consistent behaviour while tested individually, seemed to show a different behaviour while implemented in the whole system. Its float voltage was different than the earlier tested one and it also controlled the current intensity used to charge the battery. This is done through fast and short impulses of that are impossible to replicate in such model simulator.

Chapter IX - Conclusions and recommendations

The presented thesis project is articulated around clear goals: designing, modelling and implementing a hydrogen / solar hybrid propulsion system on a scale model. Meeting these objectives involved several steps composing the foundations of this project.

Electric propulsion boats market study

Prior to undertake the project itself and its successive stages, an extensive initial electric boat market study was conducted in order to bring a clear picture of the state-of-the-art in this sector. Information contained in this study is highly valuable to help take correct directions when it comes to choosing the technology to be implemented on the Hidrocat and its scale model. As far as research results informed, it is the first comprehensive and global study accomplished in this field. The latter informs that most electric boats are powered by either battery solely, battery and PV panels or battery and fuel cell. Only one sail yacht prototype gathers the three technologies but her main propulsive means remains the wind. Together with market availability, the market study outcome lead to the choice of various components of the propulsion system such as the PEM hydrogen fuel cell, photovoltaic panels, BLDC motors and lead-acid batteries.

Propeller design project

A propeller design project using NavCad software resulted in an optimized propeller configuration for the 1/1 scale Hidrocat. The latter is based on the B-series, has 3 blades and features an important 64 cm diameter for higher efficiency. The adimensional characteristic curves of this propeller were used at a subsequent stage in the Simulink® model simulator. However, due to time and economical constraints, the propellers installed on the scale model were not a downscale of the optimal one for the real Hidrocat. They were picked after browsing radio control equipment catalogues based on diameter, power and speed.

Propulsion system design

The design phase required preliminary calculation of the hull resistance of the scale model. The latter was based on previous computations of the full scale Hidrocat hull resistance. Adding the relevant efficiencies to the hull resistance, a minimal propulsive power was determined and the motors could be selected. By establishing a minimum autonomy required to carry out live testing, the battery capacity was defined and its technology was dictated by battery charge controller market availability. Considering the recharging power needs and weight limitations, the fuel cell and photovoltaic panel power was defined and specific equipment was selected and

integrated to the propulsion system. Subsequently, the electrical circuit has been designed in the most optimal manner including all connections between components, types of cables based on power to be transported, monitoring equipment and connectors. Special care has been taken as to reduce as far as feasible, the unnecessary weight, cable lengths and connections in order to diminish electrical losses and augment reliability. The architecture of the propulsion system is simple, rational and reliable. In the future, it could be fitted with added feature such as relays to manually connect or disconnect some elements with the remote control. Numerous trials showed its soundness, encouraging an upscale for the future real scale Hidrocat.
Similarly, the propulsion drive chain and steering gear were studied carefully and the best equipment available on the market was employed to limit both mass increase and mechanical losses.

Component testing

Following component selection, a thorough test campaign was initiated in order to analyze the behaviour of the main elements of the circuit, i.e. the fuel cell, photovoltaic panels and battery charge controller. Characteristic curves were obtained in a series of atmospheric conditions (temperature and RH variations) for the fuel cell, at two different tilt angles for the photovoltaic panels and with different electric loads and battery SOC for the battery charge controller. Those curves are of crucial importance to replicate the behaviour of each component in the model simulator. The FC showed higher output when humidity rises and to a lesser extent when temperature drops, the PV panels were consistent with the manufacture specifications whilst a logical output diminution was observed with the horizontal exposure and the battery charge controller similarly behaved according to its data sheet.

Propulsion system implementation

After layouts of the electric circuit and propulsion drive chain and individual component testing were concluded, the implementation phase on board the scale model commenced. First an aluminium structure to link the two hulls was designed, manufactured and mounted together with reinforcement plates to ensure sufficient mechanical strength of the hulls. A honeycomb panel was installed in the centre of this platform to host most of the electrical and monitoring equipment. The hulls were pierced and transmission shaft stern tubes were fixed to the hull with composite materials made of carbon and glass fibre impregnated with epoxy resin. The same composite material was used to bind motor supports made of carbon epoxy composite plates to the hull. Following the installation of the transmission line, steering gear, radio control equipment and batteries were installed and a preliminary test could be carried out in a swimming pool. After confirming the water tightness and reliability of the already installed equipment, the rest of the electrical circuit and monitoring equipment was set up and tested.

Simulink® model simulator

A comprehensive propulsion system simulation model has been built in Simulink® to allow computer-based simulations of the behaviour, energy fluxes and power consumption of such system in various operational and atmospheric conditions. This simulator is articulated around various blocks, namely the BLDC motor block - the main power consuming block, driven by an input voltage controlling the motor RPM, the battery block - based on the Coulomb equation of the SOC, the battery charge controller block - setting FC and PV input voltage levels in function of the battery SOC, the FC block - able to replicate the FC behaviour in function of the electrical load, the temperature and RH, the PV block - whose output current depends on the solar radiation and input voltage, the propulsive parameter block - incorporating the V/RPM of the BLDC motor, J/K_Q and J/K_T characteristic curves of the real scale propeller to calculate the speed and motor torque necessary to attain such speed. The consistency showed by the simulator model with the results acquired during live testing with scale model validates its architecture and working principles. However, the fidelity depends on the battery SOC and could be further improved by a better modelling of the battery charge controller.

Live testing

Numerous live tests were carried out along the course of this project in order to fine-tune the electrical circuit and the data acquisition system.
Two live tests - at 100% battery SOC and at 75% battery SOC - have been conducted following a strict input voltage profile, simulating a sailing scheme. During these tests, all relevant currents and voltages have been monitored and data was stored for ulterior analysis and confrontation with the outcome of the simulator model. These tests took place outdoor at specific time with high solar radiation.
The behaviour of the propulsion system encompassing two renewable energy sources i.e. a hydrogen fuel cell and photovoltaic panels has proved satisfactory and the technological choices have been validated. Consequently, the architecture and work principles of the present propulsion system can be scaled up for implementation on-board the full scale Hidrocat.

Comparison between experimental data and simulation model

Voltage and current data acquired during the live tests and similar data obtained with the propulsion system simulator have been gathered in tables, plotted in graphs and confronted. Larger gaps were found between test data and simulator data at 100% SOC. The most evident error origin being different battery charge controller behaviour in these conditions from the one observed whilst this component was tested individually. Consequently, the behaviour of the simulator differed from the reality. An SOC different from 100% at the beginning of the test, despite accurate measurements, could also have originated a distinct behaviour between the

real and simulated propulsion systems. However, at 75% SOC, voltages and currents showed consistent trends, validating the simulator in these conditions. If the characteristic curves of the above mentioned components and propulsive parameters were replaced by the relevant ones, the computer-based simulator model could be used for the full scale Hidrocat since its architecture and working principles are valid for any size and power of propulsion system. The relative errors will probably tend to diminish since the values measured will be greater.

Recommendations and further improvements

- Towing tank tests could be a good solution to validate the hull resistance data of the Hidrocat scale model.
- Tailor-made 1/8 scale propellers based on the characteristics of the optimized full scale propellers would bring the advantage of being consistent in terms of propulsive parameters with the real scale ones. This would eliminate inconsistencies in the simulator and the need for adjusting coefficient.
- NavCad provides a reliable ensemble of propeller characteristics. However, these are not comprehensive and use of more advanced softwares would advantageously complement the results obtained with NavCad and allow full characterization of the propellers prior to manufacturing them.
- Additional monitoring equipment would provide valuable information. An odometer combined with a RPM meter would allow to know exactly the speed of the boat related to the propeller RPM whereas presently in the simulator, this is based on calculations only. Another type of useful equipment includes a hydrogen flow meter to monitor the hydrogen consumption and a light sensor to determine the efficiency of the photovoltaic panels. A Wi-Fi data acquisition board (e.g. from the NI WLS range) would be ideal in order to monitor in real time all parameters of the propulsion system and not having to analyze thousands of records afterwards.
- The simulator model could be refined with a more comprehensive input data range for the PV block such as location latitude, month, time, sky conditions. From those parameters and using equations from [21]; [22]. Dynamic modelling of the battery incorporating the float voltage would turn its simulation closer to reality for SOC close to 100% as suggested in [29] and [30]. The propulsive block could be more accurate with information obtained with the above mentioned additional equipment by relating more accurately speed of the scale model and motor RPM. In fact, while conserving the main architecture of this model, the next step for the real scale simulator would be a dynamic modeling of the different components dynamically provided sufficient data is provided by the manufacturer.

Bibliography

[1] Fonseca N., Duarte F., Gonçalves G., Farias T., *Clean propulsion for marine vessels based on hydrogen and solar energy*, 9th Conference on Energy for a Clean Environment, 2007

[2] Fonseca N., Farias T., Duarte F., Gonçalves G., Pereira A., *The Hidrocat Project – An all electric ship with photovoltaic panels and hydrogen fuel cells*, EVS24 Conference - Stavanger - Norway, 2009

[3] Adamson K.-A., *Fuel Cells and Marine Applications*, Fuel Cell Today, 2005

[4] Sattler G., *Fuel cells going on-board*, Elsevier, Journal of Power Sources, 2000, 61-67

[5] Weaver G., Barrett S., *Marine applications of fuel cell technology*, Fuel Cells Bulletin, 2003, 11-12

[6] Allen S., Ashey E., Gore D., Woerner J., Cervi M., *Marine applications of fuel cells*, Naval Engineers Journal, 1998, 93-106

[7] Beckhaus P., Dokupil M., Heinzel A., Souzani S., Spitta C., *On-board fuel cell power supply for sailing yachts*, Elsevier, Journal of Power Sources, 2005, 639-643

[8] Alleau T., *Applications marines et sous-marines des piles à combustibles*, Mémento de l'hydrogène, Fiche 9.4.2., 2008

[9] Wolfe W., Taylor O., Vasilow T., Wolfe A., Pierre J., Wisse J., *Fuel Cell Powered Propulsion System*, United States Patent, 1997, 1-5

[10] Vergragt P., van Noort D., *Sustainable technology development: The mobile hydrogen fuel cell,* Business Strategy and the Environment, Vol. 5, 1996, 168-177

[11] Wee J.-H., *Applications of proton exchange membrane fuel cell systems*, Elsevier, Renewable and Sustainable Energy Review, 2006, 1720-1736

[12] Singhal S., *Solid oxide fuel cells for stationary, mobile, and military applications*, Elsevier, Solid State Ionics, 2002, 405-410

[13] American Chemical Society, *Batteries and fuel cells*, Chemical Reviews, Volume 104, Number 10, 2004

[14] Larminie J., Dicks A., *Fuel cell systems explained*, Second Edition, Wiley, 2003

[15] Langhor D., *A study on hydrogen storage through adsorption in nanostructured carbons*, PhD thesis at École des Mines de Paris, 2004

[16] Teixeira J., *Caracterização de pilha de combustível de hidrogénio*, tese de Mestrado no Instituto Superior Técnico, 2009

[17] Thounthong Ph., Raël S., Davat B., *Energy management of fuel cell/battery/supercapacitor hybrid power source for vehicle applications*, Elsevier, Journal of Power Sources, 2009, 376-385

[18] Jiang Z., Dougal R., *Design and testing of a fuel-cell powered battery charging station*, Elsevier, Journal of Power Sources, 2003, 279-287

[19] Solomon B., Banerje A., *A global survey of hydrogen energy research, development and policy*, Elsevier, Energy Policy, 2004, 781-792

[20a] Cleveland, Cutler J., *Encyclopedia of Energy*, Volume 3, Elsevier, 2004, 227, 253-281

[20b] Cleveland, Cutler J., *Encyclopedia of Energy*, Volume 1, Elsevier, 2004, 117-126

[21] Alexandre J., *Radiação solar*, 5º ano - MIEM - SFC, 2008

[22] Falcão A., *Energia Solar - Movimento e posicionamento relativos Terra-Sol*, IST, 2008

[23] Markvart T., Castañer Luis, *Practical handbook of photovoltaics - Fundamentals and applications*, Elsevier, 2003

[24] Messenger R., Ventre J., *Photovoltaic systems engineering - Second edition*, CRC Press, 2004

[25] Kininger F., *Photovoltaic systems technology*, Universität Kassel - Rationelle Energiewandlung, 2003

[26] Green M., *Third Generation Photovoltaics*, Springer, 2006

[27] Lian Dibo L., Xiaoyun F., Shuichang L., Bochuan G., *PEM fuel cell and battery hybrid system studied in Matlab®/Simulink®*, School of Electrical Engineering, Southwest Jiaotong University, 2009

[28] Spiegel C., *PEM fuel cell modeling and simulation using Matlab®*, Elsevier, 2008

[29] Ross M., *A simple but comprehensive lead-acid battery model for hybrid system simulation*, GPCo Inc. - Canada, 2002

[30] Jackey R., *A simple, effective lead-acid battery modeling process for electrical system component selection*, The MathWorks, Inc., 2007

[31] Villalva M., Gazoli J., Ruppert F. E., *Comprehensive approach to modeling and simulation of photovoltaic arrays*, IEEE Transactions on Power Electronics, Vol. 24, Number 5, 2009, 1198-1208

[32] Rai D., *Brushless DC motor - Simulink® simulator*, Department of Electronics and Communication Engineering, National Institute of Technology Karnataka - India, 2004

[33] Karnan M., Thangavel K., Chitra L., Sivakumar R., Dwarakanath G. K., *BLDC motor controlled using resonant pole inverter with variable pulse width method*, ACSE Journal, Vol. 6, Issue 4, 2006, 47-54

[34] Latour T., *Control-oriented modeling and control of an automotive fuel cell system*, Master of Science Thesis at TU Delft, 2008

[35] HydroComp Inc., *Predicting Catamaran Resistance with NavCad*, 2003

[36] HydroComp Inc., *Navcad 4.0 Help File*

[37] MacPherson D., *The ten commandments of reliable speed prediction,* Presented at the Small Craft Marine Engineering Resistance and Propulsion Symposium, University of Michigan, 1996

[38] Falcão de Campos J., *Resistência e propulsão - Aulas Teóricas: Apresentação "ppt" - Aulas Práticas - Lista de problemas*, Master in Naval Engineering and Architecture, 2007

[39] B. Huang, P. Hsu, M. Wu, P. Ho, *System dynamic model and charging control of lead-acid battery for stand-alone solar PV system*, Elsevier, Solar Energy, 2010, 822-830

[40] Zittel, *Advantages and disadvantages of hydrogen*, Hydrogen in the Energy Sector, Systemtechnik Gmbitt. 1996

[41] Mata L., *Totais Diários da Radiação Global Recebida por Superfícies com Diversas Orientações e para Diferentes Ângulos de Inclinação*, INMG Lisbon, 1981

[42] Dürr M., A. Cruden, Sinclair Gair, Mc Donald J., *Dynamic model of a lead acid battery for use in a domestic fuel cell system*, Elsevier, Journal of Power Sources, 2006, 1400-1411

[43] MW Line - Grove Boats, *Product Portfolio and Technical Data*, www.grove-boats.com, November 2009

[44] Planet Solar, *Expédition - Le Bateau*, www.planetsolar.org/expedition-boat.fr.php, November 2009

[45] E3H, *Description Technique Odonata*, http://odonata.e3h.fr/description-technique-odonata, November 2009

[46] Zemships, *Construction and design of Zemships and first - operation experiences*, www.zemships.eu/en/project, November 2009

[47] Solar Water World, *Datasheets of Suncat 13/12, Suncat 23, Suncat* 2000, www.solarwaterworld.de, November 2009

[48] Czeers, Boats, www.czeers.com, November 2009

[49] Zéro CO_2, *Le Bateau*, www.zeroco2sailing.com, November 2009

[50] H-ION Solar Inc., *Hydrogen Energy Equivalents*, www.hionsolar.com/n-heq1, November 2009

[51] MTU, *Fuel Cell Driven Yacht*, www.mtu-friedrichshafen.com, November 2009

[52] Association Française pour le Bateau Électrique, *Catalogue Bateaux Électriques*, www.bateau-electrique.com, November 2009

[53] TÜV SÜD Industrie Service GMBH, *Hydrogen and Fuel Cell Vehicles Worldwide*, www.netinform.net/H2/H2Mobility/Default.aspx, November 2009

[54] Fuel Cell Propulsion Institute, www.fuelcellpropulsion.org, November 2009

[55] LiFePO4, *Technologie et avantages*, www.lifepo4.fr/technology, November 2009

[56] Janneau, *Datasheet Janneau Cap Camarat 545 WA*, www.jeanneau.com, November 2009

[57] Bénéteau, *Datasheets Bénéteau First 31.7, Antares 13.8*, www.beneteau.com - November 2009

[58] www.fuelcelltoday.com - Visit in November 2009

[59] US Department of Energy, *Fuel Cell Technologies Program - Information Resources*, www1.eere.energy.gov/hydrogenandfuelcells/pubs_educational, May 2010

[60] Plettenberg, *Motors*, www.plettenberg-motoren.com/UK/motoren, November 2009

Appendix

Appendix 3.1 - Geometric plan

3.1.1. Front view

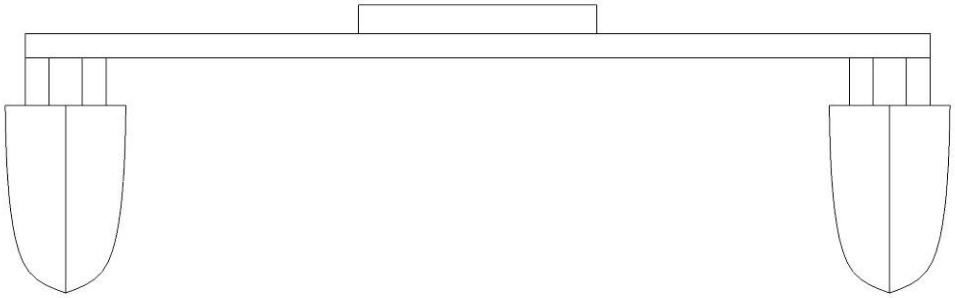

Figure A.3.1 - Front view of the Hidrocat scale model

3.1.2. Rear view

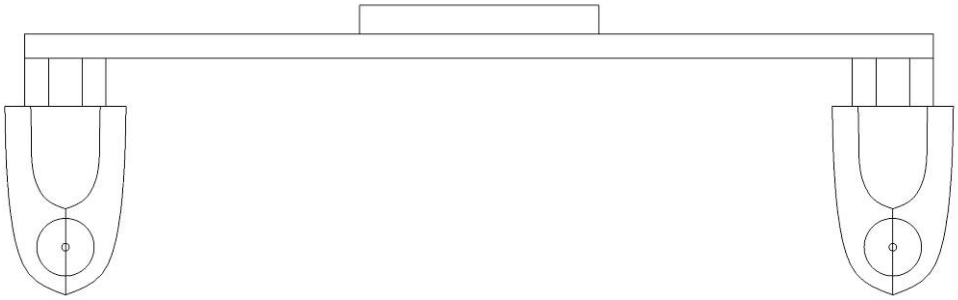

Figure A.3.2 - Rear view of the Hidrocat scale model

3.1.3. Side view

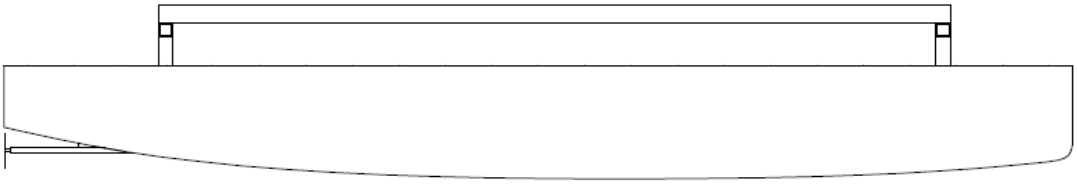

Figure A.3.3 - Side view of the Hidrocat scale model

3.1.4. Bird view

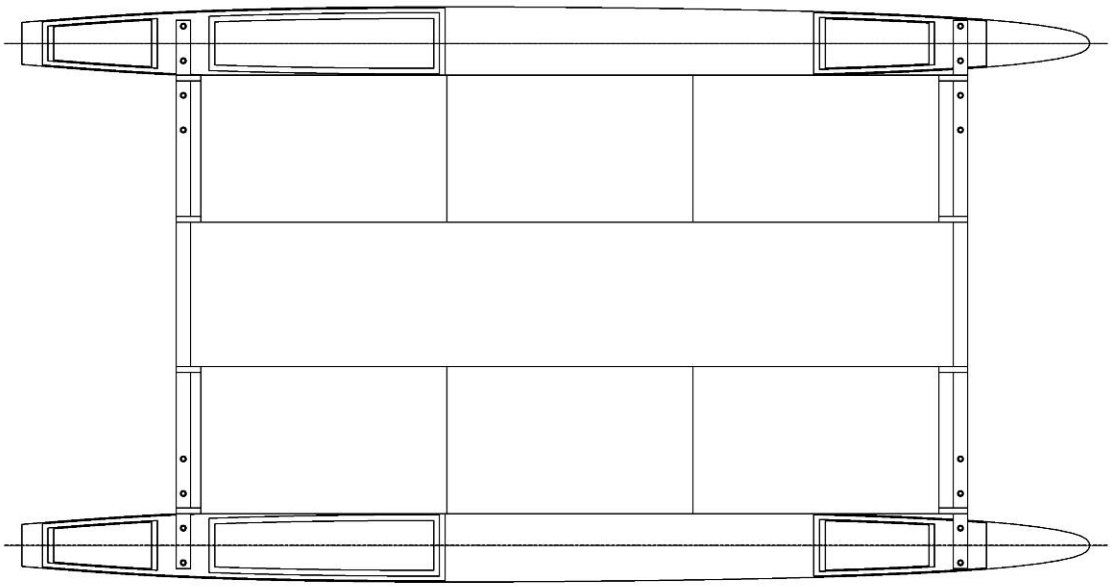

Figure A.3.4 - Bird View of the Hidrocat scale model

Appendix 3.2 - General arrangement

3.2.1. Body plan

3.2.2. Buttocks - Waterlines - Diagonals

Appendix 3.3 - Scale model finished

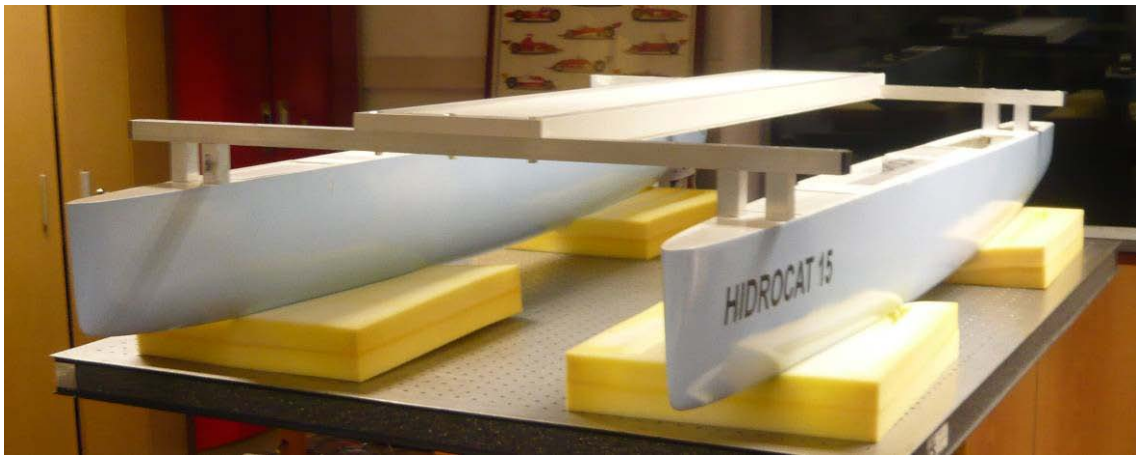

Figure A.3.5 - The Hidrocat scale model with its central platform mounted - Front view

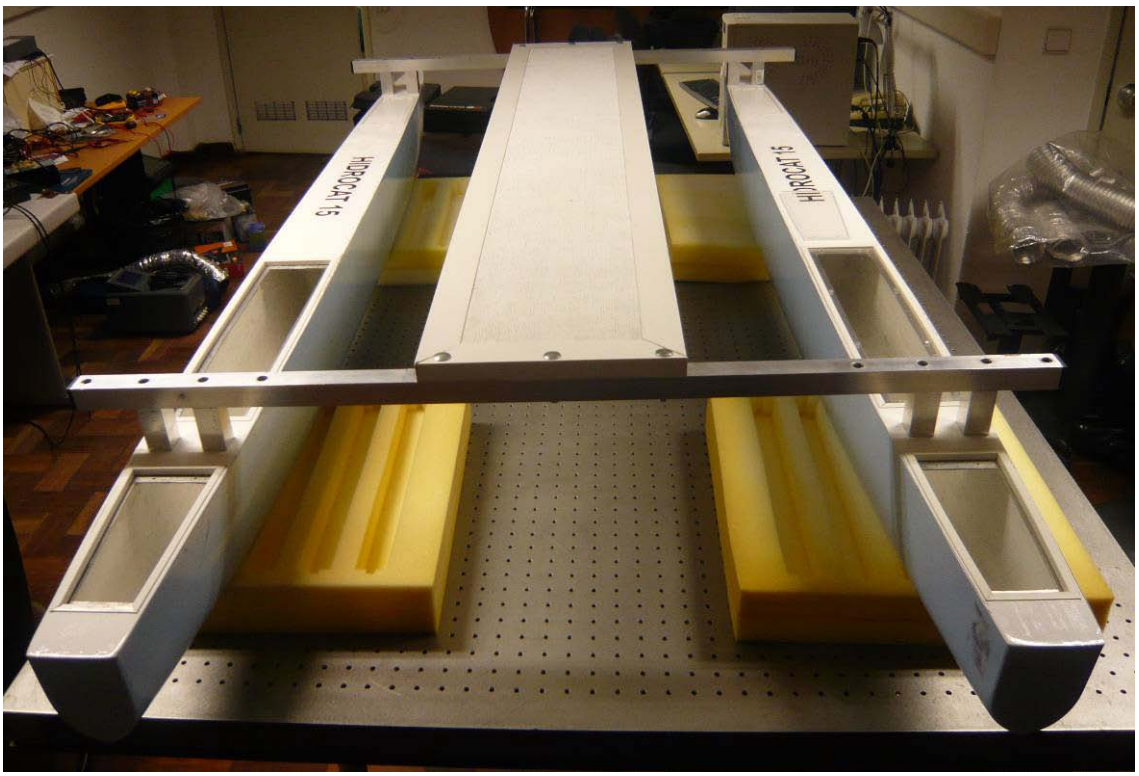

Figure A.3.5 - The Hidrocat scale model with its central platform mounted - Rear view

Appendix 4.1 - NavCad model file

```
;*******************************************
;* NavCad model file         HydroComp, Inc. *
;*******************************************

[NavCad]
Version=3.00
Release=ReleaseA
Precision=6
Description=NPL Model C5, L/B 11, B/T 2, Cp 0.693, S/L 0.3
[Units]
Length=Meter
Area=SqMeter
Weight=Kilogram
Speed=Knot
Force=kiloNewton
Power=Kilowatt
Density=KgPerCuM
KinemVisc=SqMPerSec
[Condition]
rho=999.01
nu=1.13902e-006
[Resistance]
3dFormFact=1.4
[Hull]
HullType=Displ
Loading=LoadDraft
ChineType=HardChine
SternShape=Normal
BowShape=UShape
FlapBehind=No
LengthPP=1.6
LengthWL=1.6
BeamWL=0.1455
Draft=0.0727
LCBHull=0.9024
WettedSurf=0.276
MaxSecArea=0.00597649
TraSecArea=0.003173
HullDispl=6.71
HalfEntAng=9.3
MidshiCoef=0.565
WaterpCoef=0.755
[Speeds]
Speeds=1.309,1.463,1.694,2.002,2.156,2.541,2.772,3.311,5.39,7.7

[Results]
ResiCoef=0.0027,0.0027,0.003,0.0034,0.0032,0.004,0.0037,0.0055,0.003,0
.0023
ModCfType=ITTC57
ModSource=ModelTest
ModLengthWL=1.6
FroudeLen=0.170004,0.190004,0.220005,0.260006,0.280006,0.330007,0.3600
08,0.430009,0.700015,1.00002
FroudeVol=0.495062,0.553304,0.640668,0.757153,0.815396,0.961002,1.0483
7,1.25221,2.03849,2.91213
HullReyNum=945947,1.05723e+006,1.22417e+006,1.44674e+006,1.55803e+006,
1.83625e+006,2.00318e+006,2.39269e+006,3.89508e+006,5.56439e+006
ResiMerit=0.00256523,0.00320431,0.00477343,0.00755596,0.00824765,0.014
3203,0.0157642,0.0334321,0.0483261,0.0756122
```

Appendix 4.2 - Hull resistance NavCad report

IST - CENTEC 27 août 2010 06:46 Page 1
Displacement/Resistance Project: Hidrocat
Hidrocat Aligned Prediction

---------- Analysis parameters ----------

[X]Bare-hull: Basic [X]Appendage: Holtrop-1988 method
Technique: Extrapolation [ ]Wind :
Cf type : ITTC [ ]Seas :
Align to : Rbare/W [ ]Channel :
File : C:\Documents and Settings\Julien\Ambiente de trabalho\cat1103.mdl [ ]Barge :
Correlation allow(Ca): 0,00040 [ ]Net :
[X]Roughness: 0,15 mm
[ ]3-D corr : form factor(1+k): [X]Speed dependent correction

---------- Prediction Results ----------

Vel kts	Fn	Rn	Cf	[Cform]	[Cw]	Cr	Ct
3,00*	0,127	2,03e7	0,002662	0,000000	0,000000	0,004932	0,007994
4,00*	0,170	2,71e7	0,002541	0,000000	0,000000	0,004742	0,007682
5,00	0,212	3,39e7	0,002453	0,000000	0,000000	0,004793	0,007646
6,00	0,254	4,06e7	0,002384	0,000000	0,000000	0,005215	0,007999
7,00	0,297	4,74e7	0,002328	0,000000	0,000000	0,005116	0,007844
8,00	0,339	5,42e7	0,002281	0,000000	0,000000	0,005587	0,008268
9,00	0,382	6,10e7	0,002241	0,000000	0,000000	0,005515	0,008156
10,00	0,424	6,77e7	0,002206	0,000000	0,000000	0,006821	0,009427
11,00	0,467	7,45e7	0,002175	0,000000	0,000000	0,007758	0,010333
12,00	0,509	8,13e7	0,002147	0,000000	0,000000	0,007931	0,010478

Vel kts	Rw/W	Rr/W	Rbare/W	Rw N	Rr N	Rbare N	PEbare kW
3,00	0,00000	0,00268	0,00435	0	118	192	0,3
4,00	0,00000	0,00459	0,00743	0	202	328	0,7
5,00	0,00000	0,00725	0,01156	0	320	510	1,3
6,00	0,00000	0,01136	0,01742	0	501	769	2,4
7,00	0,00000	0,01516	0,02325	0	669	1026	3,7
8,00	0,00000	0,02163	0,03200	0	954	1412	5,8
9,00	0,00000	0,02702	0,03996	0	1192	1763	8,2
10,00	0,00000	0,04126	0,05702	0	1821	2516	12,9
11,00	0,00000	0,05678	0,07562	0	2506	3337	18,9
12,00	0,00000	0,06907	0,09125	0	3048	4027	24,9

Vel kts	Rapp N	Rwind N	Rseas N	Rchan N	Rother N	Rtotal N	PEtotal kW
3,00	3	0	0	0	0	195	0,3
4,00	6	0	0	0	0	334	0,7
5,00	8	0	0	0	0	519	1,3
6,00	12	0	0	0	0	781	2,4
7,00	16	0	0	0	0	1042	3,8
8,00	20	0	0	0	0	1433	5,9
9,00	25	0	0	0	0	1789	8,3
10,00	31	0	0	0	0	2547	13,1
11,00	37	0	0	0	0	3374	19,1
12,00	44	0	0	0	0	4071	25,1

---------- Condition data ----------

Water type: Standard Fresh
Mass density: 999,01 kg/m3
Kinematic visc: 1,1390e-06 m2/s

---------- Hull data ----------

Primary:		Secondary:	
Length between PP:	15,000 m	Trim by stern:	0,000 m
WL aft of FP:	15,000 m	Bulb ext fwd FP:	0,000 m
Length on WL:	15,000 m	Bulb area at FP:	0,000 m2
Max beam on WL:	0,910 m	Bulb ctr above BL:	0,000 m
Draft at mid WL:	0,660 m	Transom area:	0,000 m2
Displacement bare:	4,5 t	Transom beam:	0,000 m
Max section area:	0,400 m2	Transom draft:	0,000 m
Waterplane area:	10,6 m2	Half ent angle:	0,000 deg
Wetted surface:	20,2 m2	Lwl/B:	16,4835
LCB aft of FP:	7,170 m	B/T:	1,3788
Bow shape:	U-shape [vert	Cb:	0,5000
Stern shape:	U-shape [vert	Cws:	2,4562
Chine type:	Round bilge	Cx:	0,6660
Loading:	Load draft	Cw:	0,7766

Parameters: Basic

Fn(Lwl)	0...0,4	0,13
Fn-high	0...0,4	0,51 Limit
Cvol(Lwl)	4,15...11,26	9,08

---------- Appendages ----------

Total wetted surface (ex. thruster):

Rudders:	0,400 m2	Drag coefficient:	1,500
Shaft brackets:	0,000	----------	0,000
Skeg:	0,000	----------	0,000
Strut bossing:	0,000	----------	0,000
Hull bossing:	0,000	----------	0,000
Exposed shafts:	0,150	----------	2,000
Stabilizer fins:	0,000	----------	0,000
Dome:	0,000	----------	0,000
Bilge keel:	0,000	----------	0,000
Bow thruster diam:	0,000 m	----------	0,000

Parameters: Holtrop-1988 method
None given

Appendix 4.3 - Solomon ST74 Datasheet

ST 74 dual motor

BOATS

displacements up to	16 tons (14.5 mT)
monohull lengths	33-50 ft (10-15 m)
catamaran lengths	40-60 ft (12-18 m)
replaces diesels up to	48+ hp (36+ kw)

SPECS

input	144 VDC
output	12 hp (9kw) @1,100 rpm
torque	74 lb-ft (100 N-m)
full load current draw	64 amps
motor type	3-phase, continuous-duty, brushless DC permanent-magnet neodymium iron boron
motor functions	acts as a motor when input voltage applied; as a generator when turned by prop
motor housing	sealed, cast-aluminum with cooling fins and mounting brackets
diameter	13 in (330 mm)
length	17 in (432 mm)
weight	143.5 lb (65 kg)
controllers (2)	- pulse width modulated (pwm) - 50 amp continuous duty, 100 amp peak (2 sec) - current loop with mechanical interface

OUTPUT

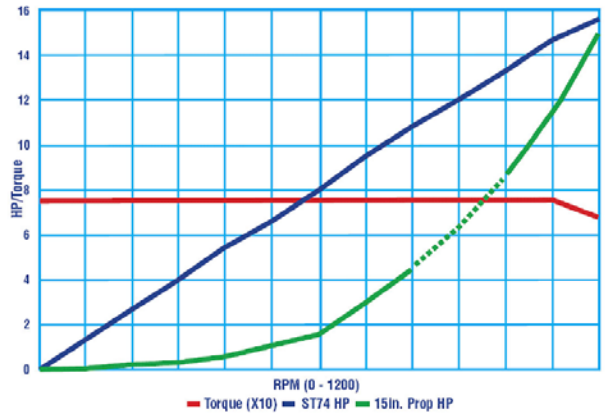

Solomon Technologies, Inc.
1400 L & R Industrial Blvd. Tarpon Springs, FL 34689
(727) 934-8778 Fax (727) 934-8779
www.solomontechnologies.com info@solomontechnologies.com

Appendix 4.4 - Optimized propeller NavCad report

IST - CENTEC 22 sept 2010 05:47 Page 3
Displacement/Optimum propeller Project: Hidrocat
Hidrocat Aligned Prediction

---------- System 3 ----------

Description: Prop 3
Series: B-series
Blades: 3
Exp area ratio: [ ]Opt 0,3700
Diameter: [ ]Opt 0,6400 m
Pitch: [X]Opt 0,7603 m

Scale corr: B-series
Kt mult: [X]Std 1,000
Kq mult: [X]Std 1,000
Blade t/c: [ ]Std 0,020
Roughness: [ ]Std 0,030 mm
Cav breakdown: [X]Apply
Propeller cup: 0,0 mm

Engine file: C:\Documents and Settings\Julien\Ambiente de trabalho\Solomom_ST37x2.eng
Rated RPM/kW: 1100,0 / 9,0
Gear ratio: 2,200
Gear efficiency: 0,98

---------- Selection parameters ----------

Load identity: Shaft power
Design speed: 8,00 kts
Cav criteria: Keller eqn
Reference load: 18,0 kW
Load design point: 100,0 %
Reference RPM: 1100,0
RPM design point: 100,0 %

---------- Analysis results ----------

Sys	Vel kts	Rtotal N	WakeFr	ThrDed	RelRot	EngRPM RPM	PropRPM RPM	Pitch m
	4,00	334	0,1400	0,1159	1,0000	335,2	152,4	0,8928
3	8,00	1433	0,1400	0,1159	1,0000	683,7	310,8	0,8928
	12,00	4071	0,1400	0,1159	1,0000	1085,7	493,5	0,8928

Sys	Vel kts	J	Kt	Kq	PropEff	HullEff	QPC	OPC
	4,00	1,0890	0,1726	0,0397	0,7537	1,0280	0,7748	0,7593
3	8,00	1,0677	0,1807	0,0411	0,7468	1,0280	0,7677	0,7524
	12,00	1,0086	0,2029	0,0447	0,7278	1,0280	0,7481	0,7332

Sys	Vel kts	Thrust N	Delthr N	PD/prop kW	PS/prop kW	PB/prop kW
	4,00	187	330	0	0	0
3	8,00	812	1436	4	4	4
	12,00	2300	4067	17	17	17

Sys	Vel kts	Fuel lph	MinP/D	TipSpd mps	%Cav	Press kPa	MinBAR
	4,00	***	1,182	5,1	1,4	1,6	0,0369
3	8,00	***	1,166	10,4	1,7	6,8	0,0702
	12,00	***	1,124	16,5	4,7	19,3	0,1499

Appendix 6.1 - Flow meter calibration for hydrogen

Table A.6.1 - Flow meter calibration for hydrogen: flow - scale

Flow [l/min]	***Corresponding scale***
0	0
0.12	0.05
0.52	0.2
1.21	0.5

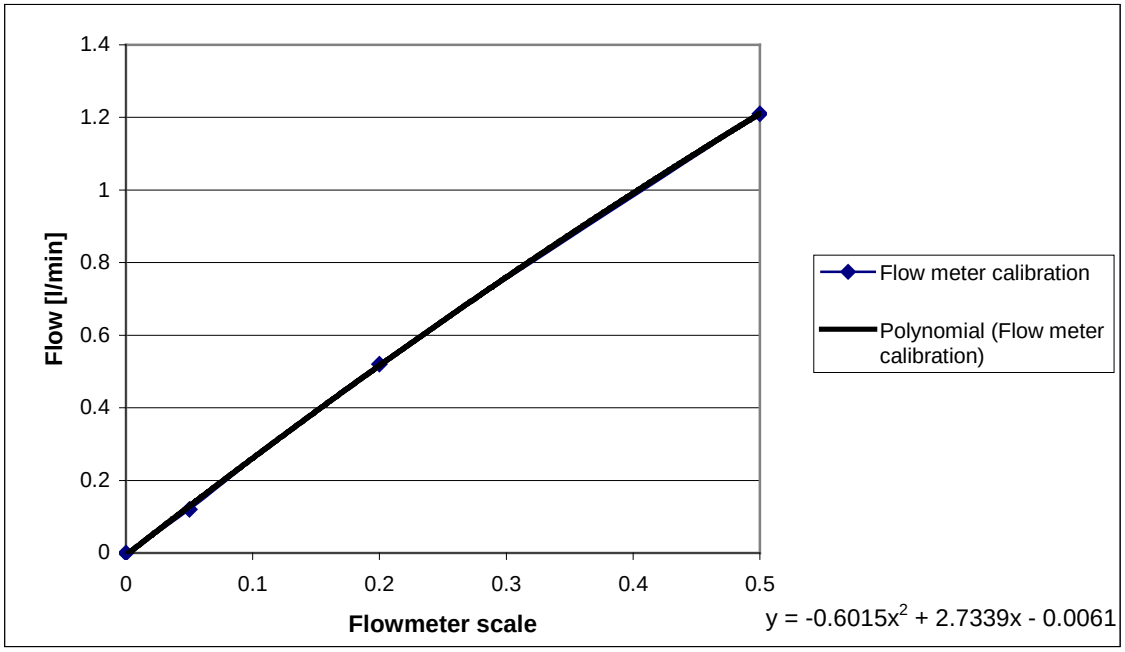

Figure A.6.1 - Flow meter calibration for hydrogen: flow/scale curve and 2nd order polynomial curve approximation

Appendix 6.2 - Solar radiation in Lisbon

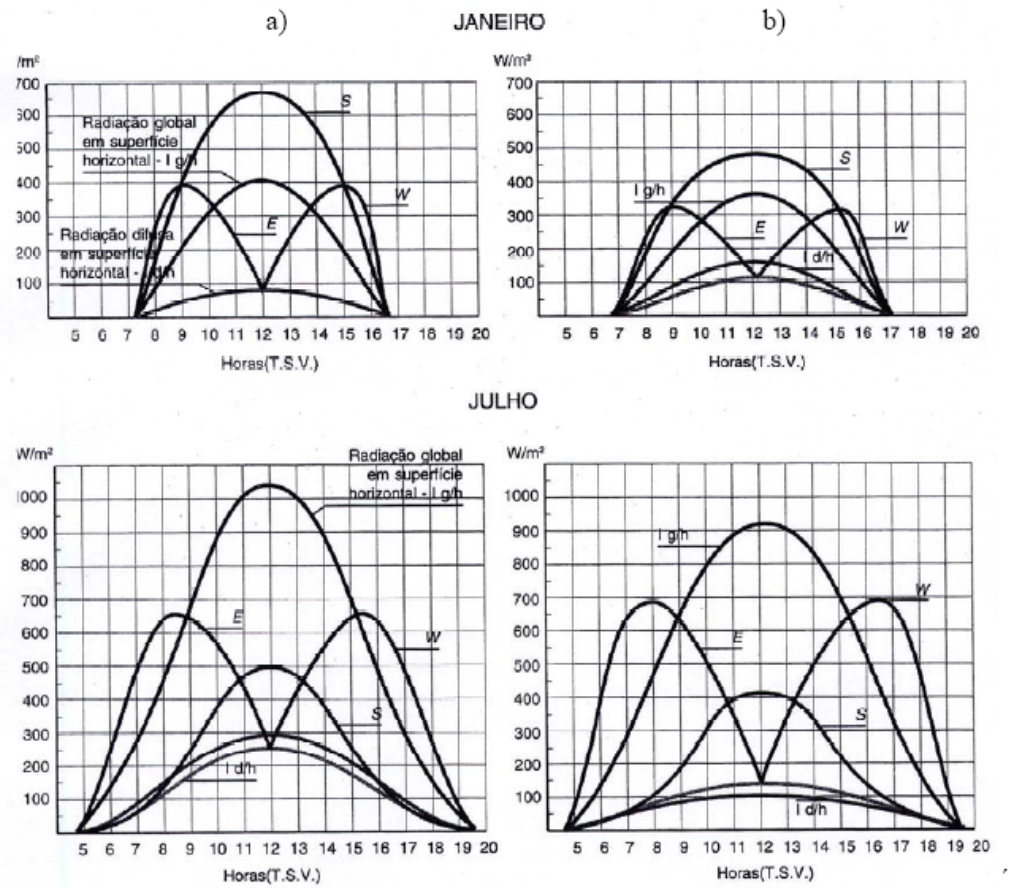

Figure A.6.2 - Average solar radiation along the day on horizontal surface in Lisbon (38º N) based on 25 year record [41]

The *Figure A.6.2* exhibits the intensity of the incident solar radiation on horizontal and vertical surface for the 4 cardinal orientations and the total radiation on horizontal surface in Lisbon (38º N latitude) from: a) equations of *Figure A.6.3* b) average values calculated by Mata and Marques from a 25 year track record [41]

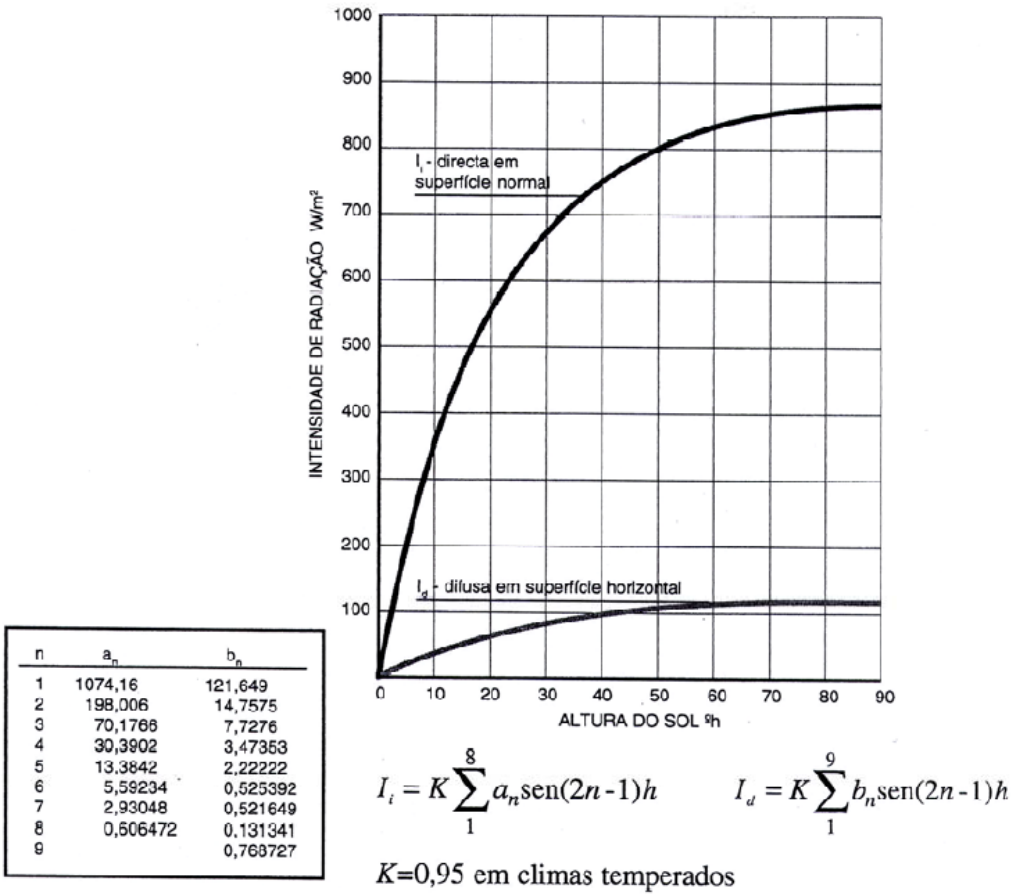

Figure A.6.3 - Intensity of direct and diffuse solar radiation in clear sky conditions [41]

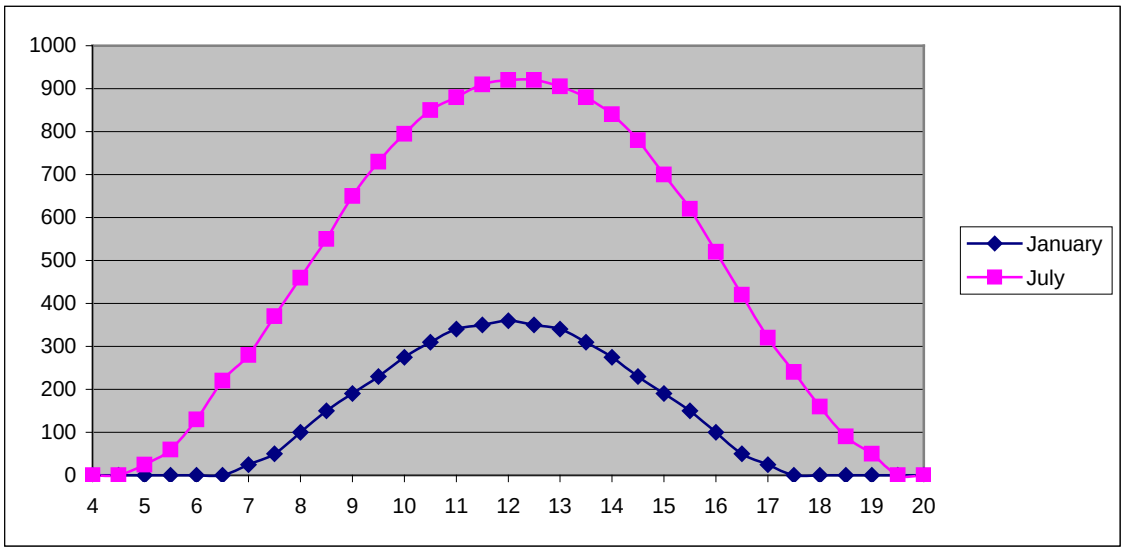

Figure A.6.4 - Average solar radiation along the day on horizontal surface in Lisbon (38º N)

Appendix 6.3 - Cable calibration for current measurement

Table A.6.2 and *Figure A.6.5* illustrate the measurements and calculation of the ohmic resistance of a copper cable of 2.5 mm diameter. The resistance is equal to the slope of the trend curve.

Table A.6.2 - Current / Voltage for calculation of electrical cable ohmic resistance - PV1

A (+/- 0.01)	***U2 (mV) (+/- 0.1)***
0	0
0.5	10
1	20
1.5	29.9
2	39.8
2.5	49.7
3	59.7
R [mΩ]	19.879

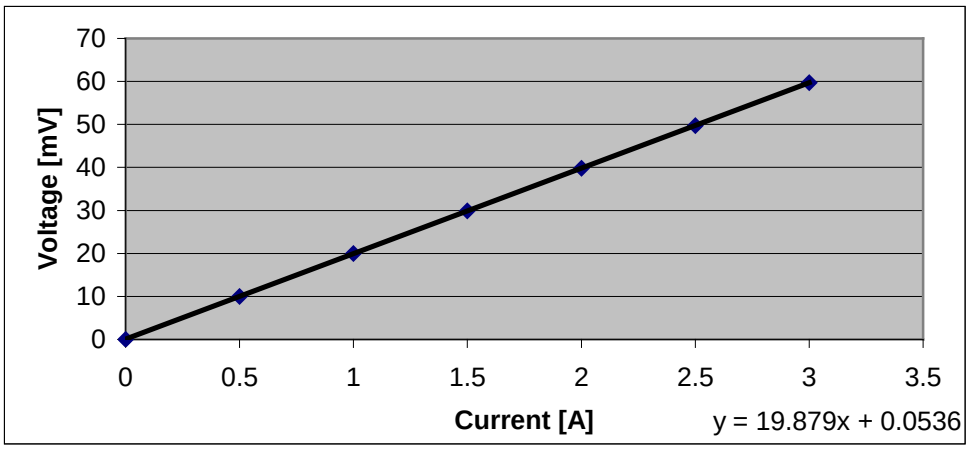

Figure A.6.5 - Current measurement for cable calibration - PV1

Appendix 7.1 - Scope simulation signal record

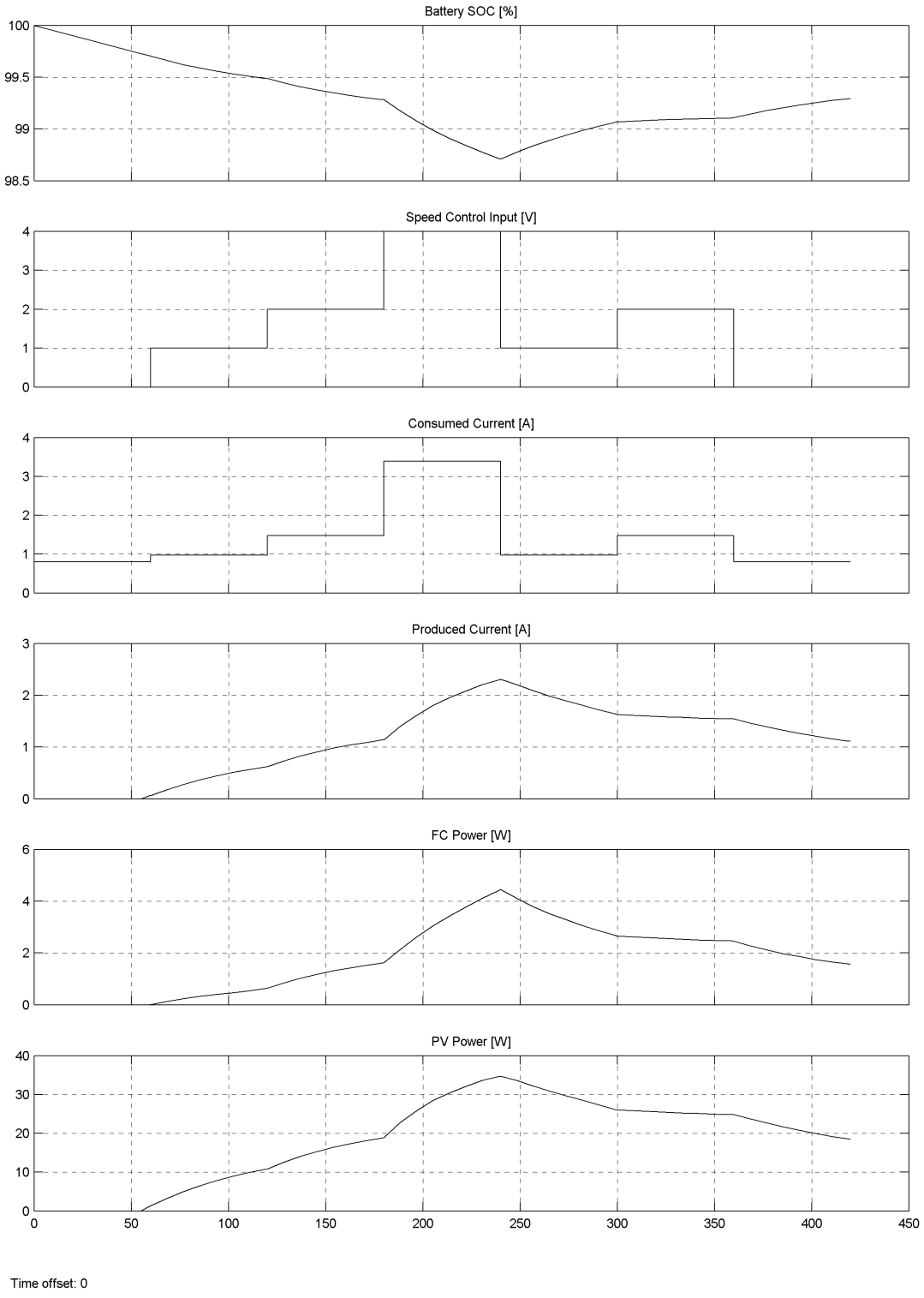

Figure A.7.1 - Scope signal record of the 7 min 100% SOC simulation